Quaternary off-axis tectonic deformation along the southern Arava segment of the Dead Sea transform as expressed by geomorphic indicators

Thesis for the Degree of Master of Science
submitted by:

Yedidia Gellman

Under the supervision of:
Prof. Ari Matmon
Dr. Amit Mushkin
30/3/2015

Department of Geology
Institute of Earth Sciences
Faculty of Mathematics and Natural Sciences
The Hebrew University of Jerusalem

Quaternary off-axis tectonic deformation along the southern Arava segment of the Dead Sea transform as expressed by geomorphic indicators

Thesis for the Degree of Master of Science
submitted by:

Yedidia Gellman

Under the supervision of:

Prof. Ari Matmon
Dr. Amit Mushkin

30/3/2015

Department of Geology
Institute of Earth Sciences
Faculty of Mathematics and Natural Sciences
The Hebrew University of Jerusalem

Abstract

The Eilat area is considered to be one of the most seismically hazardous regions in Israel in large due to the active Eilat fault system. While the Eilat fault has been studied in a series of recent paleoseismic and historical investigations, our understanding of the spatial distribution and timing of recent off-axis deformation in this region remains less clear. In this context, the goal of this study is to improve the current understanding of the spatial distribution of late Quaternary tectonic deformation in the southern Arava. To achieve this goal, interpretation of recent changes in the characteristics of drainage systems was examined using field based geomorphic mapping of middle Quaternary to Holocene fluvial units, detailed high-resolution topographic cross-sections and luminescence dating across the Zefunot, Amram and Shehoret basins in southern Israel. Results indicate recent changes in channel flow directions that appear to be most consistent with recent tectonic surface tilting. Multiple geomorphic evidences indicate coeval southward migration of the active channel in the Zefunot basin and northward migration in the Shehoret basin. These changes point towards off-axis N-S compressional deformation. OSL dating indicates that this tilting initiated in middle Pleistocene and continued at least up to middle Holocene. This research suggests that the spatial extent of late Quaternary tectonic deformation along the southern Arava segment of the Dead Sea Transform is wider than previously considered. Such off-axis deformation contradicts the localized deformation expected for the maturity and cumulative offset of the Dead Sea Transform and is most likely associated with changes in the geometry of relative movement between the Arabian plate and the Sinai sub-plate.

Acknowledgments

I would like to express my gratitude to my advisors, Prof. Ari Matmon from the Hebrew University and Dr. Amit Mushkin from the Geology Survey of Israel for their experienced and patient guidance, their enrichment of discussions and for joining on-field research trips. I would like to thank Prof. Michael Beyth from the Geology Survey of Israel, whose ideas introduced this research, for his most helpful discussions and guidance. I would like to thank Prof. Naomi Porat and Galina Faershtein who helped and guided the OSL sampling, processing and analyzing.

I am grateful to Yaakov Refael, Iyad Swaed and Yuval Levy for their assistance in the field work. I would like to thank my friends from the Institute of Earth Science for fruitful discussions, reviews and encouragement: Elchanan Zuker, Aner Paldor and Matias Groisman. I want to thank Batya Moshey, Magi Perken and Yosi Sherer for all their help. I would also like to thank all my teachers and friends whom I may have forgotten to mention in this page.

Last but not least, I am gratefully indebted to my beloved wife Rachel and our three sons: Segev, Zemer and Kedem for the moral and physical support along this journey, for accepting my long absences from home and for showing interest in my work. Without your support this work would not be possible.

This research granted me a fascinating opening to and a close observation of the marvelous wonders of nature and its evolutionary processes. During this work I was provided with many spiritual insights and above all a meaningful understanding of the saying:

"What is harder than rock, or softer than water? Yet soft water hollows out hard rock"

-Ovidius

Table of contents

List of figures

List of tables

1. Introduction

1.1. Tectonic background

1.1.1. Theoretical tectonics

Three main types of boundaries divide tectonic plates: convergent, divergent and transform. Transform boundaries are formed by parallel, opposite direction movement of adjacent plates. Examples of such plate boundaries are the San Andreas Fault (Hill and Dibblee, 1953), the New Zealand Alpine fault (Wellman and Willett, 1942) and the Dead Sea fault (Freund et al., 1970). In transform boundaries, the majority of the relative motion is confined to strike-slip faulting zones along the plates' margins.

The mechanics of strike-slip faults are often explained by two main physical mechanisms: pure shear and simple shear (Jaeger et al. 2009 and references therein). The pure shear mechanism of fault systems, also known as the "Coulomb-Anderson Model", predicts the formation of two conjugate strike-slip faults, one dextral and the other sinistral. The right angle between these faults is bisected by the maximum compression direction (Fig. 1; Wilcox et al., 1973). Folds and reverse faults are expected to form with their strike direction normal to the minimal compressional direction and extensional features are expected normal to the maximum compression direction. An example of a faulted region obeying the pure shear mechanism is the Wopmay Orogen of northern Canada (Hoffman and St-Onge, 1981).

In a simple shear system a set of conjugate strike-slip faults form as the initial stress is applied to the region (R and R' in Figs. 1 and 2; Anderson, 1905; Tchalenko, 1970; Wilcox et al., 1973). These faults are not parallel to the direction of applied shear but rather form angles of $\varphi/2$ and $90-\varphi/2$ with it (where φ is the internal friction angle (Anderson, 1905)). As the simple shear proceeds, these faults are abandoned (first the R' faults and then the R faults) and remain as passive remnant markers. In the course of inactivation of the predecessor faults, new faults are formed parallel to the direction of applied shear (also termed “D faults” by Skempton, 1966). The newly formed faults accommodate large movements (Freund, 1974) and do not change their orientation during the rest of the shear process. In a simple shear environment, folds will form normal to the maximum contraction direction. Initially, the folds form an angle of 45^0 with the direction of shearing, but as deformation continues the fold axes rotate

proportionally to the amount of shearing (Fig. 2). Examples for major strike-slip faults situated in domains of simple shear are the San Andreas Fault (Chester et al., 1993) and the north Anatolian fault (NAF) (Westaway, 1990).

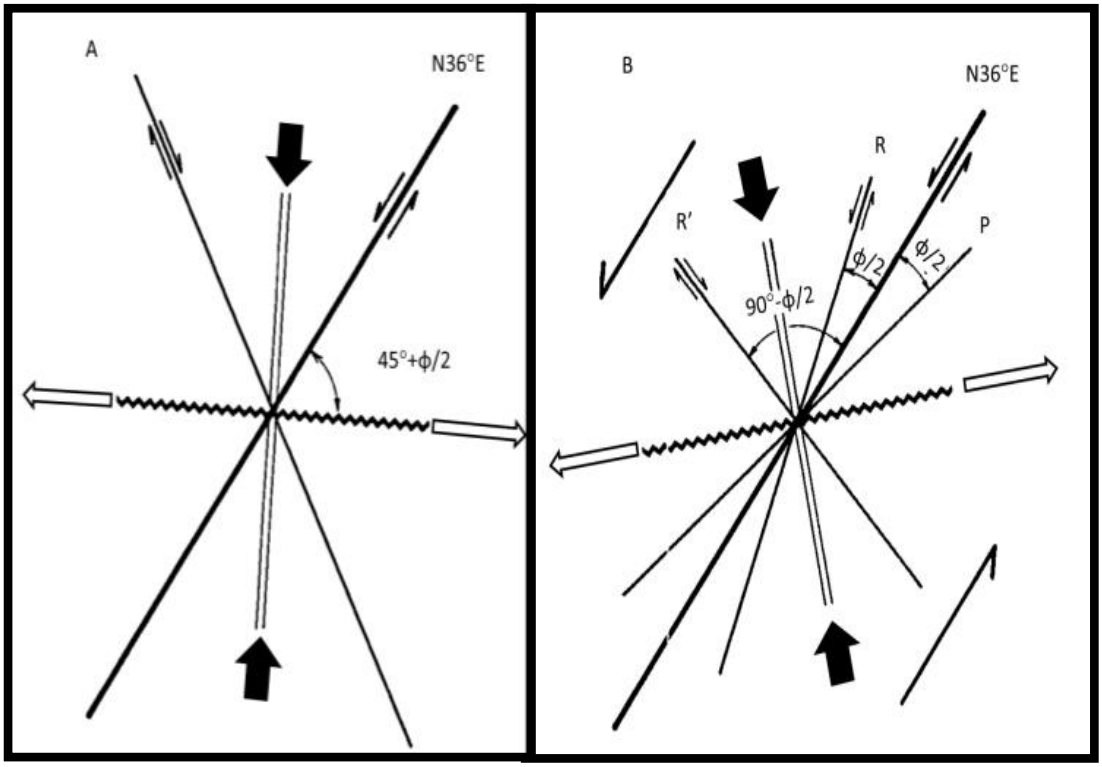

Figure 1. Strike slip structural models: **Plan view of geometric relations between strike slip structures according to basic tectonic models. A. Coulomb-Anderson model of pure shear. B. Simple shear model. The major sinistral strike-slip trend is chosen to be N36°E in both cases. Double parallel lines represent orientation of extension fractures; the corrugated line represents orientation of fold axes. P is pressure faults, R and R' are synthetic and antithetic shears, respectively; φ = angle of internal friction. Bold black arrows = shortening axis; open arrows = axis of lengthening. (Modified from Aydin and Page, 1984).**

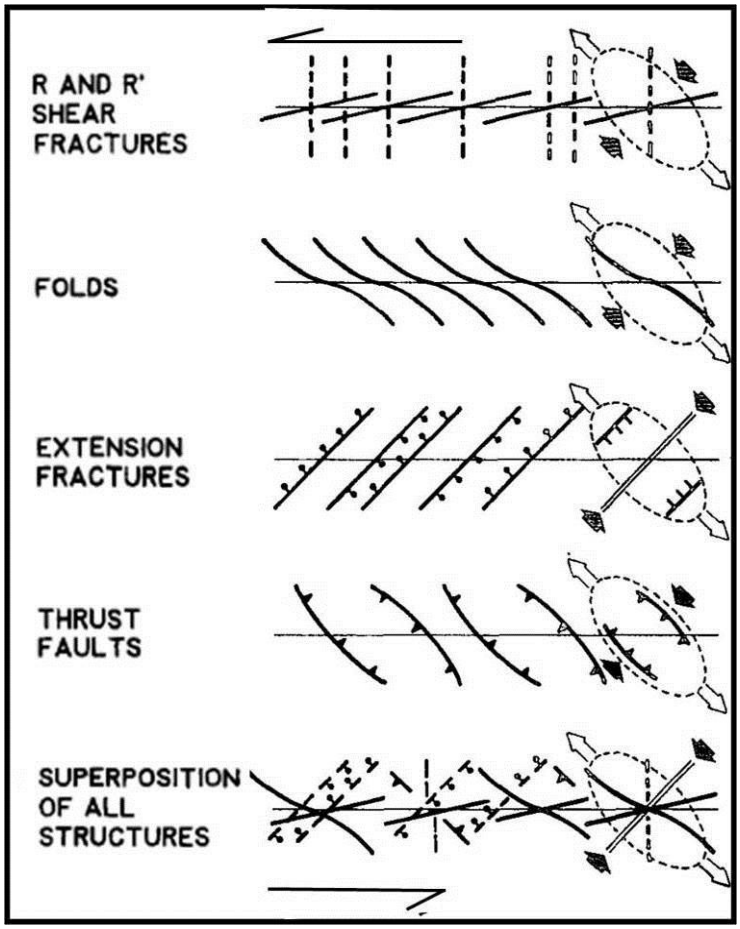

Figure 2. Simple shear model: **Orientation of folds and faults in a left simple shear strike slip tectonic model. (Modified from Sylvester, 1988).**

The extent and nature of structural deformation at the margins of strike-slip faults are controlled by (1) the degree of convergence or divergences between the adjacent blocks; (2) the magnitude of displacement along the faults; (3) the physical properties of the deformed lithology; and (4) the influence of pre-existing structures (Sylvester, 1988). Blick et al. (1985) defined a "simple strike-slip fault" as a "fault along which there is no evidence for preferential convergence or divergence." This type of fault was previously described by Wilcox et al. (1973) as a special case of simple shear, initiated with plastic deformation involving the formation of fold structures, followed by plastic distortion and fracturing. The ongoing process of deformation and increasing displacement brings on the narrowing of the shear zone, resulting in concentration of the slip displacement along a few closely spaced faults. Deformational structures may develop along certain segments of straight strike-slip faults as a result of relative convergence and divergence generated by rotation of small adjacent blocks

(Freund, 1974) (e.g. eastern Iran (Freund, 1970) and New Zealand (Freund, 1971)). In contrast to "Simple strike-slip faults", "Convergent strike-slip" and "Divergent strike slip" fault zones are accompanied by significant continual spatial deformation (Wilcox et al., 1973). These oblique deformation directions along convergence or divergence fault types are known to form at regional and local scales. Deformation along "convergent strike-slip faults" leads to the formation of reverse faults; low angle thrust faults and en-echelon folds oblique to the original displacement direction, e.g. the Western Transverse Range (WTR) (Blick and Biddle, 1985 and references therein). In contrast, deformation along "Divergent strike slip faults" leads to formation of normal faults and flexures parallel or oblique to the original displacement direction (Harding et al., 1985). In addition, changes in the orientation of the strike slip fault such as bends and step over of segments can result in the formation of rhomb shaped grabens and push-up ridges, e.g. along the Dead Sea Transform (Ben Avraham et al., 2008 and the references therein).

To summarize, the formation of off-axis deformation structures is strongly coupled to the specific strike-slip fault style and its evolution over time. The dominating mechanisms forming these structures are (1) **pure shear**: deformation that is parallel and perpendicular to the maximum compression direction; (2) **simple shear - simple strike-slip:** local relative convergence, divergence or block rotation; **(3) simple shear - convergent strike-slip:** formations of pressure structures; (4) **simple shear - divergent strike slip:** formation of elongation structures**.**

The width of the deformation zone affected by strike-slip deformation may be up to tens of kilometers (Sylvester, 1988) and tends to narrow as a function of cumulative geological offset (Wesnousky, 1988). A change in the geometric setting of the plate boundary along a fault zone can occur, leading to a rearrangement of the stress field controlling the transform boundary (Ten Brink et al., 1999). As a result, the localization stage may be interrupted by rearrangement of the deformation zone, and a wider deformation zone can be re-established. Shear localization processes may then be reinitiated (Marco, 2007).

1.2 Motivation

Previous studies indicate that tectonic deformation along the western margins of the southern Arava has been concentrated within the Arava Valley center since the Miocene (Marco, 2007). The main goal of the present research is to test this hypothesis and determine the extent of off-axis tectonic deformation in this region during the Quaternary. Answering this question relates to regional understanding the forces and deformation along the Dead Sea Transform as well as for more general understanding deformation characteristics along strike-slip plate boundaries.

1.3. Regional Geology

The Dead Sea Transform (DST) is part of the boundary between the Arabian plate and the Sinai sub-plate (Garfunkel, 1981). It extends from the Red Sea in the south to the Zagros Mountain belt in the north (Quennell, 1958; Fig. 3). Left-lateral movement along this plate boundary began in the middle Miocene and resulted in cumulative sinistral offset of approximately 105 km (Freund et al., 1970; Garfunkel, 1981). The boundaries of the transform contain numerous deformation structures that result from complex motion along strike-slip faults and form an up to several kilometer wide shear zone. Several of the strike-slip features and the regional deformation structures along the DST match many characteristics of the simple shear mechanisms (Ron and Eyal, 1985). A component of transverse separation has resulted in the formation of a rift valley along major parts of the transform, e.g., the Jordan Valley (Garfunkel, 1981). In contrast, other segments of the transform contain a compression component resulting in formation of pressure structures, e.g., along the Yammuneh faults (Garfunkel, 1981).

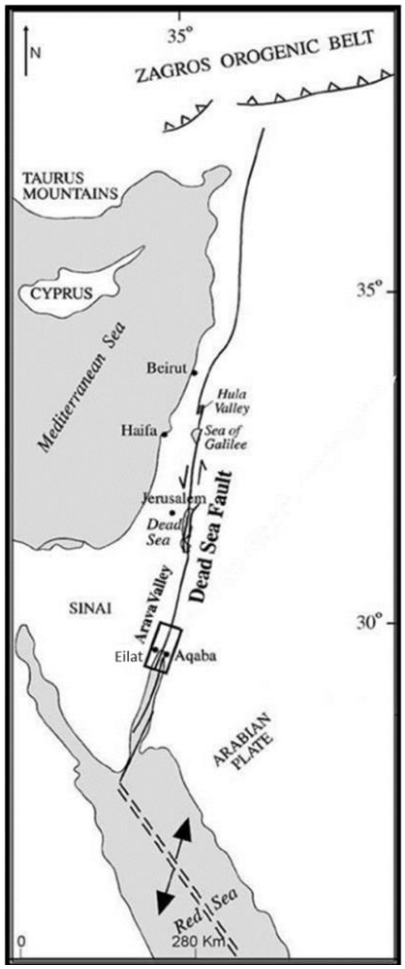

Figure 3. Regional tectonic map: **A generalized map showing the main regional tectonic settings. The study area is marked with a black open box (modified from Zilberman et al., 2005).**

The Arava Valley (Fig. 3 and 4), a part of the southern segment of the DST, formed as a consequence of a transverse component and extends from the northern end of the Gulf of Eilat to the Dead Sea basin (Picard, 1943; Garfunkel and Horowitz, 1966; Garfunkel, 1978, 1981, 1988). Since the early Neogene, motion along the Dead Sea transform in the Eilat area has been conventionally viewed as partitioned between marginal normal faults and central sinistral strike-slip faults (Garfunkel et al., 1981; Eyal et al., 1981). Local left-stepping along the strike-slip faults created a series of internal morphotectonic structural basins which accommodate the Evrona, Eilat and Yotvata playas (Garfunkel et al., 1981). Several of the marginal normal faults contain a component of horizontal displacement (Garfunkel, 1970). The Arava region consists of an assemblage of metamorphic, magmatic, and sedimentary units dating back as far as the Precambrian (e.g. Weisbored, 1961; Bentor, 1961; Garfunkel, 1970; Beyth et al., 2012). Late Cenozoic structural deformation (faulting and folding) related to the development of the DST resulted in differential uplift, erosion and exposure of the various rock types that form the crust in this area (Beyth et al., 2012 and references therein).

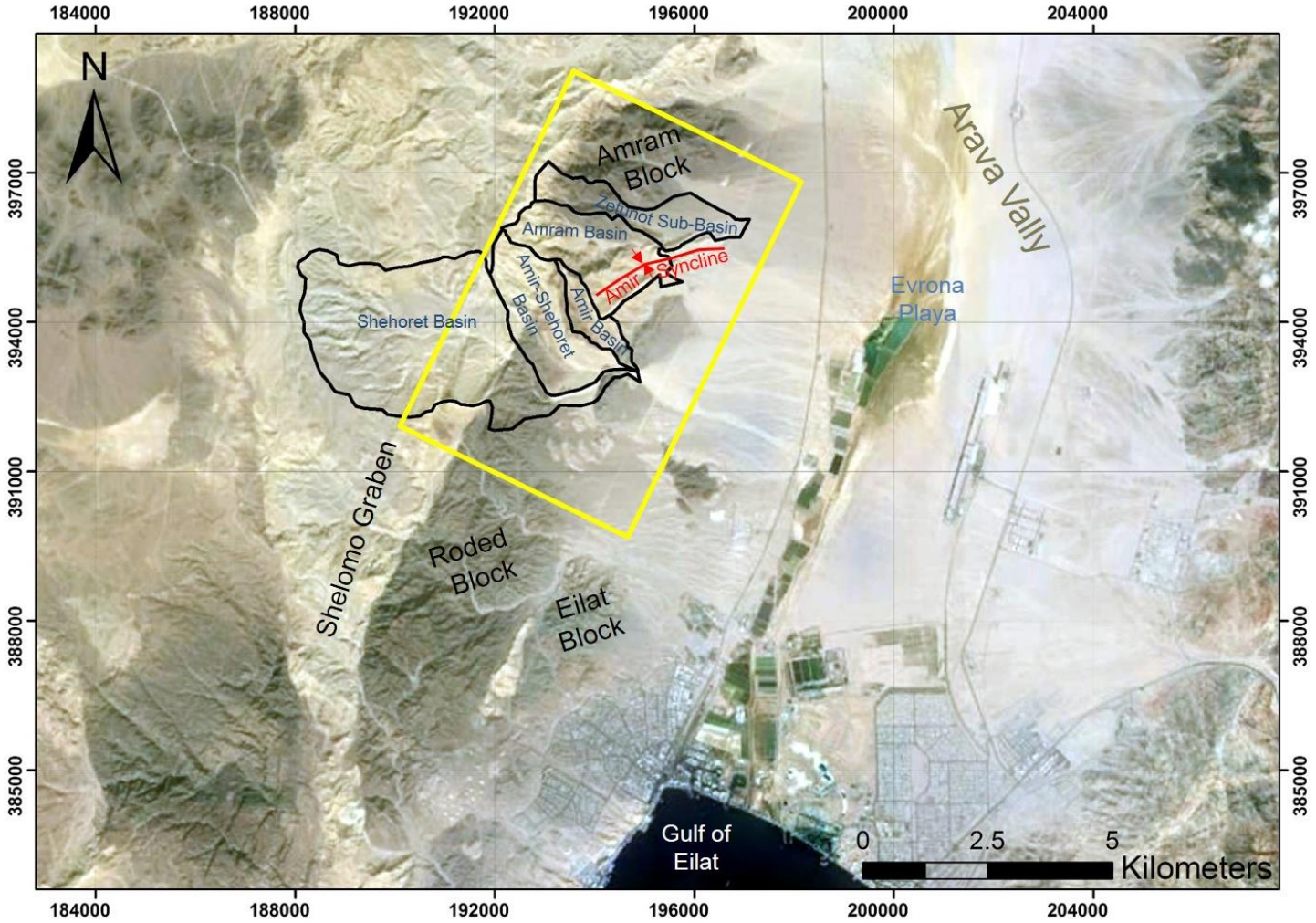

Figure 4. Arava satellite image: **A satellite image of the southern Arava and its western margins. The research area is marked with a yellow open box. Basins examined in this study are outlined in black (modified from https://maps.google.com).**

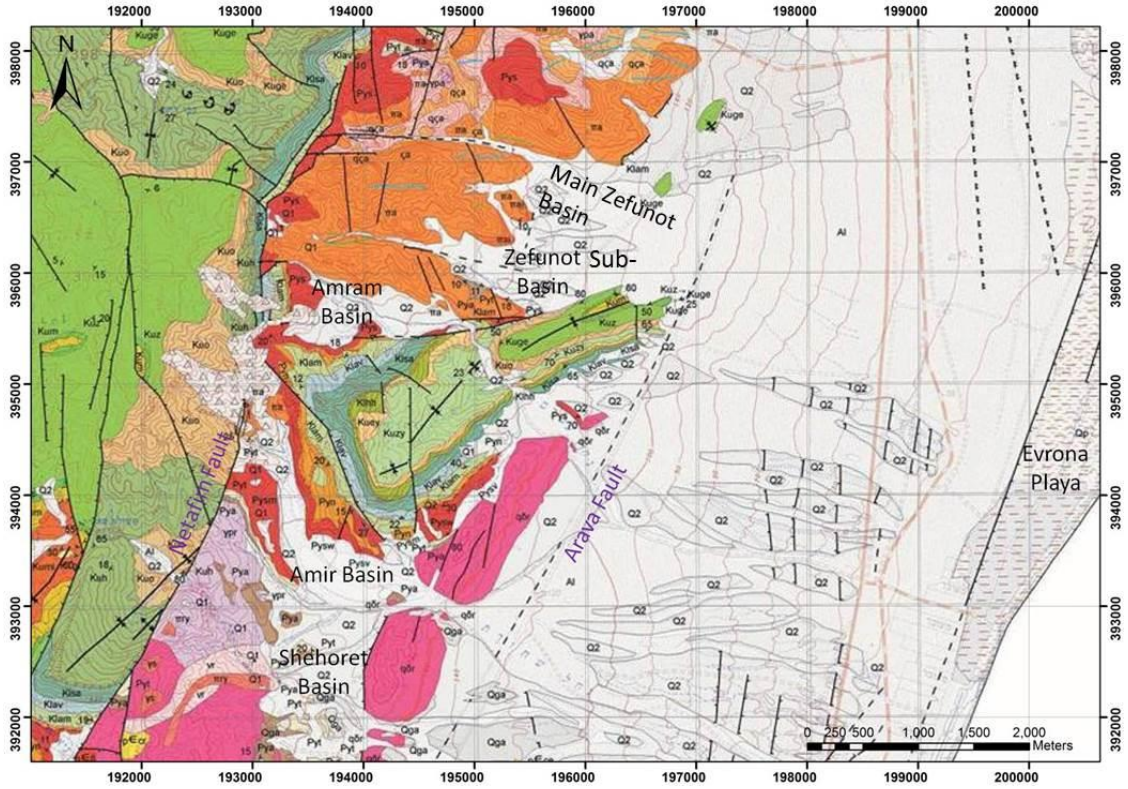

Figure 5. Geological map: **Geological map of the research area (modified from Beyth et al., 2012).**

Along the western margins of the southern Arava, a set of sub-parallel faults separate a series of structural blocks composed of crystalline basement rocks (the main blocks are the Roded, Eilat and Amram blocks) (Garfunkel, 1970; Fig. 5, 6 and 7). The width of these structural blocks ranges from a few hundred meters to 1.5 kilometers and they are 3 to 7 kilometers long (Fig. 6). Lithological offsets between the blocks enable the measurement of relative movements between them along the dividing faults (the Netafim Arava and Eilat faults). Vertical offsets of hundreds of meters as well as considerable sinistral movement are evident. The geometry of the faults changes from a NW-SE strike along their southern part to a ~N-S strike along their northern part. Bending of the faults likely forced clockwise rotation about a vertical axis (Garfunkel, 1970) (Fig. 6). Additionally, the blocks are tilted towards the center of the Arava valley.

During the Tertiary, a shear zone developed over the Sinai and Negev area, generating dextral strike slip faults that are currently perpendicular to the DST direction

(Bartov, 1967). The dextral strike slip Themed fault which is part of the Sinai-Negev Shear Zone (Bartov, 1974) strikes west-northeast and is located to the north of the research area (Fig. 6).

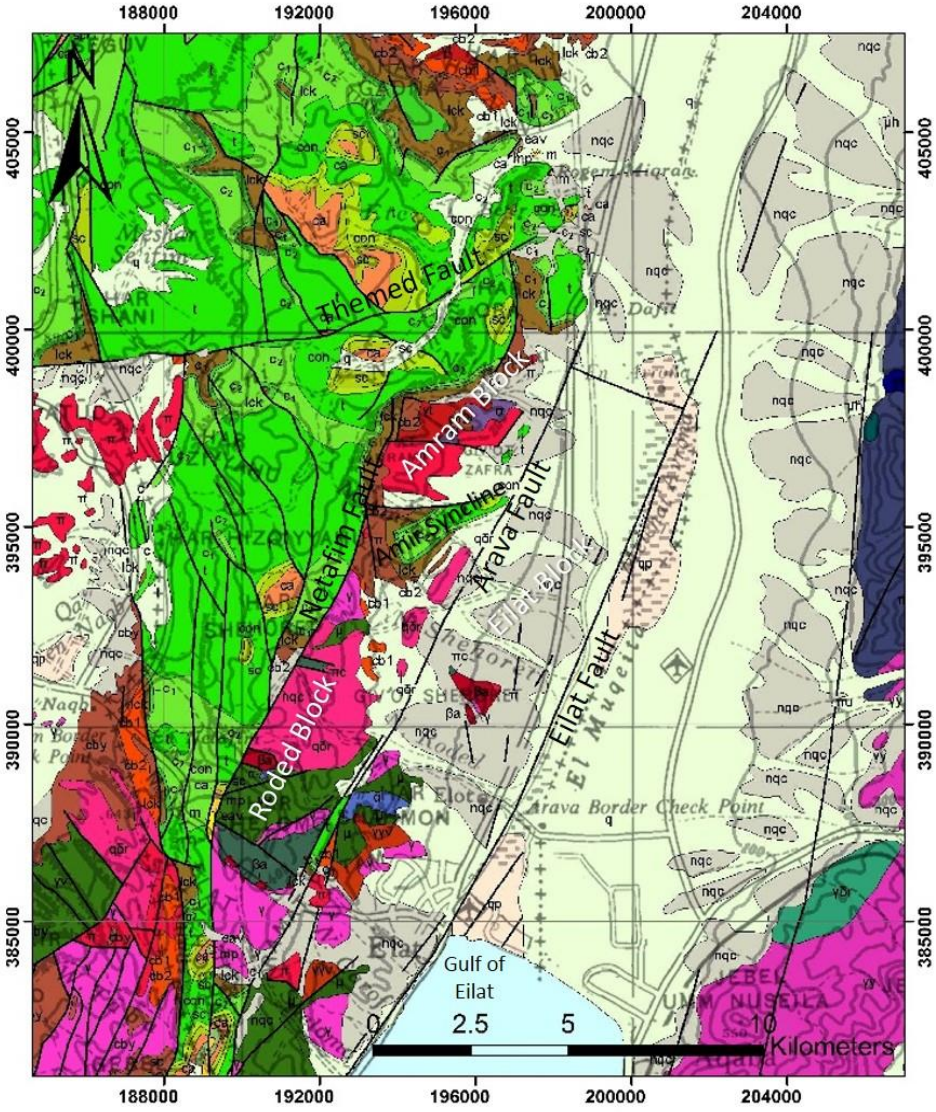

Figure 6. Main tectonic features: **The main tectonic features and structural blocks in the research area.**

The "Roded" block (Fig. 4, 6 and 7) was displaced approximately 2.5 kilometers to the north relative to the adjacent blocks along the "Netafim" fault (Garfunkel, 1970). The faults dividing the Arava's marginal blocks, including the faults along the Roded block, were initiated after the Themed fault's activity ceased as they do not displace it (Garfunkel, 1970). This implies absorption and possibly compression of the "excess" volume between the northern edge of the Roded block and the Themed fault. Rotation

of the Roded block can account for part of the volume excess. The other structures that can absorb the predicted volume excess are: (1) The "Amir" syncline between the Roded block and the "Amram" block. The axis of this pressure structure strikes E-NE and the sandstone underneath it is faulted by reverse faults (Garfunkel, 1970). (2) The Amram block is internally deformed by multiple faults and is relatively uplifted in relation to its surroundings (Beyth et al., 2012).

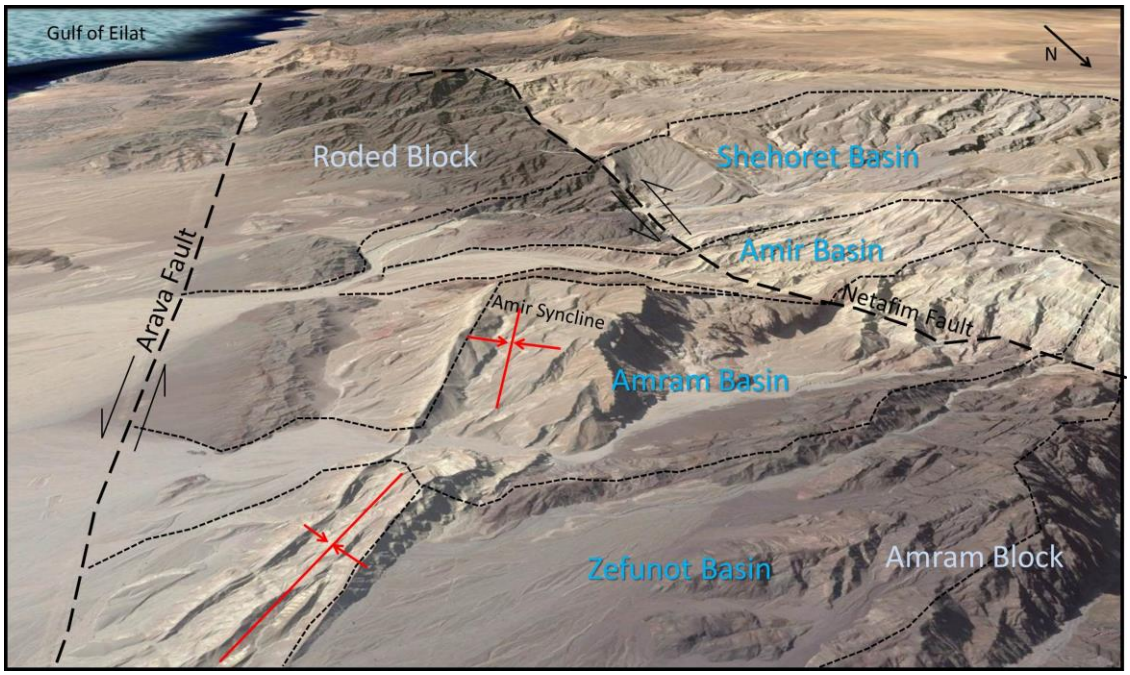

***Figure 7. Perspective view of the southern Arava's western margins*. The studied basins are outlined by thin dashed lines. The two main faults in this area are marked by a thick dashed line. (Modified from https://maps.google.com).**

The width of the deformation and faulting zone associated with the initial stages of the DST is up to 50 kilometers (Marco, 2007). With the continuation of lateral movement during the late Miocene, deformation became more localized (Marco, 2007). The southern Arava segment is conventionally regarded to follow this general trend of shear localization with time (Marco, 2007).

Paleoseismic studies (e.g., Amit et al., 2002; Gerson et al., 1993; Amit et al., 1996), geomorphic investigations (e.g., Amit et al., 1999) and interpretation of historic seismic records (e.g., Ambreseys et al., 1994; Amiran, 1994; Hamiel et al., 2009; Porat et al., 2009) together with geophysical and remote sensing investigations (e.g., Frieslander, 2000; Baer et al., 2008) were previously carried out along the Arava

segment of the DST. These studies consistently point towards late Pleistocene - Holocene seismic activity concentrated along the center of the valley.

1.4 Geomorphic background

Landscape sculpturing is promoted by the fluvial process of degradation and aggradation (Bull, 1991). Changes between degradation and aggradation through time are typically driven by fluctuations in tectonic activity and/or climatic changes. These in turn may be followed by base-level changes and variations in sediment supply. The response of the fluvial system to such perturbations may become imprinted in the evolving landscapes. Thus, studying landscape evolution in regions where one of the influencing processes can be isolated enables reconstruction of paleo-environmental conditions. In this context, the observation of changes in drainage basin characteristics and channel patterns in tectonically active areas can be used as an indicator of tectonic deformation (Schumm, 1977). Tracing tectonic deformation by geomorphic evidence is widely practiced in tectonically active regions (e.g., Burbank and Anderson, 2011; Castelltort et al., 2012; Riquelme et al., 2003; Malik and Mohanty, 2007) and has also been utilized specifically in the southern segment of the DST (Ginat et al. 2009).

Prior to the formation of the Arava's morphologic depression, the regional drainage systems flowed northwestwards, and drained into the Mediterranean Sea (Bentor and Vroman, 1957; Garfunkel and Horowitz, 1966; Zak and Freund, 1981; Zilberman, 1991). As a result of the subsidence of the Arava and the uplift of its margins during the late Neogene, new eastward draining systems formed in the southern and central Negev (Garfunkel and Horowitz, 1966; Zilberman et al., 1996; Avni, 1998; Guralnik et al., 2010). These eastward flowing drainage systems have been incising into bedrock and sediments, following the tectonic subsidence of the Arava base level. Late Cenozoic fluctuations in the base level, coupled with climatic changes, resulted in the formation of several generations of morphostatigraphic surfaces, fluvial terraces, and fans that shape the Arava Valley and the surrounding margins (Ginat et al., 1998; Beyth et al, 2012).

The tectonic deformation and relative movement of the Arava's marginal structural blocks were followed by landscape development that expresses deformation occurring at greater depths (Garfunkel, 1970). Geomorphic evidence, mainly the

behavior of drainage systems, can be used to infer the character and timing of such deep deformation. Furthermore, it can be assumed that geomorphic perturbations occurred since the initiation of deformation in the region and accompanied it ever since. In this context, studying and interpreting recent changes in geomorphic features and reconstructing past drainage system flow patterns will achieve the goal of this research.

In the case that deformation of the Roded and the Amram blocks continued during the Quaternary, the Zefunot and Amram drainage systems of the Amram block and the Amir and Shehoret drainage systems of the Roded block would be expected to possibly show geomorphic indications for this deformation.

1.5 Climatic background

The climate in the southern Arava segment of the DST is hyper-arid with annual mean precipitation of less than 30 mm, usually occurring in one or two rainfall events (Israel Meteorological Service web site- http://www.ims.gov.il, last update - 10/2007). As a result, runoff occurs as short high-energy flash floods that can transport large sediment volumes (Barzilai et al., 2000). The average maximum daily temperature is 31ºC and mean annual temperature is 25°C (Israel Meteorological Service web site- http://www.ims.gov.il, last update - 10/2007). Summers are extremely hot and winters are warm to mild. These hyper-arid climate conditions account for scarce vegetation. Though indications of temporal changes in storm and flood frequency were described in nearby basins through the Quaternary (Enzel et al., 2012) climatic conditions in the southern Negev and Arava did not significantly vary from the present conditions despite global glacial and interglacial cycles (Horowitz, 1979; Amit et al., 2006; Enzel et al., 2008). Steady climatic conditions suggest that geomorphic perturbations in this region during the Quaternary were not climatically controlled.

2. Properties & Methods

2.1 Study site

The research area is located along the western margin of the DST in the southern Arava Valley of southern Israel, approximately 10 kilometer north of the Gulf of Eilat (Fig. 3 and 4). The geomorphic surfaces investigated in this study are fluvial terraces and fans within four drainage basins. The Shehoret basin in the south is the largest basin in the research area draining a total area of approximately 12.5 square kilometers. The Amir-Shehoret basin drains an area of approximately 4 square kilometers (a small basin drains the area between the Amir-Shehoret basin and the Amram basin named the "Amir basin"). The Amram basin drains an area of approximately 3.9 square kilometers. The Zefunot basin in the north drains an area of approximately 2.6 square kilometers, (Fig. 4). The base-level of all four basins is the Evrona playa, a morphologic depression formed by sub-parallel left-stepping faults (Amit et al., 1999).

Field mapping and OSL optical stimulated luminescence dating were aimed to trace and characterize changes in the fluvial systems flow vectors. Using these results, the former channel flow directions were compared to the present opposed active channels flow directions and the former geomorphic features were placed in a time frame.

2.2 Mapping

Initial mapping was performed on high-resolution orthophotos and was based on color and texture differences between proposed mapping units. This was followed by actual Field characterization of fluvial fan surfaces which was carried out according to the following criteria (Bull, 1991):

Relative age:

- Surface roughness: Examination of the maturation degree of desert pavements and advancement of surface smoothing process was used as criteria for unit definition. Comparison of pavement development, surficial particle size, spacing between the particles, and preservation degree of original

flow pattern (bar and swale) were used as criteria for distinguishing between the mapping units and constraining their relative age (Bull, 1991). These comparisons must consider the original size, lithology, and abundance of particles within the originally deposited sedimentary sequence.

- Soil development: Characterizations of soil profiles, developed on top of the fluvial terraces surfaces, are useful for comparison and definition of mapping units. The gypsic–salic Reg soils in the study area (Amit et al., 1993) can be used as relative age indicators by comparison of three main soil properties: A. The thickness of the Av horizon (Gerson and Amit, 1987); B. The degree of gravel shattering by salts (Amit et al., 1993); and C. Depth of accumulation and thickness of the salt and gypsum horizon (Amit and Yaalon, 1996).

Lithological composition:

- The different lithological components of the fluvial sediments were examined and identified. Lithological composition can be used to determine the bedrock source that supplied the material and was thus exposed during the deposition period. Tracing of bedrock sources of fluvial sediments can also be used to infer possible flow directions at the time of deposition.

Sediment characteristics

Enhancement of sphericity, roundness, and sorting of the sediments is generally an indication of fluvial sediment transportation maturity. Increase or decrease in channel power typically results in growth or decay, respectively, of sediment particle size. Variation between grain supported and mud supported bedding horizons can indicate changes from a high channel power flow regime to a low channel power flow, respectively. However, the short transportation distance in the mapped basins does not allow the full development of such distinct sediment characteristics, which were therefore only used as an aid in the mapping process and not as a unit defining parameters.

- Cross-bedding patterns: Examination of cross-bedding patterns (such as bedding thickness variation, formation of lens type bedding, bedding dip and dip direction) within the fluvial sequences can indicate changes in channel power, flow direction, and sediment supply variations within the drainage basin.

Once identified and characterized, the units were mapped in the field and projected onto the ortho-images**.** GPS recordings were used to assist in the mapping process. Schematic cross-sections were constructed to examine field relations between the units. The mapping data was digitized using the ArcGIS Arcmap10 program.

High-resolution, topographic cross-section measurements along selected profiles were carried out in order to understand the field relations between the different map units and to identify tectonic related deformation within the drainage basins. These measurements were executed using the "Sokkia 50x total station" (EDM) and GPS measurements.

A geometric method was used to determine the relative geomorphic maturity of the different drainage basins. The planimetric shape of a basin evolves over time as result of channel capturing and drainage divide migration (Bull, 2009). A basin evolving over time will tend to have a more circular shape as opposed to tectonically active basins that will preserve an elongated shape (Strahler, 1964). In order to quantify the geometric planimetric evolution of the basins the **Elongation ratio (R_e - Index of circularity, dimensionless)** was used. This geometric method estimates the relative geomorphic maturity of the basin by examining the ratio between the diameter of a circle with the same area as the basin **(R_c)** and the map length between the most distant points in the basin **(L)**:

$$R_e = \frac{R_c}{L}$$

A value of 1.0 indicates a perfectly circular basin (Bull, 2007). The index of circularity decreases below 1.0 as the elongation of a basin increases.

2.3 OSL dating

Optical stimulated luminescence (OSL) dating was utilized to place the studied fluvial terraces in an absolute temporal framework. OSL dating is based on the determination of the time elapsed since last exposure of semi-conducting mineral grains (such as Quartz or feldspar) to heat or sunlight (Stokes, 1999; Murray and Wintle, 2000; Lian and Roberts, 2006). In fluvial systems, sediments that are sampled and dated provide the date of their last exposure to sun light, i.e. their burial age. By dating the base of a mapping unit and the sediments immediately under its surface it is possible to

determine the time of beginning of the deposition process and the time of abandonment of the surface (Aitken, 1998).

Grains with reset luminescence signal may accumulate in the upper part of the soil sequence as the result of several post deposition processes such as pedogenic perturbations or young grain invasion. In order to avoid sampling such grains, samples were extracted from below the salic-gypsic accumulation horizons where this contamination is minimal (Porat et al., 1997; Porat et al., 2010).

OSL samples were processed at the Geological Survey of Israel Luminescence laboratory according to the SAR protocol (Aitken, 1998) and according to the protocol detailed in Porat (2007). Luminescence dating using the single grain (SG) method following the procedure described by Duller (2008) was applied to samples that required more precise results. Thermally transferred OSL (TT-OSL) was applied to samples collected from units that exhibited very mature morphologic characteristics and where the 'traditional' OSL methods yielded poor results. TT-OSL extends the age range of dating to provide quartz OSL dates for Middle Pleistocene sediments (Wang et al., 2006). The TT-OSL signal is measured after the depletion of the conventional OSL signal and a subsequent pre-heat induces the thermal transfer of charge.

All OSL measurements were executed on small aliquot samples (2mm in diameter). The ages of samples measured on small aliquots were calculated using the average De value (Fig. 9; App. C). The ages of samples measured by the SG method were calculated using the Finite Mixture Model (FMM; Roberts et al., 2000) and the minimum age model of Galbraith et al. (1999). Samples YEG-10, 11 and 12 were additionally measured on larger aliquots (5mm in diameter), following poor results on the small aliquots of 2mm. In addition, samples YEG-4, 7, 10 and 16 were measured using the SG (Single Grain) method.

The Preheat and Cut heat sensitivity tests yielded results of 260°C and 240°C respectively. Samples were clean of Feldspar grains. The OSL signal in all samples was dominated by the fast component, and decayed significantly within a few seconds (Fig. 8).

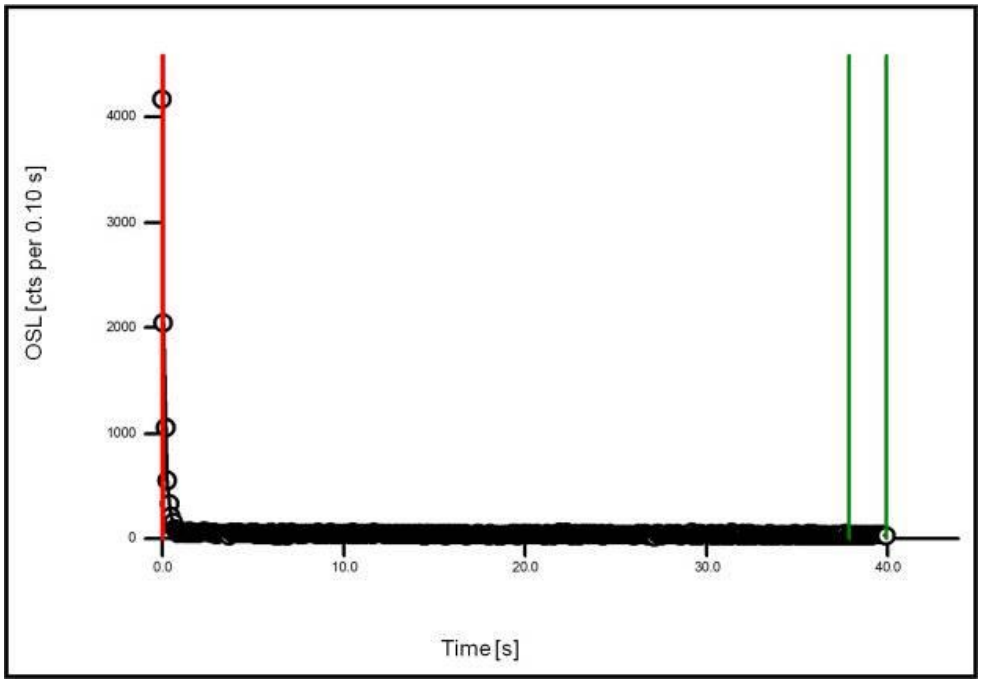

Figure 8. OSL signal: **A typical OSL signal from one measurement disc (sample YEG-15, collected from the base of unit SQ5). The OSL signal is controlled by the fast component and decays to less than 1% of its original strength within less than two seconds (marked by the red line).**

The nature of fluvial transportation of the quartz grains over a short distance during flash flood events may result in insufficient bleaching by sunlight and considerable dispersion of the De values (Olley et al., 2004). This phenomenon is also expressed in the high over dispersion (OD, represents the statistic variability in the data set) values of the samples in these basins - 29% to 86% in the Zefunot basin and 16% to 65% in the Shehoret basin (App. C). To overcome this large distribution of De values, outliers were excluded, based on the assumption that the lower De values represent the well-bleached grains in the sample, while the high De values represent the unbleached grains (e.g. Fig. 9).

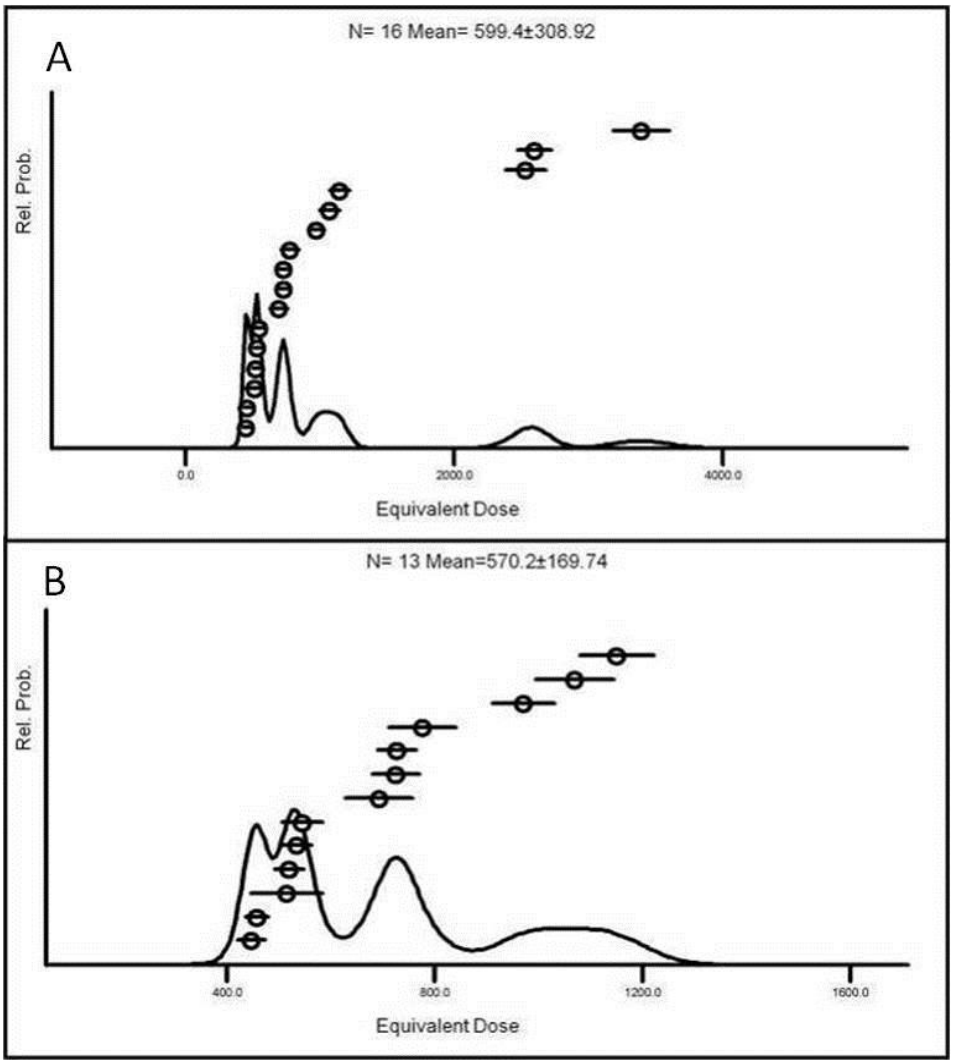

Figure 9. OSL cumulative distribution curves: **An example of cumulative distribution curves (sample YEG-15, collected from the base of unit SQ5). A. All results for discs that showed a normal growth curve (16 discs out of 18 that were measured), the mean equivalent dose includes all discs (appears above the graph). B. The outlying discs (those showing the highest equivalent dose) were excluded (assuming they represent partially bleached samples) and a more geologically consistent mean equivalent dose was recalculated. To obtain the samples age, the equivalent dose is divided by the dose rate.**

3. Results

3.1 The Zefunot Sub - Basin

3.1.1 General

To the west of the Arava fault, the Zefunot basin is divided into two separate drainage systems: the main Zefunot basin and the "Zefunot sub-basin" (the subject of this work) (Fig. 5). The Zefunot sub-basin, a 2.6km^2 elongated shaped basin, has an elongation ratio (R_e) of 0.45. The Netafim fault crosses the basin from north to south close to the headwater (Fig. 7). To the west of the Netafim fault the Zefunot channel drains carbonate lithologies (the Upper Cretaceous Judean group (Beyth et al, 2012)). East of the Netafim fault the Zefunot channel flows through a narrow elongated valley flanked by steep slopes carved into magmatic rocks (Precambrian crystalline basement (Beyth et al., 2012)) (Fig. 5). Isolated relicts of terraces are found along the elongated valley flanks. Deposition and accretion of fluvial terrace deposits occurs at an opening of the valley at the foothill of the surrounding magmatic hills .Flow gradients for these fluvial surfaces are approximately 3^0 in the flow direction and a maximum of 1^0 perpendicular to the flow direction. Further east, the basin changes to braided flow, extending from the foot of the marginal mountains of the Arava to the Evrona playa (the base level of this basin; Fig. 4). The fluvial sediments in the basin are of two origins: the carbonate formations from the western hanging wall of the Netafim fault and the magmatic slopes within the basin to the east.

3.1.2 Mapping results

Four generations of fluvial terraces (fill-cut type terraces) and one playa were mapped (ZQ1-ZQ4 and ZP; Fig. 10). These fluvial terraces consist of variable mixtures of carbonate and magmatic lithologies, grain sizes, and depositional structures.

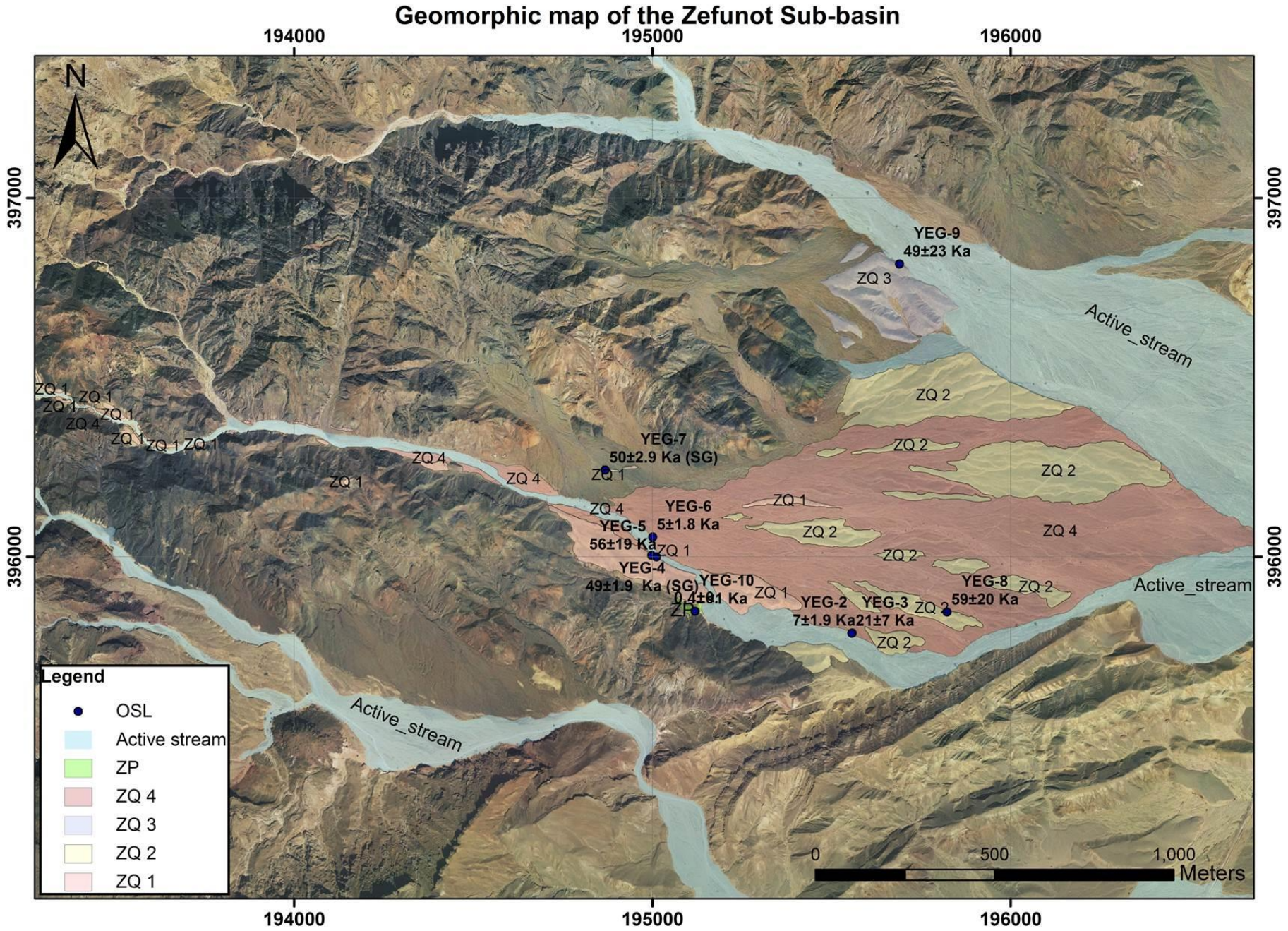

Figure 10. A geomorphic map of the Zefunot basin.

Unit	Total surface Area[%] *	Desert pavement development	Sediment lithology	Sphericity	Rounding	Sorting	Matrix	Grain size [cm]	Gravel shattering	OSL Age [ka]	Comments
ZQ1	3	**Well**	50%-*Carbonate* 50%-*Magmatic*	Carbonate-Moderate Magmatic-Poor	**Poor**	**Poor**	Mud supported, silty, contains gypsum	1-10	**Highly** in top 35 cm	Top surface - 1) 48±2(SG) 2) 50±3(SG) Middle of sequence - 40±10 Bottom of sequence- 58±23	Boulders larger than 40 cm are sparsely scattered all through the deposited sequence
ZQ2	10	**Moderate**	30%-*Carbonate* 70%-*Magmatic*	Carbonate-Moderate Magmatic-Poor	**Poor**	**Poor**	Mud supported, silty, contains gypsum	1-5	**Highly** in top 25 cm	Top surface - 59±20	A soil sequence with a large concentration of gypsum and salt at the depth of approximately 5cm developed upon this unit
ZQ3	<1	**Well**	10%-*Sand* 30%-*Carbonate* 60%-*Magmatic*	Sand-Moderate Carbonate-Moderate Magmatic-Poor	**Poor**	**Poor - Moderate**	Mud supported, silty, Moderate consolidated	1-10	Moderate in top 25 cm	Top surface - 49±23	-
ZQ4	20%	**Poor**	30%-*Carbonate* 70%-*Magmatic*	Carbonate-Moderate Magmatic-Poor	**Poor**	**Moderate**	Mud supported, silty, contains gypsum	1-30	**Poor**	Top surface - 1) 7.1±1.9 2) 5.2±2 Bottom of sequence - 24±9	Immature soil sequence
ZP	<1	**Poor**	*Silt*	-	-	**Well**	-	<1	-	Bottom of sequence - 0.4±0.1 (SG)	-

Table 1. Zefunot basin units: ***Detailed description of the mapping units of the Zefunot basin.*** ***"Total surface area" refers to % area of the total basin area (including: Bedrock, Colluvium and the Active channel). Sediment features refer to the entire sediment sequence.**

Unit ZQ1 is the most elevated terrace in the current drainage basin and covers about 3% of the basin's total surface area. It contains a relatively high fraction (~50%) of carbonate clasts. This unit directly overlies Precambrian magmatic and Cambrian sandstone bedrock. A Well-developed soil sequence occurs at the top of this unit and its surface is fairly smooth (App. B. Table 1 Fig. 11). Small channels incised into this unit disturb the smooth surface (Fig. 12). Luminescence dating (Appendix C) indicate the unit's base was deposited at 58±23 ka and its deposition ceased shortly after 49±1.9 ka (Fig. 10; Table 1).

Figure 11. Unit ZQ1: **A. Characteristic well-developed desert pavement. B. Typical soil profile with shattered clasts and a thick gypsum and salt accumulation horizon at 10 cm depth. (Figure location in Appendix A.)**

Relicts of ZQ1, found north of the active channel, are partially buried by a low angle colluvium of magmatic clasts (Fig. 12). Luminescence dating (Table 1; App. C)

yielded a deposition age of 50±2.9ka for the upper sediments of unit ZQ1's northern relicts thus implying that deposition ceased shortly after that time.

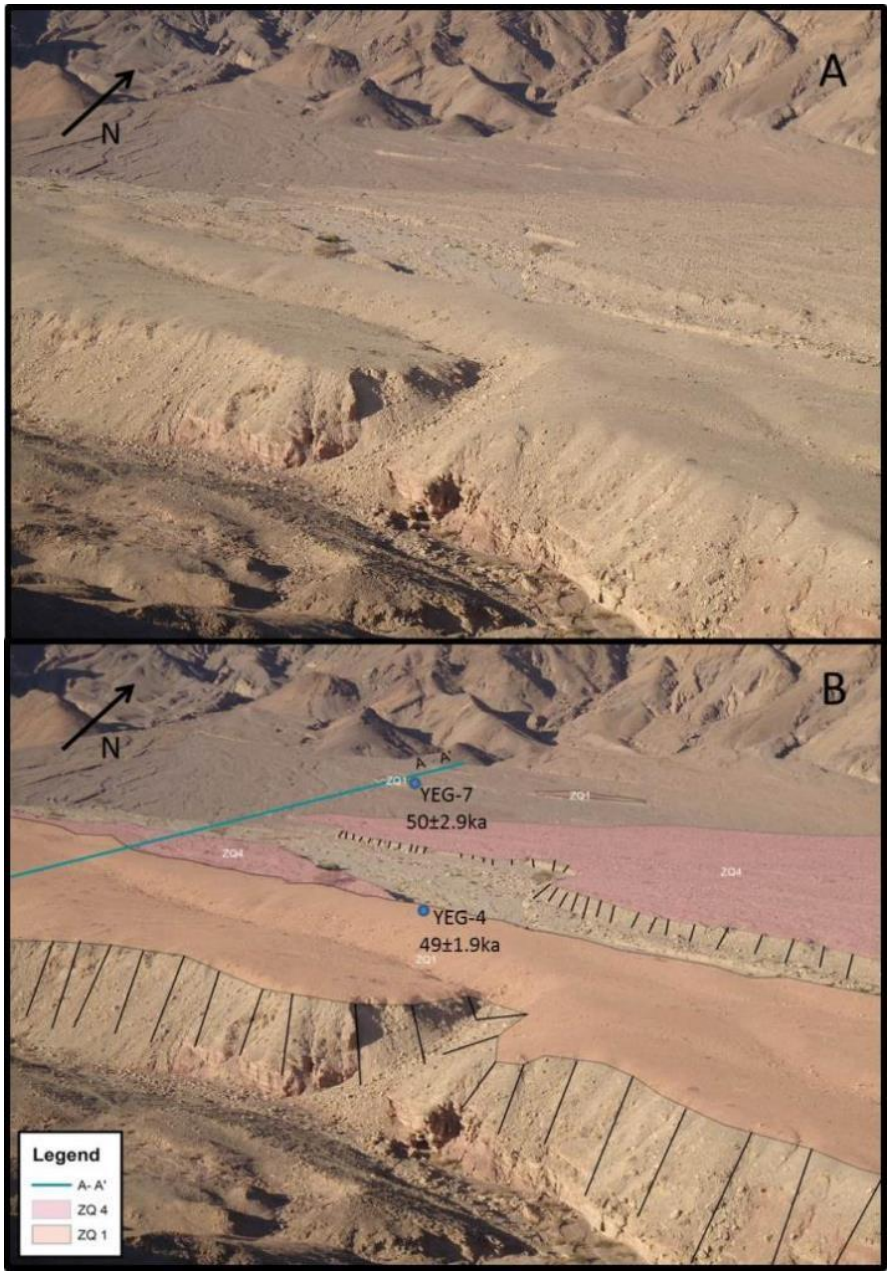

Figure 12. ZQ1 in the Zefunot basin: **A. Northward view across the active channel. B. Same as A with geomorphic interpretation. Unit ZQ1 in the foreground and the northern relicts of ZQ1 north of the active channel and ZQ4. OSL sampling locations are indicated by blue dots. Cross section A-A' in turquoise (see Fig. 19).**

Unit ZQ2 covers about 10% of the basin's total surface area. The unit's surface is typically one to a few meters lower than unit ZQ1. A well-developed soil sequence occurs at the top of ZQ2 and its surface is smooth (App. B. Table 1 Fig. 13). The unit is composed mostly of magmatic clasts characterized by poorly rounded and poorly sorted

clasts (Table 1 App. B). Luminescence dating (Table 1; App. C) yielded a deposition age of 59±20ka for the upper sediments of unit ZQ2 (Fig. 10).

Figure 13. Unit ZQ2: **Well-developed desert pavement and soil of unit ZQ2. B. Local occurrences of gypsum accumulation are found within unit ZQ2. (Location of figure appears in Appendix A.)**

Unit ZQ3 The unit directly overlays Cambrian sandstones. A moderately developed soil sequence is developed at the top of this unit and its surface has a fairly smooth desert pavement (App. B. Table 1). Small channels deeply incise into this unit exposing in places the underlying bedrock. Luminescence dating (Table 1; App. C) yielded a deposition age of 49±23ka for the upper sediments of unit ZQ3 (Fig. 10). Sediment source is from the adjacent basin to the north (the main Zefunot basin) (Fig. 5), as indicated by the distinct lithologic assemblage containing sandstones (the Cambrian Yam-Suf formation (Beyth et al., 2012); Table. 1; Figs. 5, 10 and 14). Discontinuity observed in the unit's cross-beddings in one location could imply post-deposition faulting (Fig. 14; see further discussion, chapter 4.1.4).

Figure 14. Discontinuity in unit ZQ3: **Discontinuity in ZQ3 sedimentary beddings (coordinates: 195684/396819 ITM). Bedding structures on the right side of the figure are abruptly truncated as they reach the area marked with the dashed line. (Location of figure appears in Appendix A.)**

Unit ZQ4 covers about 20% of the basin's total surface area. This terrace was truncated by the active channel (Fig. 10). A poorly developed soil sequence occurs at the top of this unit and its surface preserves original bar and swale morphology (Fig. 15; Table 1l; App. B.). The unit's bottom horizons yielded an OSL age of 24±9ka and the top horizons yielded OSL ages of 5±1.8 ka and 7±1.9 ka (Table.1), thus indicating late Pleistocene to mid Holocene deposition of this unit.

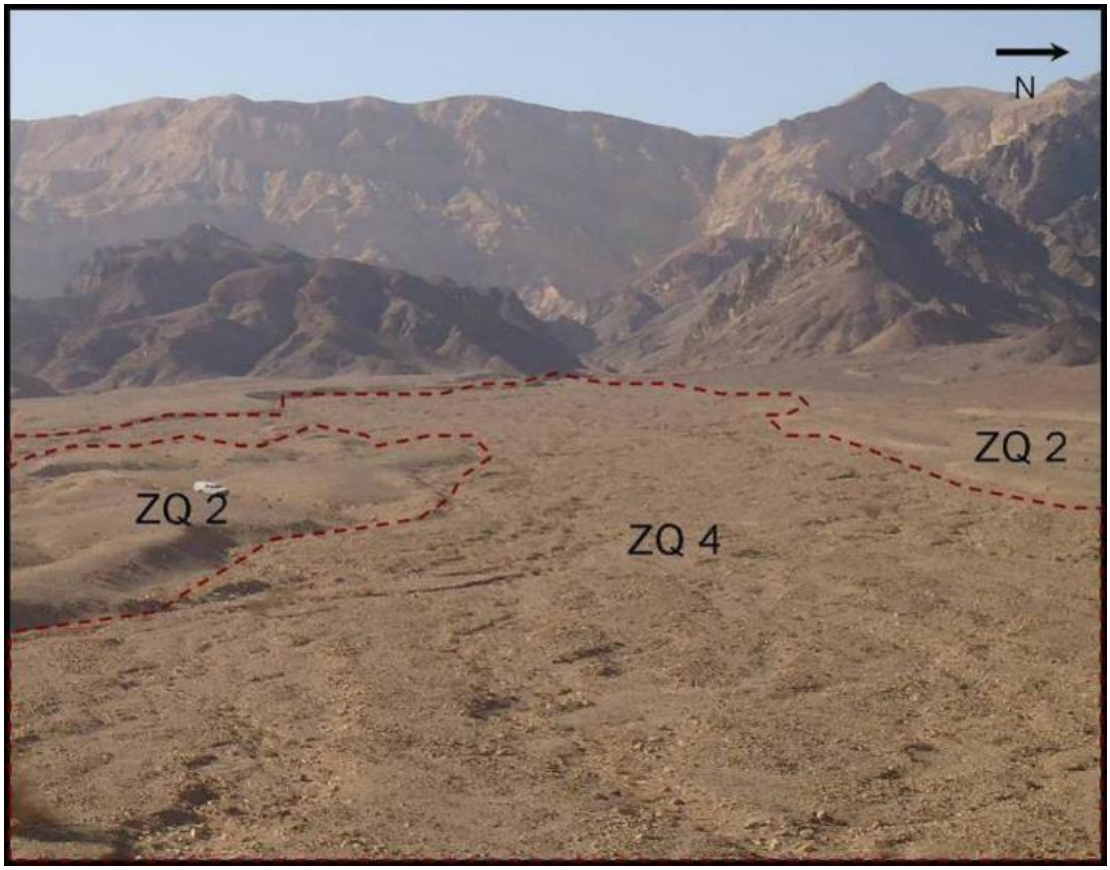

Figure 15. Unit ZQ4 in the Zefunot basin: **Red dashed line outlines the limits of ZQ4 in this image. (Location of figure appears in Appendix A.)**

Unit ZP covers less than 1% of the basin's total surface area. This fine-grained playa deposit is located at the intersection between the Zefunot sub-basin's active channel and a small, easterly flowing tributary located to the south of the active channel. Coarse sediment from the main channel impeded the flow of the smaller tributary, resulting in the accumulation of fine-grained silt deposits (Fig.16). The unit's bottom horizons yielded an OSL age of 0.4±0.1ka (Fig. 10; Table 1).

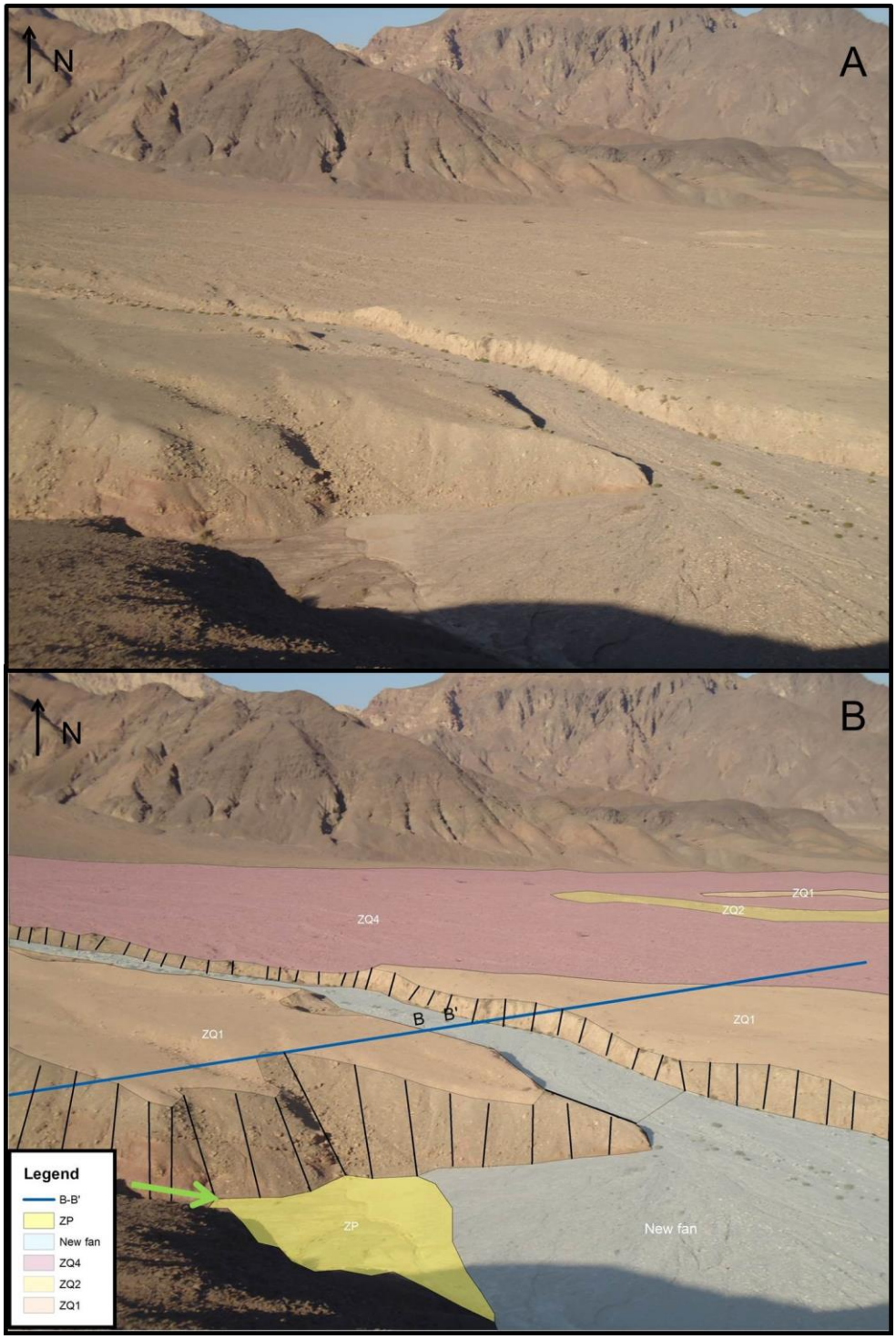

Figure 16. Accretion of fan and playa in Zefunot sub-basin: **A. Northward view across the active channel. B. Same as A with geomorphic interpretation. A fan formed as the channel incised southwards through ZQ1 and partially dammed a small east-flowing tributary (marked with a green arrow). As a result a small playa (ZP) formed. Cross section B-B' was measured along the Blue line (see Fig. 17 and 18).**

3.1.2.1 Topographic cross sections

Eight topographic profiles were measured in the field (Fig. 17).

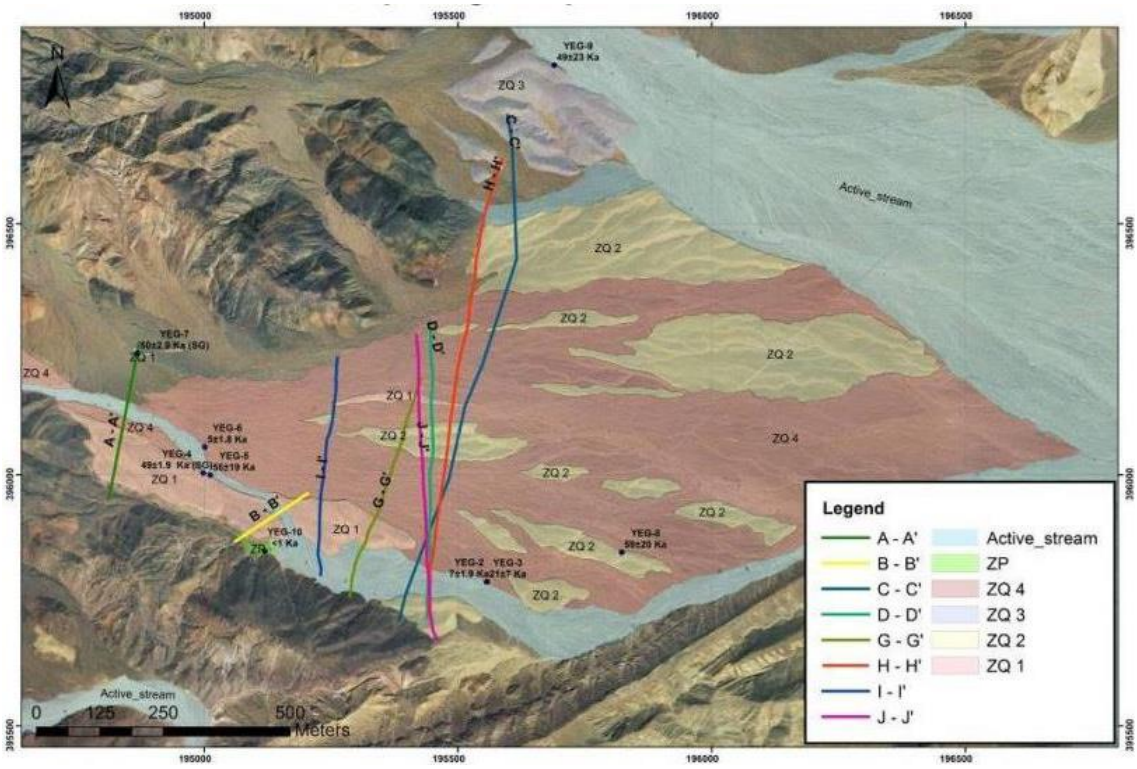

Figure 17. Cross section location map: **Locations of the eight topographic cross sections measured in the Zefunot basin.**

The highest morphostratigraphic surface in the basin is the main relict terrace of unit ZQ1. Topographic cross-sections I-I' & G-G' (Fig. 18) display the elevation of ZQ1 above units ZQ2 and ZQ4 at mid-fan. Cross-sections A-A' & B-B' display the relative elevation of ZQ1 above ZQ4 at the apex of the fan. Conflicting data as to the morphostratigraphic relation between an elongated relict of unit ZQ1 located in the center of the fan and the adjacent relicts of unit ZQ2 was obtained from cross-sections I, G and C. Part of these measurements show that the elongated relict of unit ZQ1 is higher than those of unit ZQ2 (e.g. cross-sections G Fig. 18) while other show the opposite (e.g. cross-sections I Fig. 18). Cross-section A, perpendicular to the general flow direction of the basin, measures the reciprocity between the main relicts of unit ZQ1 and its relicts to the north of the active channel (see definition, 4.1.2 Fig. 12). The northern relicts are currently located 4.75 m higher than the highest point on the southern terraces, at a distance of 158 m, forming a southwards gradient of 1.72 degrees.

Figure 18. Zefunot measured topographic cross sections: **The locations of the cross sections are drawn on the map in Fig. 17. (Two of the measured cross sections are not shone as they reveal the same trend as the other cross sections)**

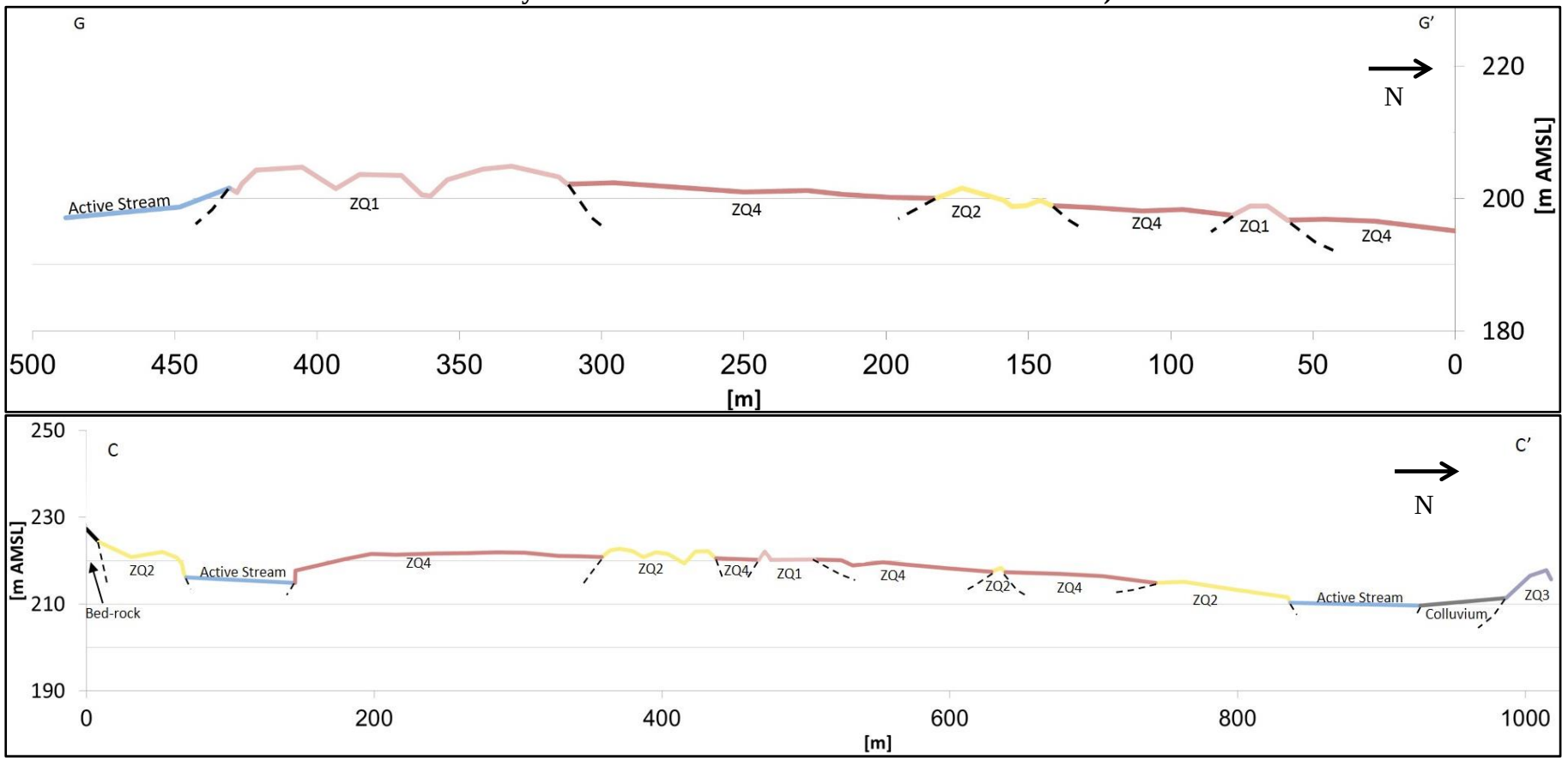

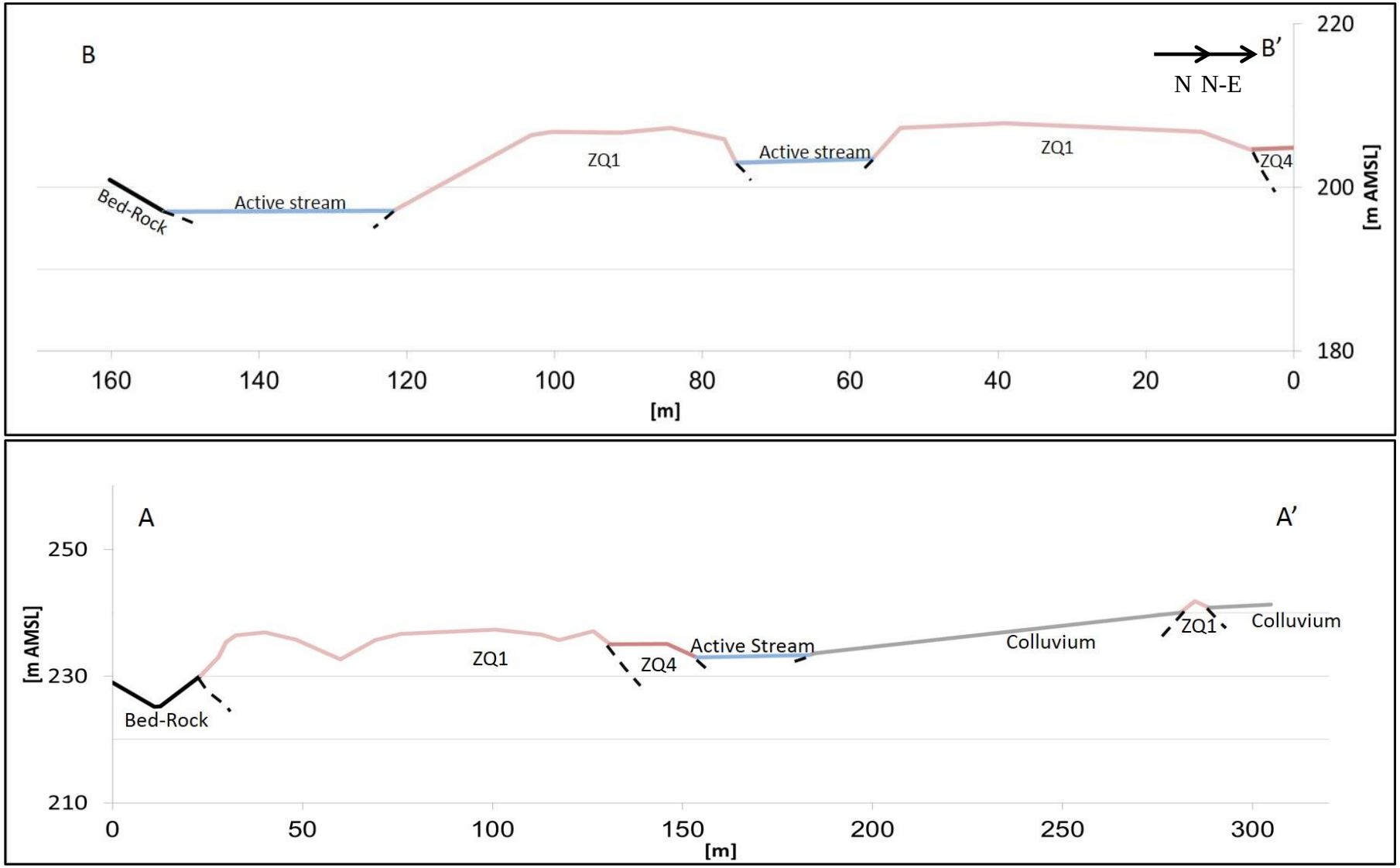
B
B'
N N-E
220
200
180
[m AMSL]
Bed-Rock
Active stream
ZQ1
Active stream
ZQ1
ZQ4
160
140
120
100
80
60
40
20
0
[m]
A
A'
250
230
210
[m AMSL]
Bed-Rock
ZQ1
ZQ4
Active Stream
Colluvium
ZQ1
Colluvium
0
50
100
150
200
250
300
[m]

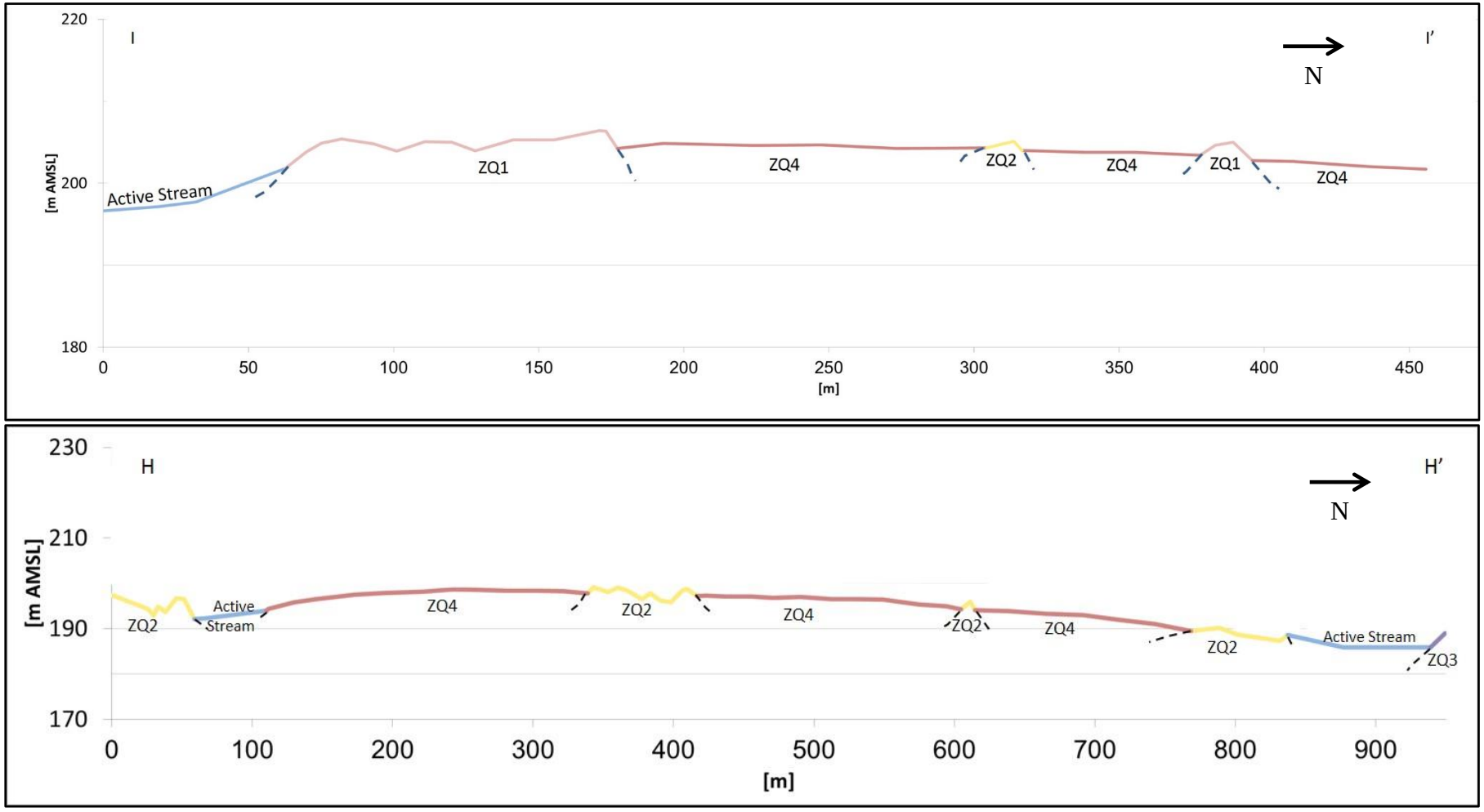
I
I'
N
220
200
180
[m AMSL]
Active Stream
ZQ1
ZQ4
ZQ2
ZQ4
ZQ1
ZQ4
0
50
100
150
200
250
300
350
400
450
[m]
H
H'
N
230
210
190
170
[m AMSL]
ZQ2
Active Stream
ZQ4
ZQ2
ZQ4
ZQ2
ZQ4
ZQ2
Active Stream
ZQ3
0
100
200
300
400
500
600
700
800
900
[m]

The elevation of Unit ZQ3 is relatively lower than unit ZQ1 and ZQ2 (as indicated by cross-section C (Fig. 18). All measurements indicate that unit ZQ4 is lower than all its predecessors (e.g. cross-sections I, C and H Fig. 18).

The flow direction during deposition of the various terraces is indicated by the preserved gradient direction of the fluvial fan. Cross-sections (e.g. H and G) show a decrease in height of all the units and a general surface inclination from south to north (Fig. 18) (the surface inclination from north to south shown in cross section A is in the opposite direction due to possible tectonic surface tilting). Thus the flow gradient reconstruction based on these measurements indicates flow to the east direction, in comparison to the current south-east direction.

3.1.3. OSL dating

In the Zefunot basin, ten sediment samples were collected for OSL dating (YEG-1-10, see locations in Fig. 10). Samples YEG-2 (ZQ4), YEG-4 (ZQ1), YEG-6 (ZQ4), YEG-8 (ZQ2) and YEG-9 (ZQ3) were collected from directly under the salic-gypsic accumulation horizons at the base of the soil sequence overlying the fluvial terraces. Samples YEG-3 (ZQ4) and YEG-5 (ZQ1) were collected from the lowest exposed sediment horizons of the terrace. Sample YEG-1 was collected from the middle of ZQ1's sedimentary sequence (~2.5 m below the surface). Sample YEG-7 was collected from under the buried soil sequence of unit ZQ1 relicts; though the terrace is currently covered by overlying colluviums deposits (Fig. 19). Sample YEG-10 was collected from the contact layer between the bottom of the silt sediments and the underlying gravelly sediments in mapping unit ZP.

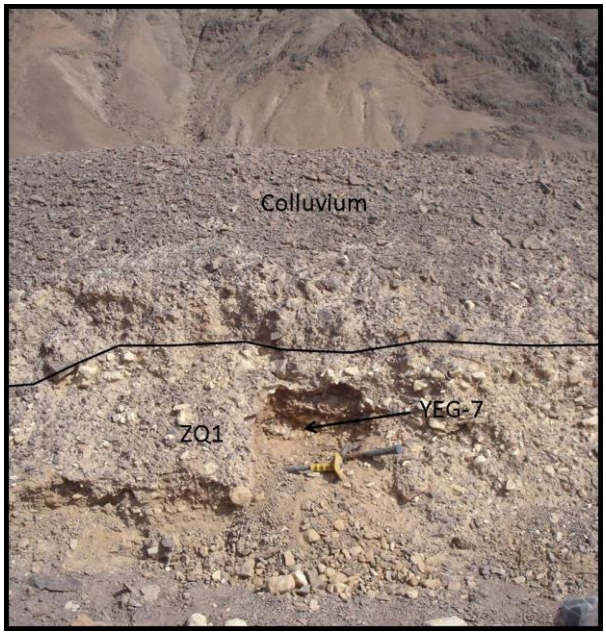

Figure 19. Sampling location for YEG-7 within the northern relicts of ZQ1: **The sample was collected from the notch marked by the black arrow. ZQ1 is covered by colluvium. (Location of figure appears in Appendix A.)**

Single grain measurements were performed on samples YEG-4 and YEG-7 to accurately validate deposition timing correlation of the main ZQ1 terrace and the northern relicts. The De values used to calculate the FMM age of sample YEG- 4 were obtained from the first component that represents the value of 10% and up of the grains (Table 2). The De value used to calculate the age of sample YEG-7 (Table 2) was obtained from the second component, representing over 10% of the grains, for two reasons: (a) during the sampling process, grains from the overlying magmatic colluviums were suspected to have dropped into the sample and contaminated it with grains that have lower De values, (b) the first component provided De values that were much younger than expected taking into account the unit's morphostratigraphic relations and the maturation degree of its surface and soil. Using the average De value method for calculating sample YEG- 10 age yielded poor results, therefore single grain measurements were performed and the sample's age was obtained using the minimum age model.

YEG-4				
Component	1	2	3	
Dose [s]	1099±204	3610±140	5850±215	
% of component	2.7	52	44	
YEG-7				
Component	1	2	3	4
Dose [s]	620±99	2524±204	4201±244	5990±220
% of component	2.6	17.4	40.8	39.2

Table 2. Zefunot SG FMM: **Results of the FMM for the Zefunot, SG samples. The component chosen for calculating the age is marked in blue.**

3.1.4 Zefunot sub-basin Discussion

3.1.4.1 Geomorphic outcomes

The existence of an older drainage system is evident from fluvial relicts found on hilltops and bedrock slopes throughout the research area (Fig. 20). These relicts do not relate to the current basin configurations. Obviously, it is impossible to correlate between relicts of this ancient drainage system although they could be relicts of a single older drainage system.

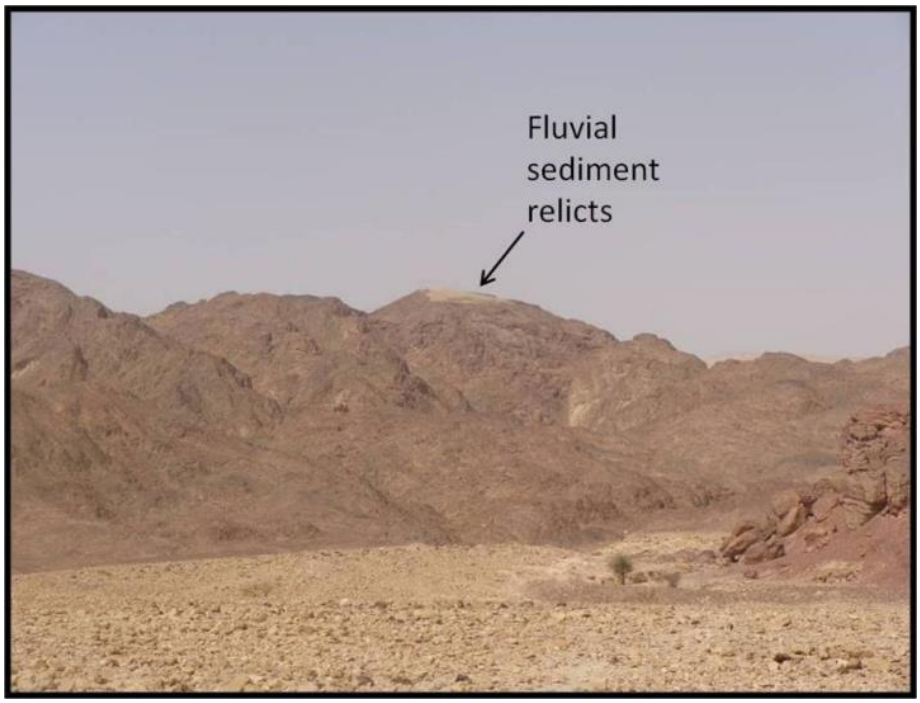

Figure 20. Fluvial sediments on hilltops: **Relicts of fluvial sediments found on hill tops high above the active channels and do not relate to the current basin configurations. (Location of figure appears in Appendix A.)**

Field relations, surface maturity, soil development stage and the OSL ages of units ZQ1 and ZQ2 suggest these two units represent an aggradation period between 58±23ka and 48±2ka with possibly a short degradation event that separates them. The lithological composition of unit ZQ1 (i.e., large percent of large carbonate pebbles – Table1; App. B) suggests significant sourcing from the carbonate bedrock outcrops west of the Netafim fault. ZQ2 lithology (i.e., large percent of small angular magmatic clasts – Table 1; App. B) suggests more contribution from the magmatic bedrock slopes flanking the channel compared to ZQ1.

Its location within the Zefunot sub-basins catchment area suggests that during its deposition, unit ZQ3 was linked to the catchment area of the Zefunot sub-basin though its sediment source was from the main Zefunot basin. Thus, it is of significance to the Zefunot sub-basin due to its southward sedimentation direction and the diversion of the main Zefunot basin's flow direction southwards.

Fluvial sediments found on present day topographic saddles along the ridge dividing the Zefunot sub-basin and the Amram basin, imply physical connection between these basins at some time. During the deposition of these mapped units the channel bed's level was higher than these topographic saddles located between the basins (Fig. 21). This suggests that when the sediments passed the height of the saddles, an instantaneous enlargement of the Zefunot basin occurred, connecting to the Amram basin.

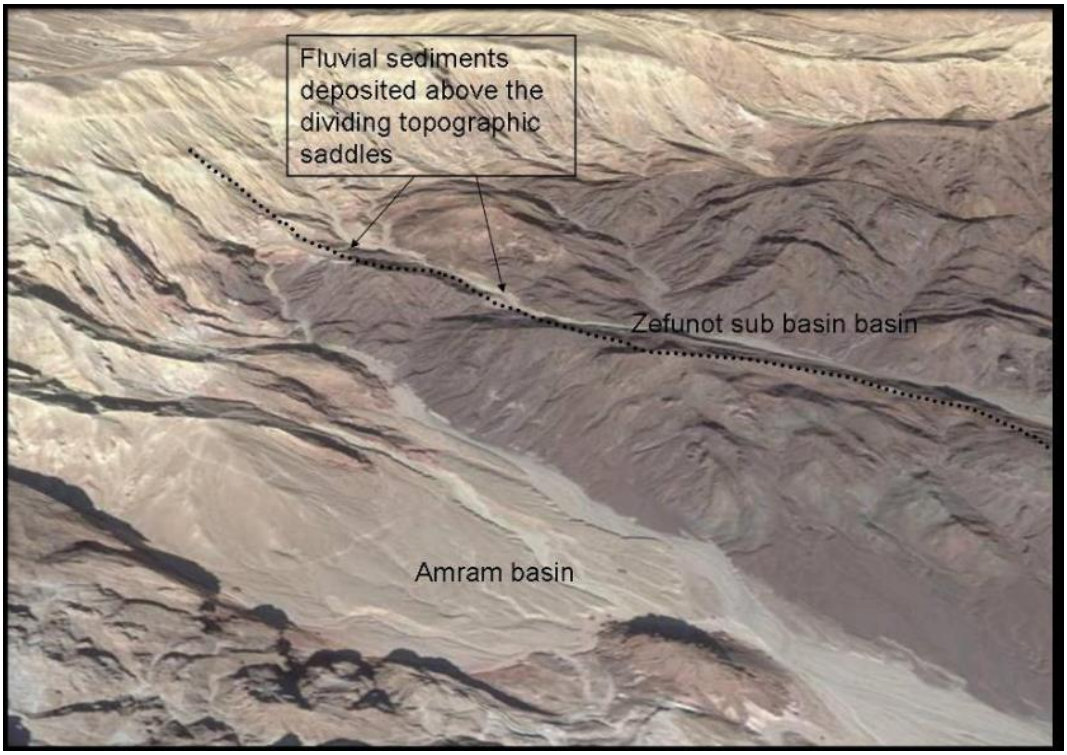

Figure 21. Perspective image of Amram/Zefunot basins: **Google Earth image of the dividing ridge crest between the Zefunot and Amram basins. Present topographic divide is marked with dashed line.**

The aggradation period in which units ZQ1 and ZQ2 were deposited was followed by a degradation period. This degradation activity removed a large volume of the ZQ1and ZQ2 terraces forming a wide channel system with relicts of the former terraces left as isolated highs. Shortly before 24±9ka aggradation resumed and unit ZQ4 was deposited in the eroded void between the relicts of ZQ1 and ZQ2. Units ZQ1, ZQ2 and ZQ4 mark a general flow direction to the east. Incision of a single channel (the present active channel) initiated after the aggradation period ended. As opposed to the flow patterns of the previous aggradation and degradation periods in which flow activity occurred throughout the whole width of the basin's fan and with a general average flow direction to the east, this incision is confined to a restricted channel with a preferred southward flow direction. This channel cut across the elevated terrace (unit ZQ1) between 7±1.9ka and 5±2ka, as indicated by the OSL ages of unit ZQ4's surface, obtained from two locations along the channel channel, the first southeast to the elevated terrace and the second to its northwest. As this newly formed channel passes the elevated terrace, the widening of the channel bed caused the formation of a small fluvial fan. The formation of the fan blocked off a small tributary located to the south of the main channel and as result a small playa formed at the contact point between the fan

and the end of the tributary. The age of the beginning of accumulation of silty sediments in the playa, obtained from a sample collected from the contact layer between the bottom of the silty sequence and the underlying gravel was found to be 0.4±0.1ka (this is a minimum age for the playa since its deeper sediments are not exposed).

3.1.4.2 Tectonic outcomes

The low elongation ratio of 0.45 of the Zefunot basin suggest that the height of the basin's base level relative to the basin's head waters were constantly evolving over time, resulting in the immature basin's geometry.

The three geomorphic observations described above appear consistent with a recent southward tilt of the Zefunut basin, possibly through tectonic deformation.

(a) Holocene change of flow direction - The abandonment of the former eastward flow direction indicated by incision through an elevated relict of ZQ1 in a south-southeast direction (Fig. 16) is consistent with a southward tilt of the basin.

(b) Southward flow direction bend of the main Zefunot basin – The abrupt truncation feature in unit SQ3's sedimentary sequence (Fig. 14) is located along the projected direction of an inactive fault scarp mapped by Garfunkel (1970) and Byeth et al. (2012) (Fig. 5). However, as no additional evidence for faulting was found on the surface of unit SQ3 or along the projected direction of the purported fault plane the mapped disturbance cannot be classified as a fault. An alternative mechanism for the formation of this disturbance is the existence of a former cannel incised perpendicular to the units flow direction that was later filled by debris. The southward linkage of the main Zefunot basin to the Zefunot sub-basin doesn't necessarily oblige solely a tectonic forcing in the form of surface tilt, but the presence of the southward bend of the flow direction at an additional location and timing (Unit ZQ3 was dated to 49±23ka) reinforces the other tectonic evidence in the basin.

(c) Elevation of ZQ1 relicts - The higher elevation of the northern relicts of unit ZQ1 relative to the southern relicts of ZQ1 (Fig. 18), suggests basin-scale tilting after the deposition of ZQ1. Flow gradients for the fluvial units of the Zefunot basin show a calculated approximate 3^0 gradient parallel to the flow

direction and a maximum approximate 1^0 deposition gradient perpendicular to the flow direction. The height difference between the northern and southern relicts of ZQ1 cannot be explained as a natural deposition gradient of the fan, since its gradient (1.7^0) is perpendicular to the deposition direction (Fig. 18). Subtracting the maximum perpendicular natural gradient of the fan from the measured height difference between the relicts (4.75 m) leaves a residual ~2 meters tectonic uplift of the northern relict after the deposition of ZQ1. The surfaces of these relicts were abandoned shortly after ~50 ka, placing the tectonic surface tilt in that time span.

3.2 The Amram basin

3.2.1 General

The Amram basin drains a total surface area of 4km^2. The basin's headwater crosses the Netafim fault (Fig. 22) where small tributaries drain the area close to the fault and coalesce into the main channel as the basin bed widens. This widening causes a drop in channel power and deposition of sediments. The basin narrows again downstream as it cuts through the Amir syncline (Fig. 22) and then once east past the Amir syncline the channel bed widens and forms a braided fan that drains further eastwards into the Evrona playa (Fig. 4). A strike-slip fault crosses the basin from north-east to south-west and approaches the Netafim fault (Figs.4 and 22). Along this fault, marks of both left and right lateral displacement were found (Beyth et al., 2012). A topographic saddle formed where the fault crosses over into the basin from the north-east.

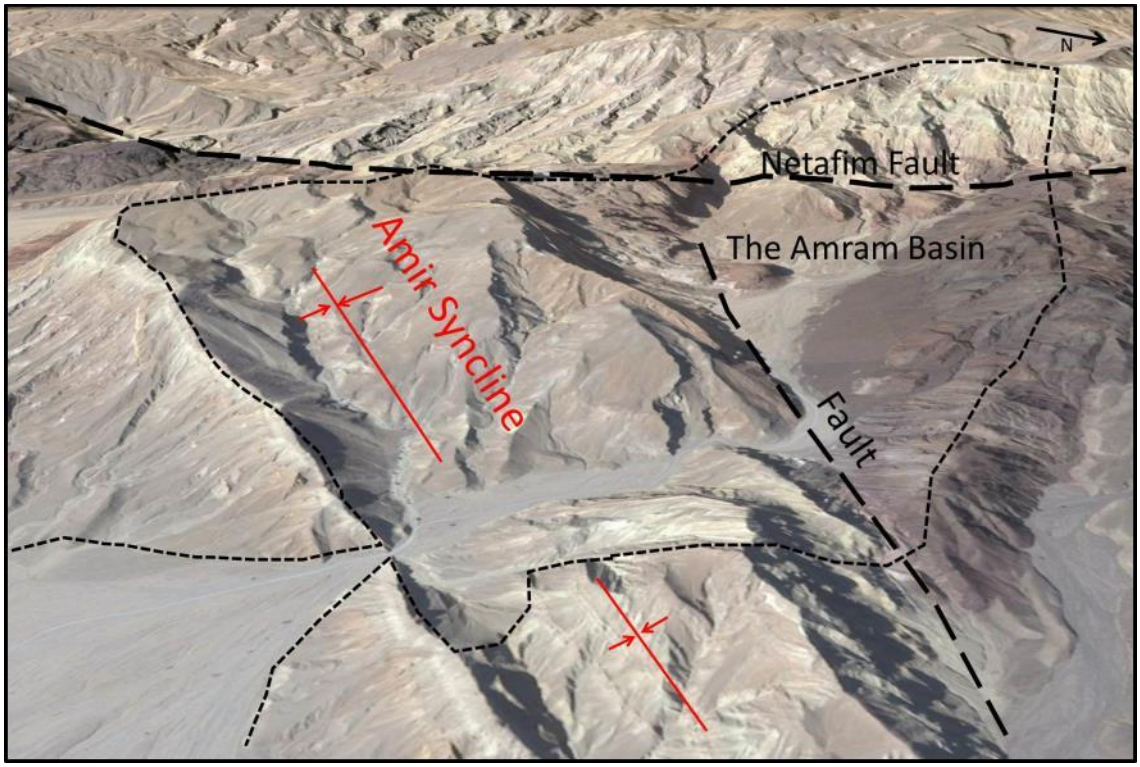

Figure 22. Perspective view of the Amram basin: **Google Earth perspective view of the Amram basin. Red lines mark the axis of the Amir Syncline. The Amram basin is marked with a thin dashed line. (Modified from https://maps.google.com).**

Bedrock lithology within the Amram basin area consists of magmatic rocks, carbonates and sandstones (Figs. 5 and 22). Fluvial sediments have two primary sources: (a) Phanerzoic carbonate and sandstone formations from the western hanging wall of the Netafim fault and the southern slopes along the basin, and (b) magmatic clasts from the northern slopes. As a result of the high erodibility of sandstone and marl units within the Phanerozoic sequence, together with the physical weathering caused by the Netafim fault, most of the fluvial sediment is of the carbonate and sand stone source. Massive rock falls and landslides transfer sediments from the fault area into the basin (Beyth et al., 2012). As a result, the sediments sourced from such high-energy events display larger grain size distributions than sediments supplied through 'regular' lower-energy colluvial processes (as indicated by comparison of grain size distributions of the different lithologies found in the basin's fluvial terraces (Table. 3, App. B.)).

3.2.2 Mapping results

Detailed geomorphic mapping of the fluvial units in the upper part of the Amram basin (upstream of the Amir syncline) revealed five fill/cut-fill terrace units (AQ1-AQ5 in fig. 23).

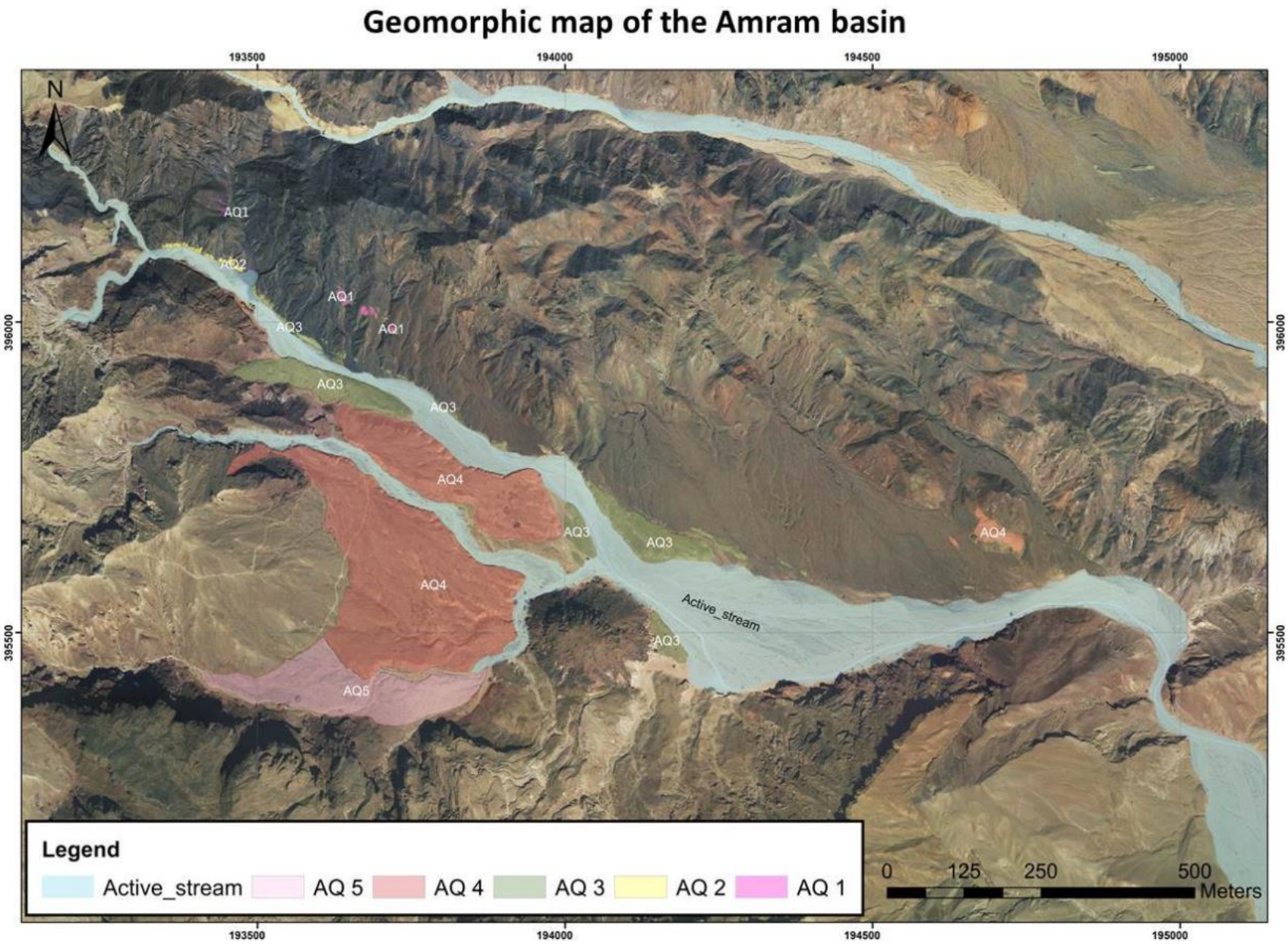

Figure 23.Geomorphic map of the Amram basin.

Unit	Total surface Area[%] *	Desert pavement development	Sediment lithology	Sphericity	Rounding	Sorting	Matrix	Grain size [cm]	Gravel shattering	Comments
AQ1	<1	-	85%-*Carbonate* 15%-*Magmatic*	Carbonate-Moderate Magmatic-Poor	**Poor - Moderate**	**Moderate**	Mud supported, silty, contains gypsum	1-10	-	Top of unit not exposed
AQ2	<2	**Moderate**	90%-*Carbonate* 10%-*Magmatic*	Carbonate-Poor - Moderate Magmatic-Poor	**Poor**	**Well**	Mud supported, silty, well to Moderate consolidated	5-20	Moderate in top 25 cm	there are scattered boulders of varies sizes up to 150cm
AQ3	5	**Moderate**	40%-*Carbonate* 60%-*Magmatic*	Carbonate-Moderate Magmatic-Poor	**Poor**	**Well**	grain sported	1-5	**Poor**	A 40cm thick horizon containing gypsum and salt developed at a depth of 120cm from the top of the unit
AQ4	5	**Poor**	20%-*Sand* 80%-*Carbonate* <1%-C*hert*	**Moderate**	**Moderate**	**Poor - Moderate**	Mud supported, silty, Moderate consolidated	1-10	**Poor**	Scattered boulders that range in size between 30 and 100cm within the sequence
AQ5	2	**Poor**	70%-*Carbonate* 30%-*Sand*	**Moderate**	**Moderate**	**Poor - Moderate**	Mud supported, silty, Moderate consolidated	2-10	**Poor**	The surface of the unit is very rough.

*T*able 3. Amram basin units**: Detailed *description of the mapping units of the Amram basin. .* *"Total surface area" refers to % area of the total basin area (including: Bedrock, Colluvium and the Active channel). Sediment features refer to the entire sediment sequence.**

Unit AQ1 consists of the most elevated terrace relicts in the basin. These relicts are located along the northern, magmatic slopes of the basin. The predominately carbonate lithology in these relicts distinguishes them from their surrounding magmatic colluvium (Fig. 24). Some of these relicts are found in a tributary descending from a topographic saddle situated on the ridge crest between the Zefunot sub-basin and the Amram basin (Figs. 21). The relicts of this unit were covered by colluvium deposits and then re-exposed by weathering of the colluvium cover together with the unit's upper horizons.

Figure 24. Unit AQ1: **Fluvial sediments of unit AQ1 located within a tributary between the Zefunot and Amram basin. (Location of figure appears in Appendix A.)**

Unit AQ2 covers less than 2% of the basin's total surface area and is stratigraphically below AQ3. The base of the unit is deposited on Pre-Cambrian magmatic bedrock. A soil sequence developed on top of this unit and its surface is moderately smoothed (App. B. Table 3). The sediments are coarse and exhibit relatively low maturation features (Fig. 25). The majority of the sediments are carbonate.

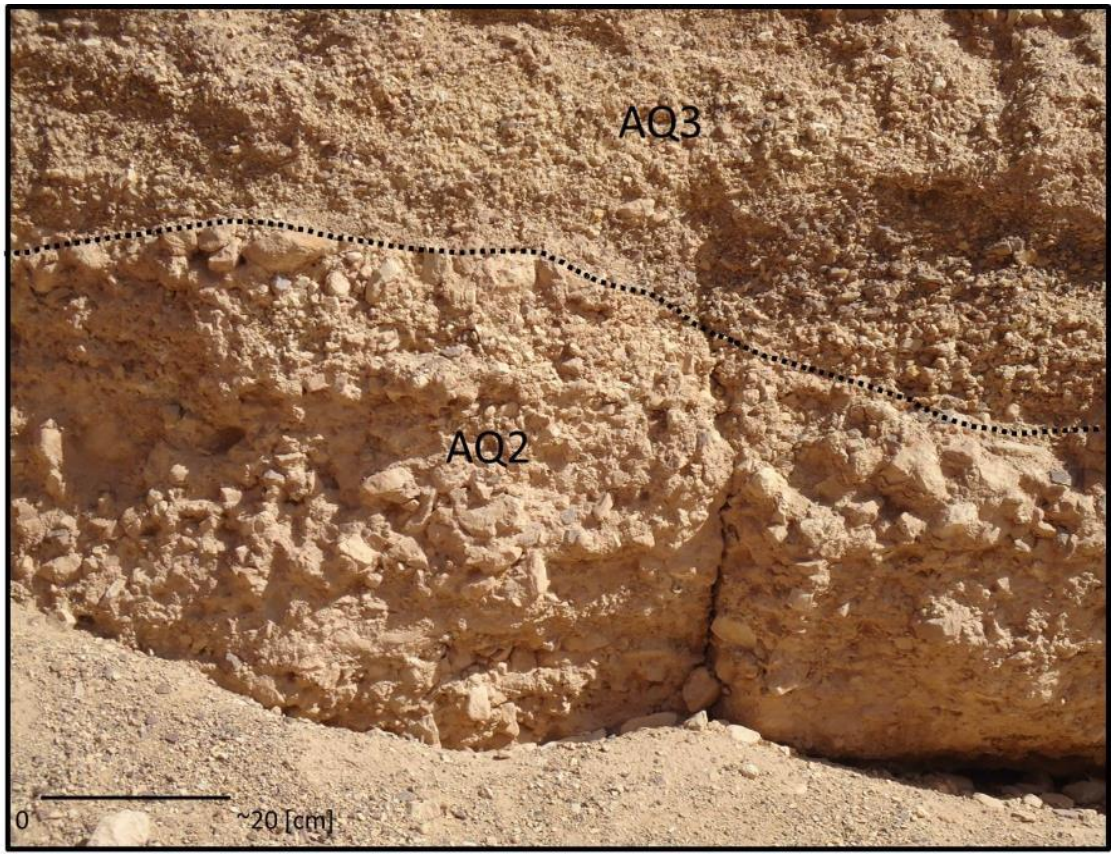

Figure 25. Unit AQ2: **Sediments of unit AQ2 and the overlying sediments of unit AQ3. (Location of figure appears in Appendix A.)**

Unit AQ3 covers approximately 5% of the basin's total surface. In places, it overlies unit AQ2. A moderately developed soil sequence caps the top of this unit and its surface is moderately smoothed (App. B; Table 3). A 40cm thick horizon containing gypsum and salt developed at a depth of 120cm from the top of the unit (Fig. 26). In places the unit consists of up to 60% angular magmatic clasts.

Figure 26 Unit AQ3: **Sediments of unit AQ3 and overlying recent colluvium derived from magmatic sources. Note the gypsum-cemented horizon within the unit (backpack for scale). (Location of figure appears in Appendix A.)**

Unit AQ4 covers about 5% of the total surface area**.** The base of the unit is deposited in places on Cambrian sandstones and in places on unit AQ3. A poorly developed soil sequence developed at the top of this unit and its surface is fairly rough (App. B; Table 3). The unit consists of carbonate clasts only.

Unit AQ5 is a cut-fill terrace and covers about 2% of the total surface area. This unit was deposited after the channel incised into unit AQ4. The unit's surface height is lower than unit AQ4's surface by a few meters. The surface of the unit is very rough and is not leveled. 4.2.2.1 Topographic cross section

A topographic cross-section was measured perpendicular to flow direction (cross-section A-A', Fig. 27 and 28). This cross section demonstrates the elevation of unit AQ1's base relative to the elevation of units AQ3, AQ4 and the current base level thus indicating that it was deposited during a higher stand of the base level.

.

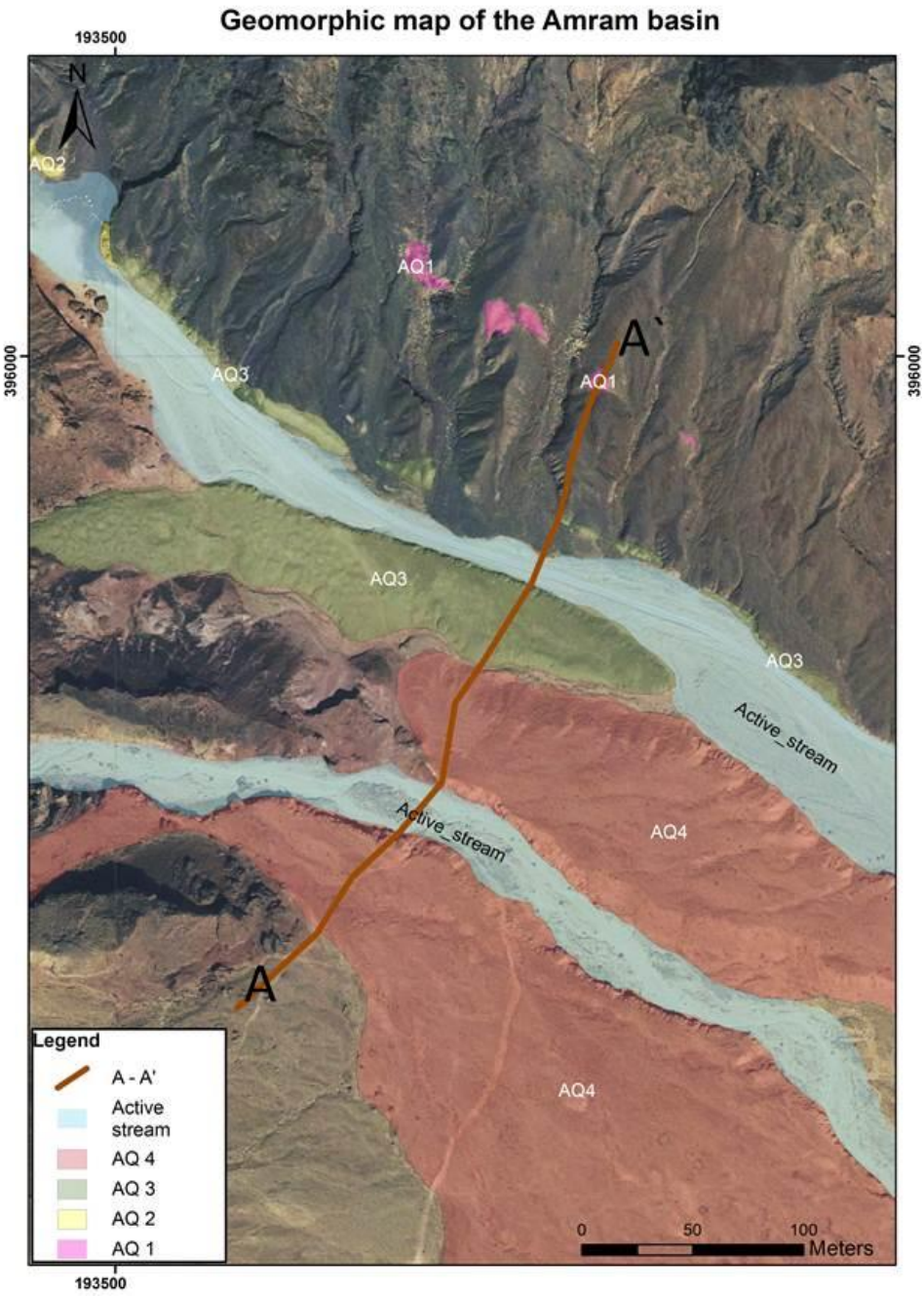

Figure 27. Cross section location map for the Amram basin.

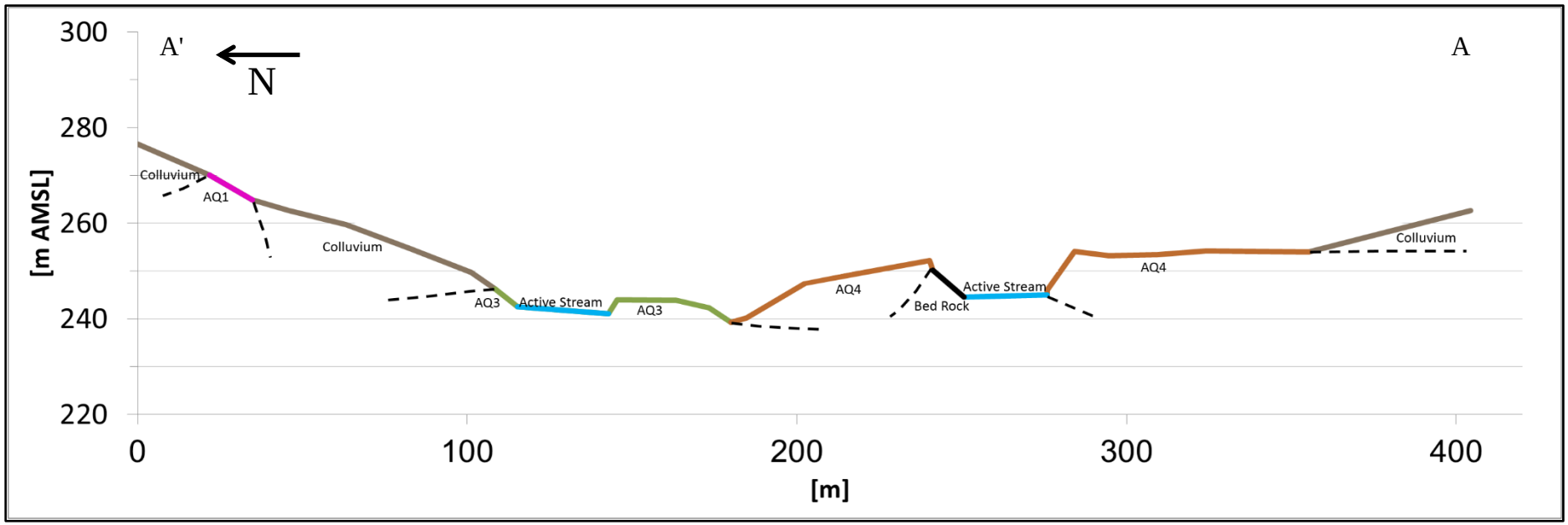

Figure 28. Amram measured topographic cross section: **The location of the cross section is drawn on the map in figure 29.**

3.1.4 Amram basin Discussion

3.1.4.1 Geomorphic outcomes

Unit AQ1 is the highest preserved fluvial sediment found in the basin. After the deposition of this unit ceased, incision activity formed a wide channel. Units AQ2, AQ3 and AQ4 are fill terraces deposited in this wide channel. AQ2 and AQ4 differ in their lithological composition (AQ2 and AQ4 are mostly of carbonate composition while AQ3 is mostly of magmatic composition). It is possible that this difference in lithologic composition is due to temporal fluctuations in sediment supply from the carbonate outcrops upstream of the Netafim fault.

Aggradation ceased after the deposition of unit AQ4, and the channel has been continually incising into the fluvial sediments as well as the underling bedrock. This incision was interrupted by a short period of surface stability evident in the formation of the mapped surface AQ5, located in the southern tributary of the basin.

Fluvial sediments of carbonate lithology found on the magmatic slopes above the topographic saddles between the Amram and Zefunot sub-basin can be explained in two ways: a) these basins were linked in the past through these saddles causing one basin to flow into the other and b) these sediments are relicts of a thick sedimentary cover that overlay both basins and the dividing magmatic ridge.

Units ZQ1 and ZQ4 of the Zefunot sub-basin that were mapped above topographic saddles in the western part of the dividing ridge (Fig.10) postulate that the first mechanism applies to this area during the deposition of these units (Fig. 29). Conversely, Sediments found on the saddle located between the Amir syncline and the Amram-Zefunot magmatic ridge lack specific evidence as to the source of the fluvial sediments and therefore can be explained by both mechanisms.

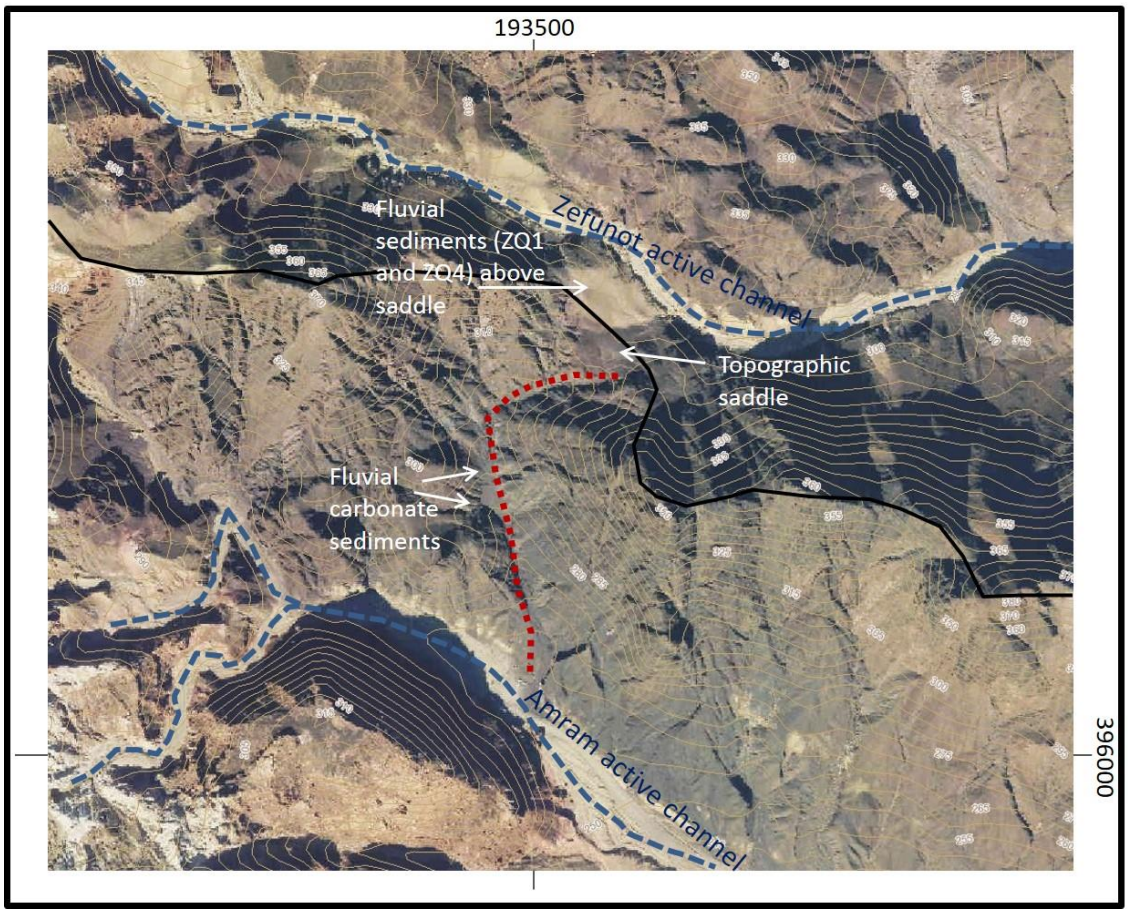

Figure 29. Connection of the Amram and Zefunot basins: **Proposed past connection of the Zefunot sub-basin and the Amram basin through the western saddles upon the dividing magmatic ridge. The current water divide between the basins is marked with a black line. The tributary that previously connected the basins is marked in red. (Modified from: http://www.govmap.gov.il/)**

3.1.4.2 Tectonic outcomes

The elongation ratio of the Amram basin (~0.62) is higher than that of the adjacent Zefunot basin (~0.45), but still low enough to indicate that changes in base level elevation are still occurring. The relatively mature elongation ratio of Amram basin relative to the Zefunot basin may partly be explained by the differences in bedrock of these two basins. While most of the Zefunot basin's flanking slopes consist of slower eroding magmatic rocks, the Amram basin's southern flank consists of fast eroding sandstone. Nevertheless, this lithology difference cannot entirely explain the large difference between the basins elongation ratios (30% larger) thus postulating that a tectonic component seems responsible for this difference.

The southward bend of the Amram channel through the Amir syncline uplifted flanks is a unique flow path in the generally eastward dipping drainage pattern of this

region. Furthermore, the crossing of the syncline's elevated flanks is an unusual phenomenon that requires an explanation. Two scenarios can be considered for such a deflection in flow path: (1) the southward bend of the Amram channel existed before the formation of the late Miocene syncline and the channel continued incising at a faster rate than the uplift of the syncline flanks, (2) during a period of high elevation of the basins channel bed, tectonic deformations shifted the channel southwards, thus forcing it to incise and cross the syncline. No direct evidence was found to support either of the proposed scenarios, yet the southward tectonic surface tilt described in the adjacent Zefunot sub–basin implies such a configuration of tectonic deformation is possible in this area thus suggesting a preference to the second mechanism.

3.3 The Amir-Shehoret basin

3.3.1 General

The Amir-Shehoret basin drains a total area of 4 km^2 and has an elongation ratio of ~0.57. The basin extends westwards beyond the Netafim fault (Figs. 4,7 & 30) and includes a sharp morphologic transition between steep (~25^0) slopes and channels west of the Netafim fault and a low-gradient (~2.5^0), wide channel bed east of the Netafim fault. The Amir-Shehoret basin drains into the Shehoret basin just west of the foothill of the Roded block (Fig. 7) and follows a broad fan towards the Evrona playa (Fig. 4). Carbonate bedrock lithologies characterize the Amir-Shehoret basin west of the Netafim fault and sandstone and magmatic lithologies crop out east of it.

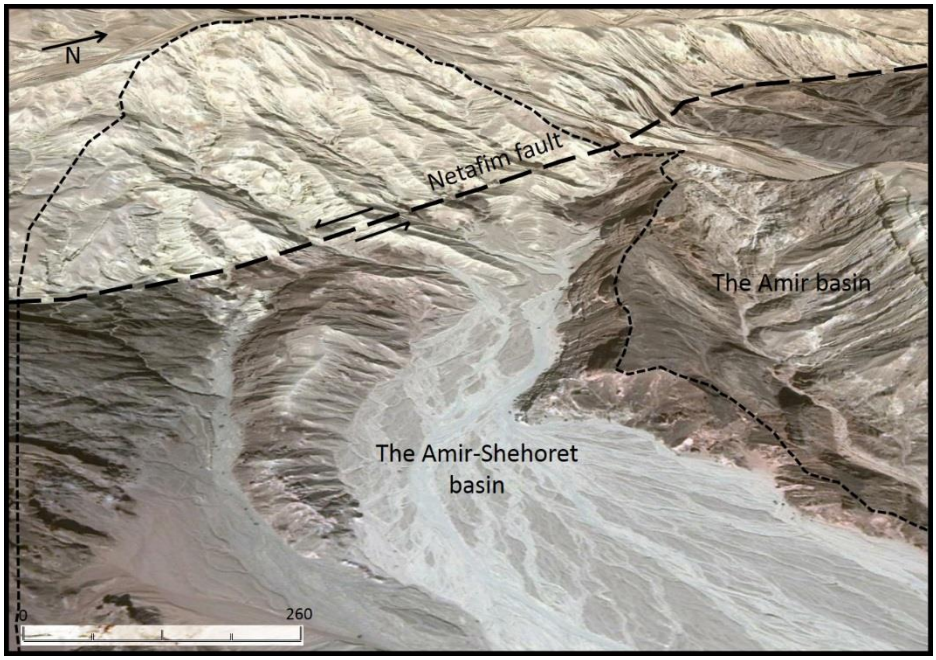

Figure 30. Prospective view of the Amir-shehoret basin: **A Google Earth perspective view of the Amir-Shehoret basin.**

Fluvial sediments in the Amir-Shehoret basin consist almost exclusively of carbonate lithologies. This observation points towards a dominant source of sediments beyond the Netafim fault (to the west), possibly from landslides along the fault (Byeth et al., 2012)(Fig. 5).

3.3.2 Mapping results

Geomorphic mapping of the fluvial units revealed two cut-fill terrace units (Fig. 31).

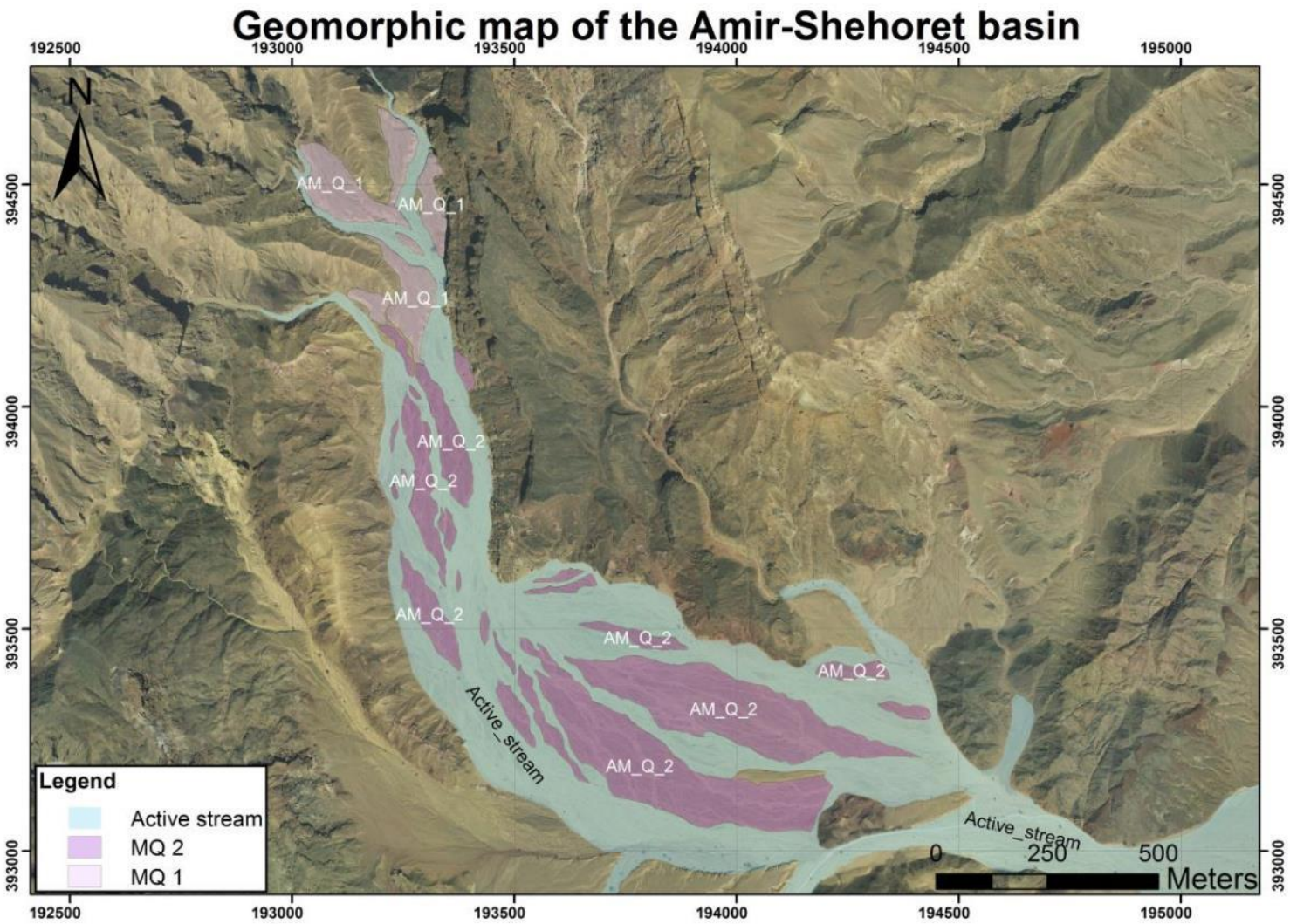

Figure 31. A geomorphic map of the Amir-Shehoret basin.

Unit	Total surface Area[%] *	Desert pavement development	Sediment lithology	Sphericity	Rounding	Sorting	Matrix	Grain size [cm]	Gravel shattering	Comments
MQ1	2	**Poor/Moderate**	*Carbonate*	**Moderate**	**Poor - Moderate**	**Moderate/ Well**	Mud supported, silty, contains gypsum	1-5	**Poor**	-
MQ2	7	**Poor**	*Carbonate*	**Poor**	**Poor**	**Moderate**	Mud supported, silty	1-10	**Poor**	-

Table 4. Amir-shehoret basin units: **Detailed description of the mapping units of the Amir basin. . *"Total surface area" refers to % area of the total basin area (including: Bedrock, Colluvium and the Active channel). Sediment features refer to the entire sediment sequence.**

Unit MQ1 covers about 2% of the basin's total surface area and is the higher terrace in the basin. The terrace consists of carbonate clasts (Fig. 32 Table 4). A moderately developed soil sequence is developed at the top of this unit and its surface is fairly smoothed. The sediments are of relatively small particle size and exhibit moderate maturation features.

Figure 32. Unit MQ1: **The fluvial sediment sequence of unit MQ1 (backpack for scale). (Location of figure appears in Appendix A.)**

Unit MQ2 covers about 7% of the basin's total surface area and is the lower terrace in the basin. The terrace consists primarily of carbonate clasts (Table 4). A poorly developed soil sequence is developed at the top of this unit and its surface still preserves depositional bar and swale morphology and is rough. The sediments are of medium particle size and exhibit moderate maturation features.

3.3.3 Discussion

During the formation of the current configuration of the Amir-Shehoret basin, a wide bedrock channel formed. Unit MQ1 was deposited during an aggradation period, its sediment source predominantly from the carbonate outcrops. This unit is only found in the northern part of the basin. After the deposition of unit MQ1 an incision formed

the MQ2 cut surface. This cut terrace is only found in the southern part of the basin (Fig. 31). This degradation activity continued and formed the current active channel bead.

The geomorphic observations in the Amir-Shehoret basin do not indicate direct evidence of tectonic influencing forces within the basin area.

3.4 The Shehoret basin

3.4.1 General

The Shehoret basin drains a total area of 12.9km^2 and has an elongation ratio of 0.56. The headwaters of the basin are at the western boundary of the Shlomo graben (Fig. 4) and its base-level is at the Evrona playa (Fig. 4). The basin is crossed by the Netafim and the Arava Faults. Small tributaries with steep gradients characterize the upstream section of the basin in the western part of the Shlomo graben. Further downstream, flow is concentrated into a steep walled canyon. High terraces were deposited where a widening of the valley previously existed (at the foothills of the magmatic mountains of the Roded block). The Amir and the Amir-shehoret basins join the Shehoret basin as they exit the foothills creating a wide braided fan (Fig.4, 7 and 33). As will be discussed in chapter 3.4.4.1, the catchment area of the basin changed over time and therefore units now located outside of the present-day catchment area were also examined. The majority of the sediments in the basin are of carbonate sources. From the east side of the Netafim fault, small channels connecting to the main channel contribute magmatic clasts to the transported sediment load. Upstream of the Netafim fault, the channel bed is wide and a significant amount of carbonate sediment is currently stored above the Shehoret canyon.

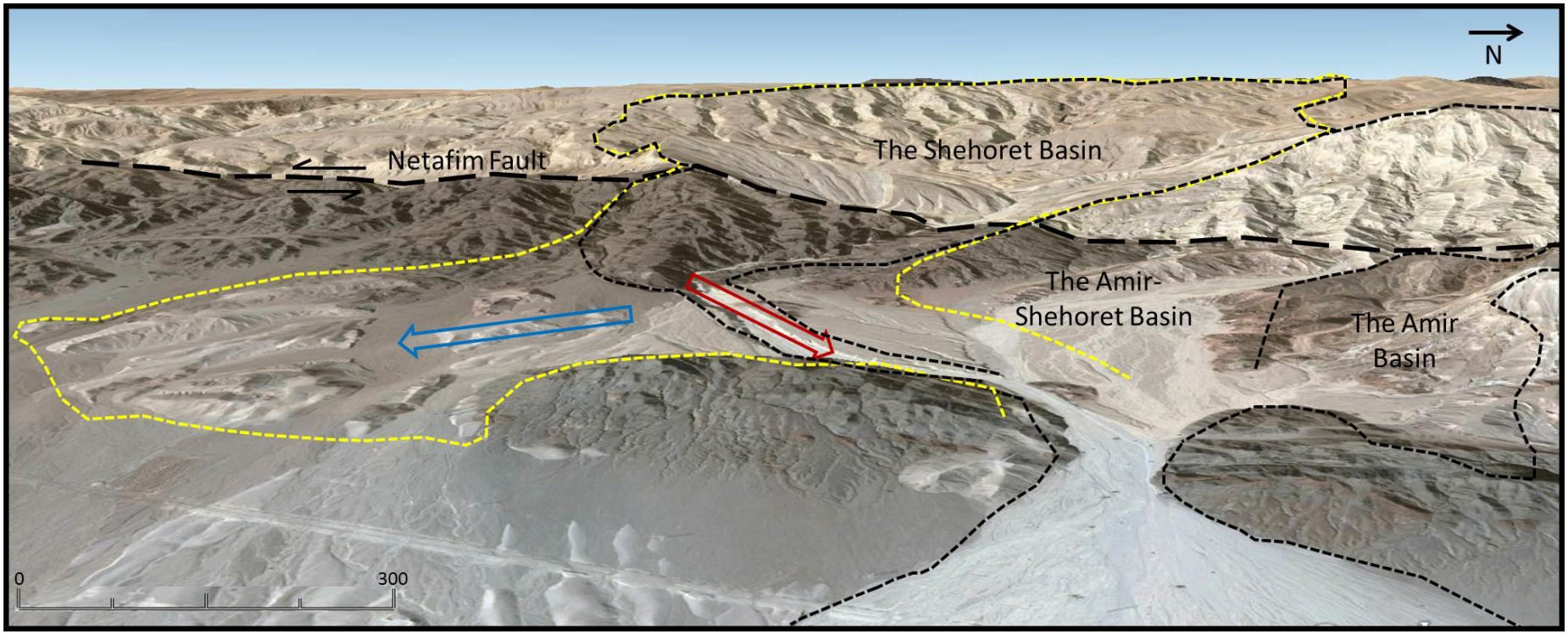

Figure 33. Perspective view of the Shehoret basin: **A Google Earth perspective view of the Shehoret, Amir-Shehoret and Amir basins. The former flow direction of the Shehoret basin is marked by a blue arrow and the former catchment area is marked by a yellow dashed line. The present flow direction is marked by a red arrow.**

3.4.2 Mapping results

Geomorphic mapping of the fluvial units east of the canyon revealed six generations of fluvial terraces (fill-cut type terraces) (SQ1-SQ6; Fig. 34).

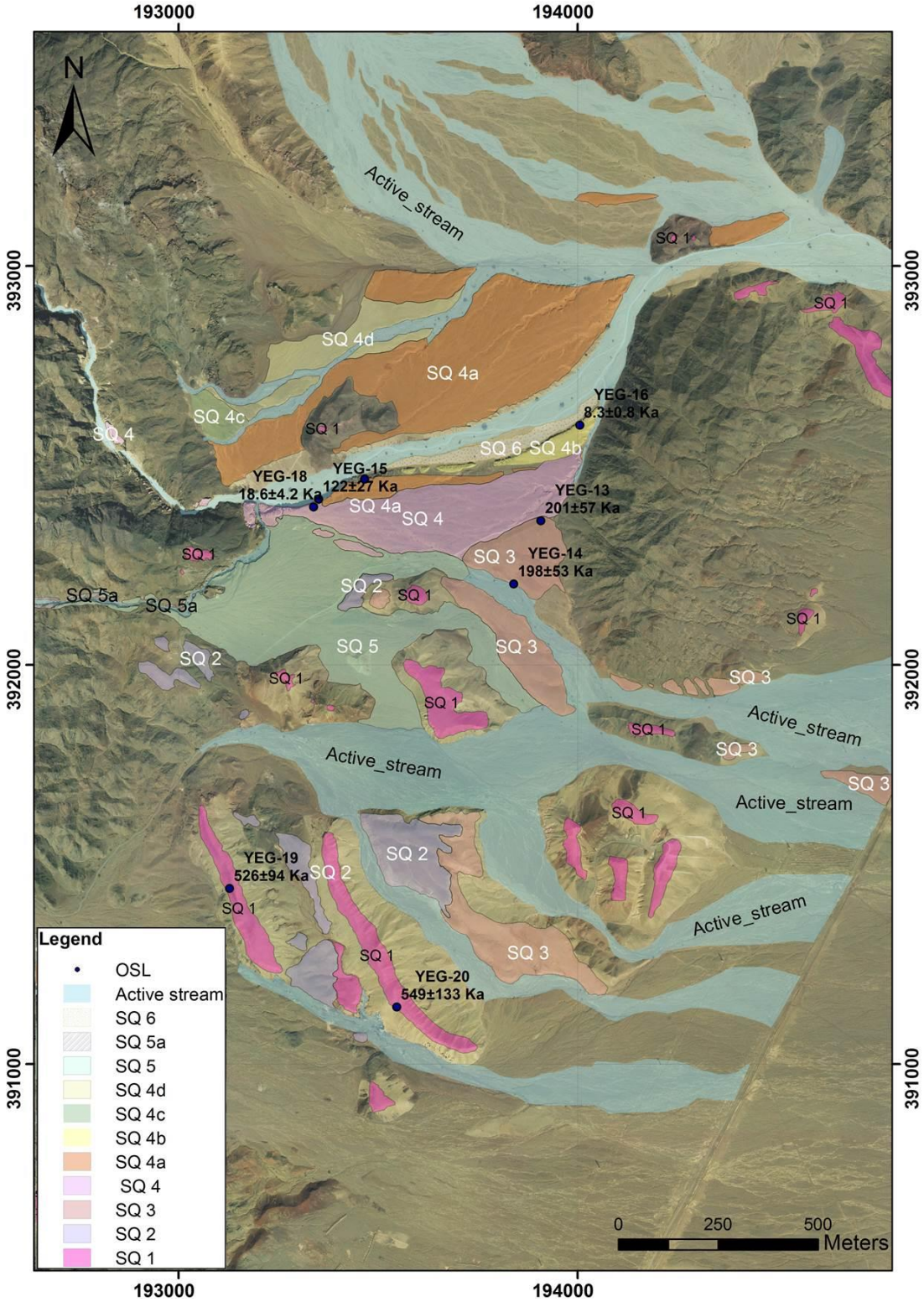

Figure 34. A geomorphic map of the Shehoret basin.

Unit	Total surface Area[%] *	Desert pavement development	Sediment lithology	Sphericity	Rounding	Sorting	Matrix	Grain size [cm]	Gravel shattering	OSL Age [ka]	Comments
SQ1	3	**Highly**	30%-Magmatic 60%-*Carbonate* 10%-*Chert*	Magmatic-Poor Carbonate-Moderate Chert-Poor	**Poor**	**Poor**	grain supported, well to Moderate consolidatedwith silty matrix containing gypsum and salt	1-100	**Well**	Top surface - 526±94 (TT) Bottom of sequnce - 549±133 (TT)	Ocasinoly contains sandrock sediments
SQ2	1	**Well**	95% -*Carbonate* 5%-*Magmatic*	Carbonate-Moderate Magmatic-Poor	**Poor**	**Poor**	grain supported, Poor to Moderate consolidated	1-100	**Well**	Top surface - 202±68 Bottom of sequnce - 202±60	As the distance from the basin's origin increases there is an increase in the carbonate and chert component
SQ3	<1	**Moderate**	95%- *Carbonate* 5%-*Magmatic*	Carbonate-Moderate Magmatic-Poor	**Moderate**	**Moderate**	grain supported, Poor consolidated	1-20	**Moderate**	-	-
SQ4	12	**Moderate**	*Carbonate*	**Moderate**	**Poor**	**Poor**	grain supported, Poor consolidated	1-100	**Moderate**	Top surface (under subunit SQ4b) - 8.3±0.3(SG) Top surface - 18±4 Top surface (under subunit SQ4a) - 30±9	-
SQ5	3	**Moderate**	*Magmatic*	**Poor**	**Poor**	**Moderate**	grain supported, Poor consolidated	1-20	**Poor**	-	-

Table 5. Shehoret basin units: *Detailed description of the mapping units of the Shehoret basin.* **. *"Total surface area" refers to % area of the total basin area (including: Bedrock, Colluvium and the Active channel). Sediment features refer to the entire sediment sequence.**

Unit SQ1 is the most elevated terrace in the Shehoret basin and the most elevated Quaternary dated fluvial sediment relict found in the research area. SQ1 directly overlies bedrock of either magmatic, sandstone or carbonate lithology depending on location. The sediments comprising this unit are predominately carbonate (Fig. 35B, App. B. Table 5). The highest relicts of this unit contain sediments derived from rock formations, such as the Eocene Avedat Group, that are no longer found within the catchment area of the Shehoret basin. A well-developed soil sequence occurs at the top of this unit. The unit's sediments are well cemented by a silty and calcite matrix (App. B, Table. 5; Fig. 35B) and its surface presents a well-developed desert pavement (composed mostly of magmatic and chert clasts) (Fig. 35A). The margins of SQ1 are eroded, thus creating secondary deposition of the unit's sediments along the slopes of the elevated terraces. At one location in the southern part of the basin (Fig. 36) SQ1 is deformed by north striking normal faulting. The deposition age of the unit's base and top were found to be 526±94 and 549±133 ka, respectively (Table 5).

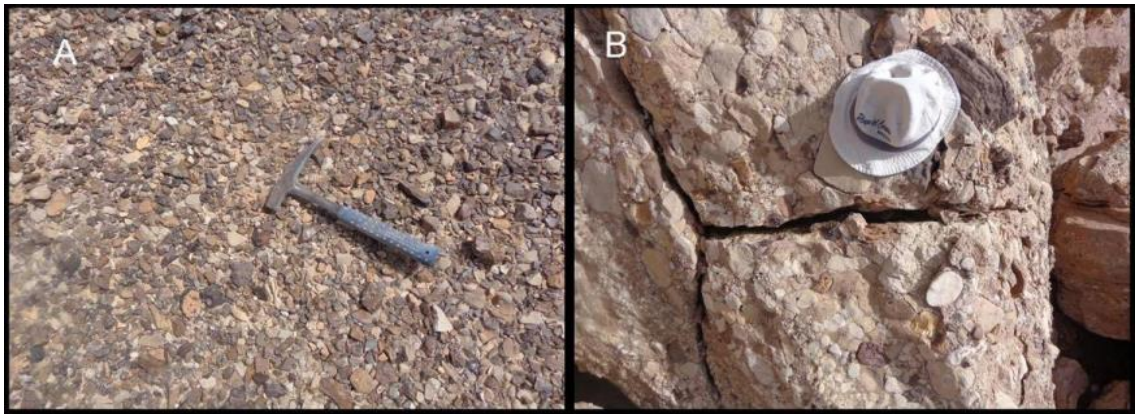

Figure 35. Unit SQ1: **A. The desert pavement at the surface. B. The well-cemented basal layer of SQ1. Some of the pebbles are fractured thus indicating the strength of the surrounding matrix. (Location of figure appears in Appendix A.)**

Figure 36. Normal faulting of unit SQ1: **A. The area between the dashed lines is filled with breccia, calcite veins and rotated pebbles. B. SQ1 sediments faulted together with the underlying sandstone bedrock (total displacement of ~1.5m). (Location of figure appears in Appendix A.)**

Unit SQ2 was deposited at least 20m lower than unit SQ1 after an incision period created elongated flow channels within the surface of unit SQ1. The base of this unit is deposited on magmatic and sandstone bedrock. The lithologic composition of the unit is predominately carbonate. A well-developed soil sequence occurs at the top of this unit and its surface is fairly smooth (App. B; Table. 5). The deposition age of the unit's base and top was found to be 202±60 and 202±68 ka, respectively (Table 5).

Unit SQ3 is at the same level as unit SQ2. The unit's lithologic composition is predominately magmatic. A well-developed soil sequence occurs at the top of this unit and its surface is fairly smooth. This unit was deposited simultaneously or shortly after the deposition of unit SQ2 and therefore shares its depositional properties. The sediment source of this unit, which is different than that of unit SQ2, is probably from the tributaries to the south of the main channel bed that flow on magmatic bed rock (Fig. 37). Field relations, mainly inter-fingering between the two simultaneously deposited units, enable to associate the ages of unit SQ3 with unit SQ2.

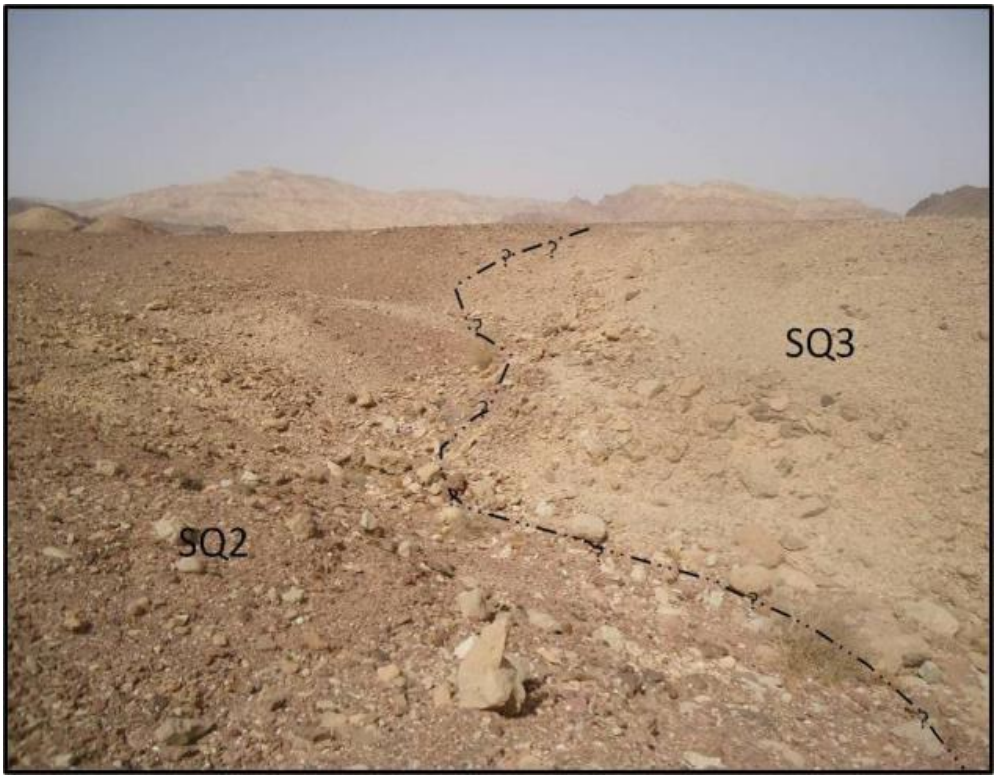

Figure 37.Contact between units SQ2 and SQ3: **SQ2 and SQ3 are composed of different lithologies and sourced from different channels and yet they connect to form leveled contemporaneous surfaces. (Location of figure appears in Appendix A.)**

Unit SQ4's base was deposited approximately 30m lower than units SQ2 and SQ3 top surface. SQ4 was deposited on magmatic and sandstones bedrock, OSL dating yielded an age of 122±27 ka for the deposition of the base of the unit (Fig. 34; Table 5). The lithologic composition of the unit is predominately carbonate (Table. 5; App. B.). The exposed thickness of unit SQ4 reaches approximately 25m. Inspection of the sediment section at all the location it is exposed in the basin does not reveal any significant indications of depositional hiatuses. The OSL dating of two additional locations within the sedimentary sequence (a) a bedding horizon, approximately 15m above the unit's base yielded an age of 30±9 ka, and b) the top-most sediments of unit SQ4 yielded an age of 18±4 ka) indicate that the unit was deposited within an overall continues aggradation period. The soil sequence at the top of SQ4 is moderately developed and the surface is moderately smoothed with remnant bar and swale morphology (App. B; Table. 5).

Although the unit was deposited in a consistent continues sequence, four cut terrace surfaces currently shape the unit (Fig. 34 and 38). Sub-unit SQ4a is an erosional

surface approximately 2.5 m lower than SQ4's surface that was incised into SQ4. Subunit SQ4b surface is approximately 2.5 below SQ4a. The sediments directly under the surface of subunit SQ4b yielded an OSL age of 8.3±0.3ka (Table 5). This age is not compatible with the field observation showing that Unit SQ4 was deposited during a continuous aggradation period and that the stepping surfaces that presently carve it are a result of a continues incision . A possible explanation for this observation is that the sampled sediments represent an episodic sedimentation within the overall incision.

Units SQ4c and SQ4d (Fig. 34) are located north of the main active channel. These subunits were formed as a result of the incision of a small tributary that drains the magmatic slopes to the north of the main active channel and joins the Shehoret basin further to the east (Fig. 7 and 34). Though the formation age of these subunits is uncertain, it is certain they formed after the formation of subunit SQ4a (they are cut into the surface of SQ4a), thus, they postdate the initial incision into SQ4 (18±4ka).

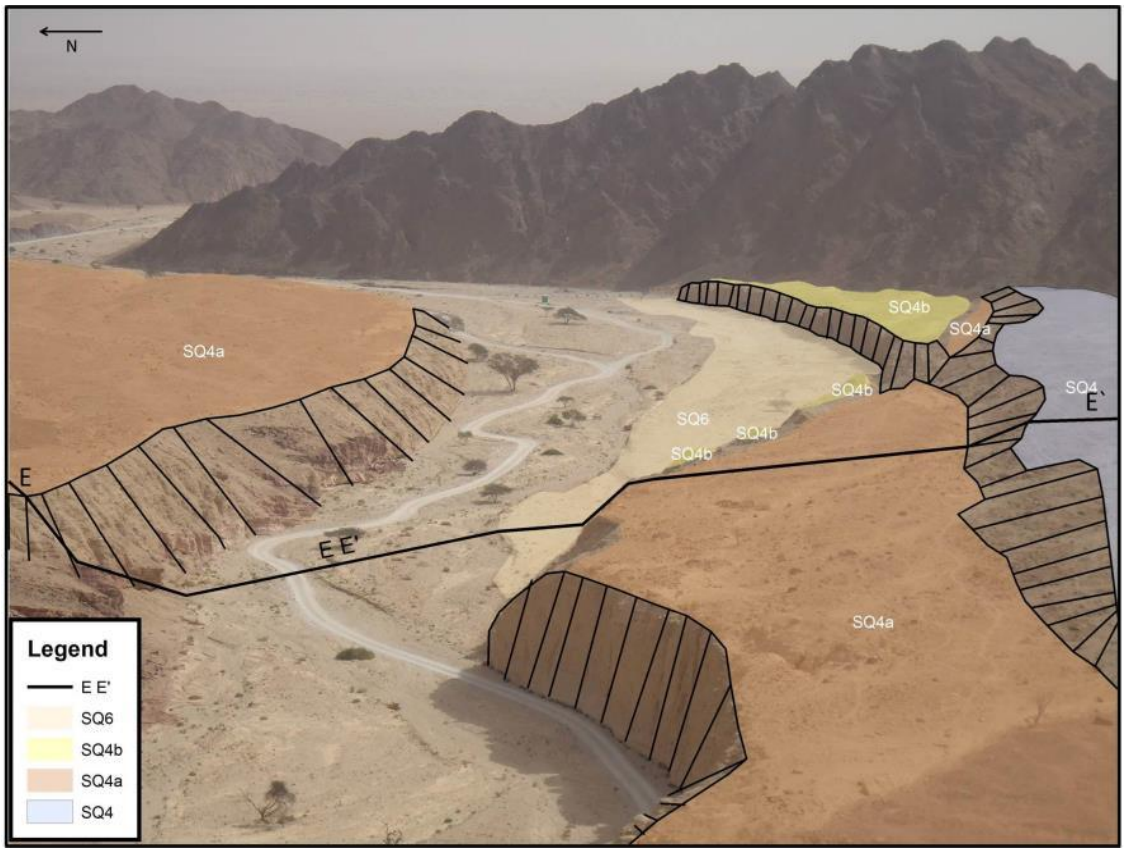

Figure 38. Active channel and SQ4 sequence: **An eastward view at the SQ4 terrace sequence and the main active channel of the Shehoret basin. SQ4a, and SQ4b are cut surfaces incised into unit SQ4. (Dirt road is ~4 m wide).**

Unit SQ5 consists primarily of magmatic clasts sourced from a channel that drains the magmatic slopes south of the Shehoret canyon. SQ5 was deposited on magmatic bed rock and partly upon unit SQ4. Depositional inter-fingering between SQ5 and SQ4 (Fig. 39) indicate that the lower layers of SQ5 were deposited simultaneously with the upper layers of SQ4. The upper layers of SQ5 were deposited after the deposition of unit SQ4 ceased, as indicated by sediments of unit SQ5 that deposited into SQ4 swales and surround QS4 bars (Fig. 34 and 40). A poorly developed soil sequence occurs at the top of SQ5, and its surface is moderately smooth with remnant bar and swale morphology (App. B, Table. 5). Sub-unit SQ5a is a cut-terrace incised ~ 2m into SQ5 (Fig. 40).

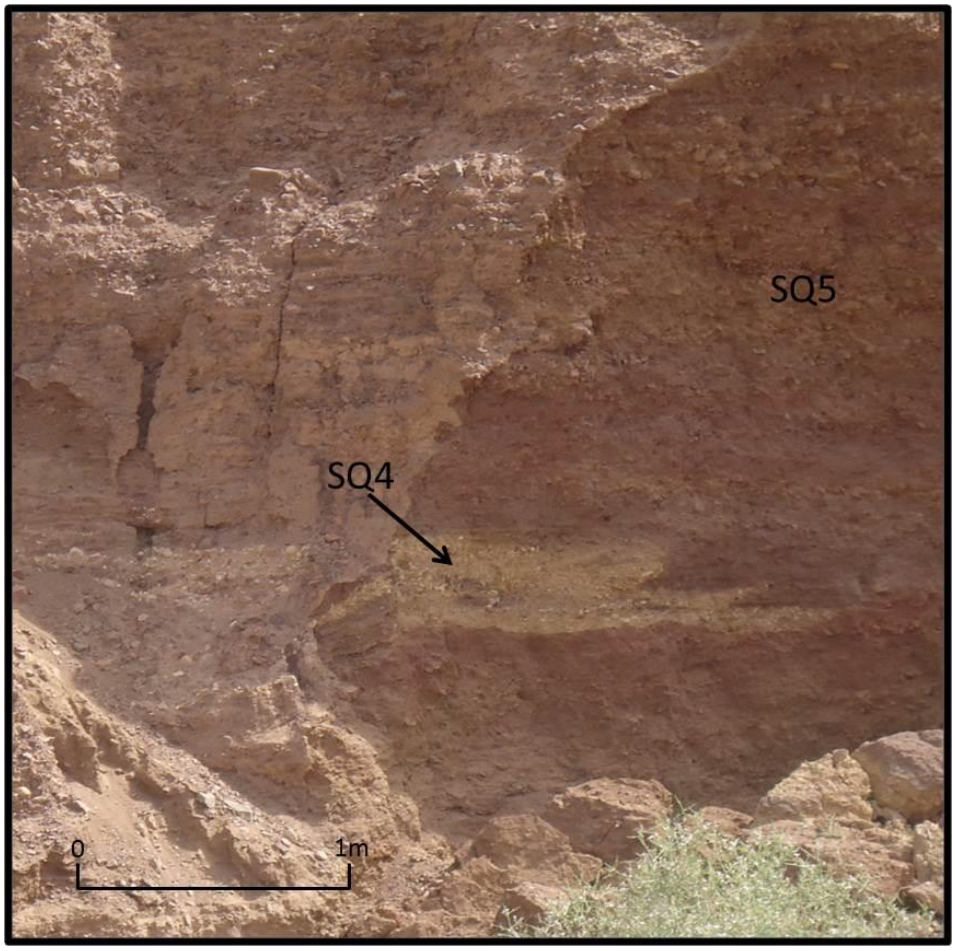

Figure 39. Interfingering between the sediments of units SQ4 and SQ5. **(Location of figure appears in Appendix A.)**

Rinat (2014) dated, using OSL, the sediments of SQ5. The sedimentary horizon dated by Rinat does not represent the actual base of SQ5 sequence but rather the base of a local accumulation of the later deposits of this unit against the flanking bedrock slopes. According to his findings, the sediments of SQ5 began accumulating shortly

after 6.2±0.8ka. Sediments at the top of SQ5a and directly under a fallen bolder yielded an age of 3.4±1.4ka. These ages constrain the incision into SQ5 and the formation of SQ5a. Since this incision occurred in response to the incision of the main channel into SQ4 these ages indicate a mid-Holocene age for the major incision to form the present level of the active channel.

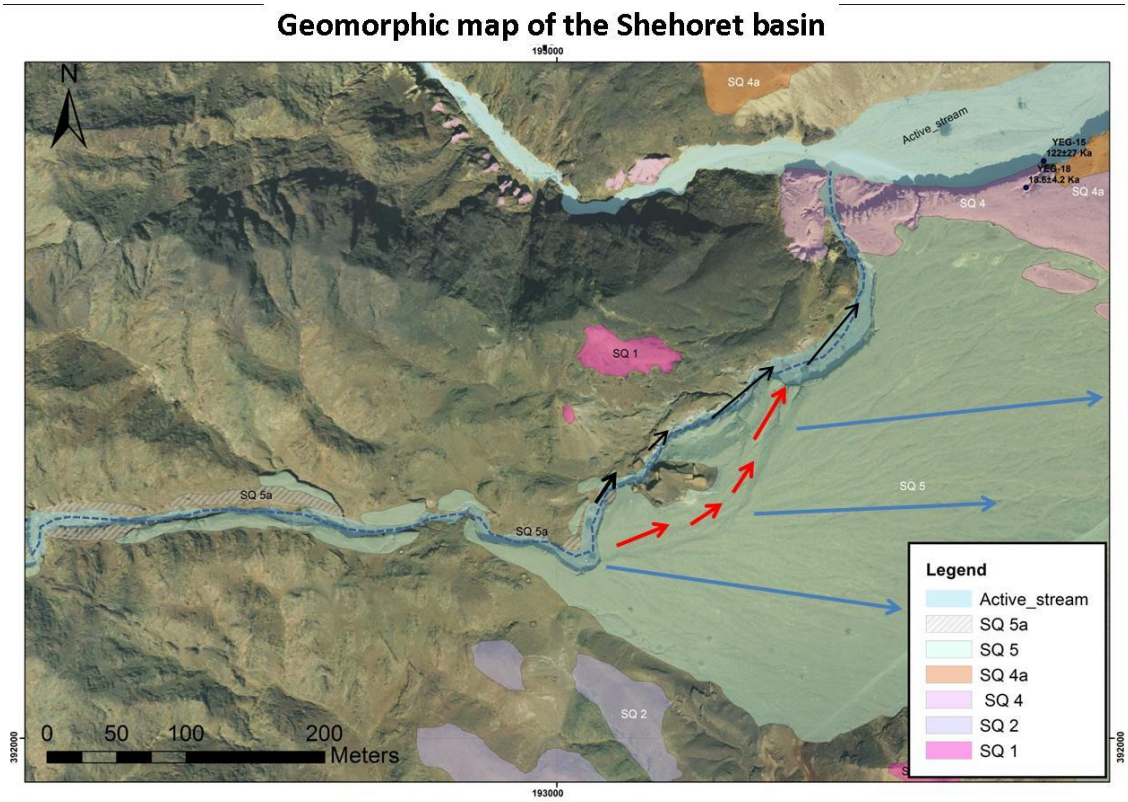

Figure 40. A geomorphic map of the fluvial units south of the Shehoret main channel: **The three evolution stages of a tributary channel south of the main active channel are shown: At first the channel supplied the sediments that were deposited as unit SQ5. Flow direction, indicated by the bar and swale pattern was to the east and to the east-northeast (blue arrows). Second stage, channel capture shifted the channel to the northeast flowing into the main active channel of the basin (red arrows). Stage three, the channel incised deeper into unit SQ5 and shifted further northwards (black arrows).**

Unit SQ6 is found approximately 2m above the active channel bed in the main active channel. No soil sequence is developed; its surface is rough with prominent bar and swale morphology (Fig. 34).

3.4.2.1 Topographic cross sections

Four topographic cross-sections were measured in the Shehoret basin (Fig. 41).

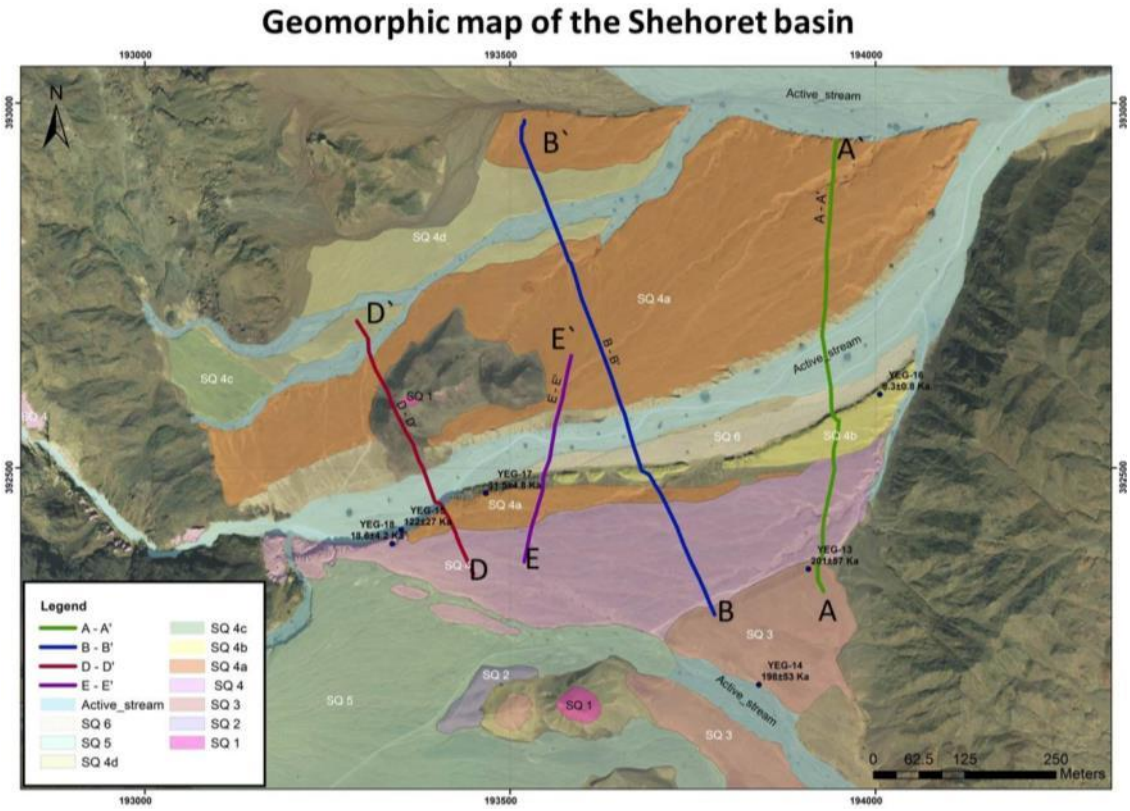

Figure 41. Cross section location map, Shehoret: **A geomorphic map of the Shehoret basin showing the locations of the four topographic cross sections.**

Relicts of SQ1 are typically found on top of bedrock hills (Fig. 42), it's measured elevation above SQ4 surface as appears in cross section D-D' is approximately 17m (although at other locations the height difference between SQ1 and SQ4 can reach up to approximately 90m). No contact between unit SQ1 and the other mapping units was found. Unit SQ2's surface is elevated approximately 5m above unit SQ4's surface (cross sections A-A' and B-B', Fig. 42). SQ4a is lower than SQ4 by approximately 2.5m (Fig. 42). SQ4b is lower than SQ4 by approximately 5m and. Units SQ4d and SQ4c are lower than SQ4 by approximately 5m (Fig. 42). Unit SQ6 is elevated approximately 2m above the active channel and approximately 15m below unit SQ4 (Figs. 42).

Figure 42. Measured topographic cross sections, Shehoret: **The locations of the cross sections are drawn on the map in figure 41. The following legend applies for all cross sections.**

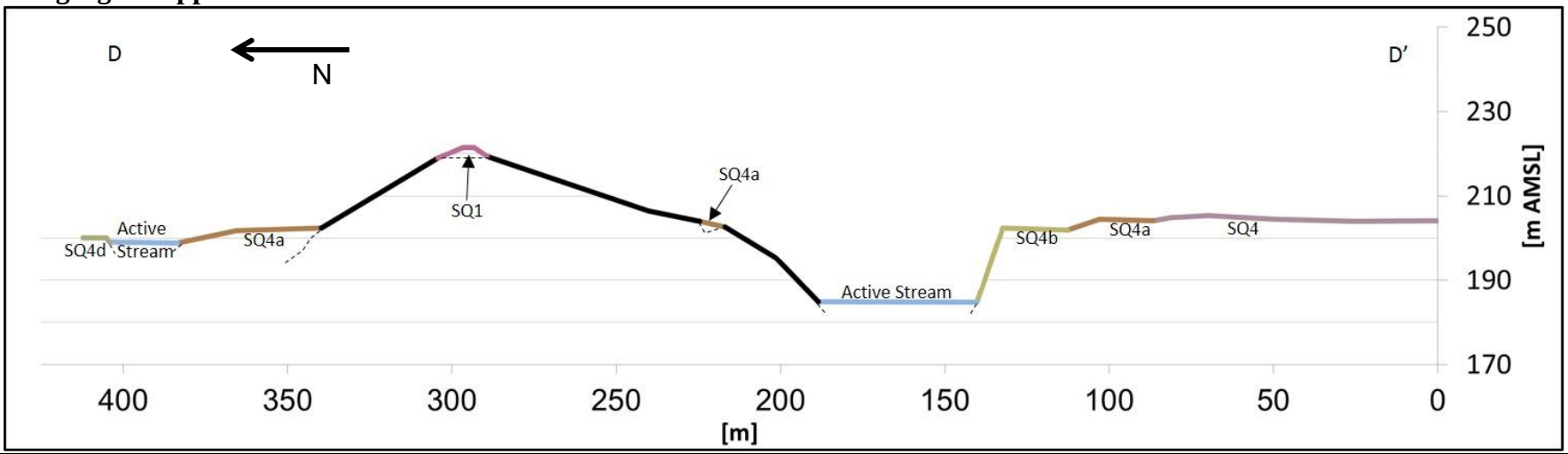

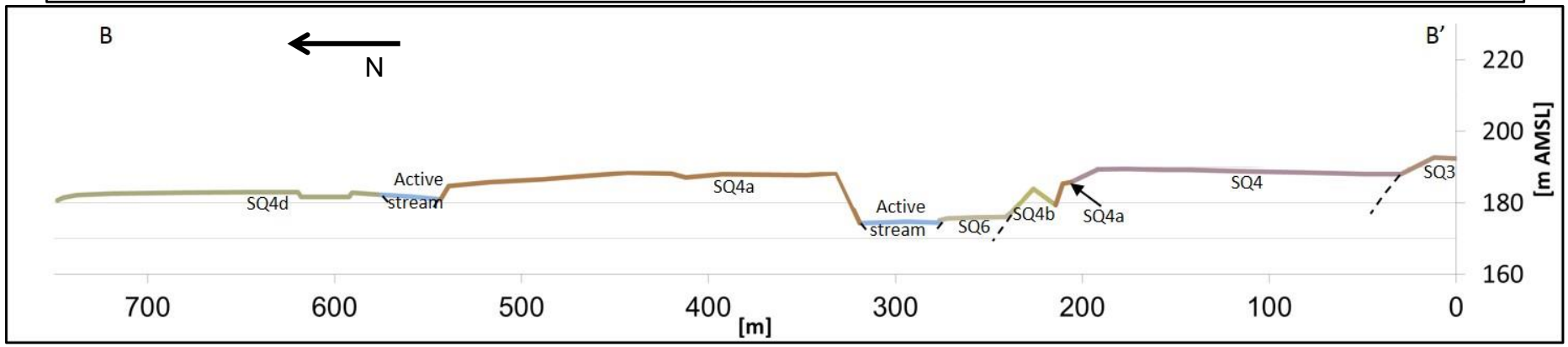

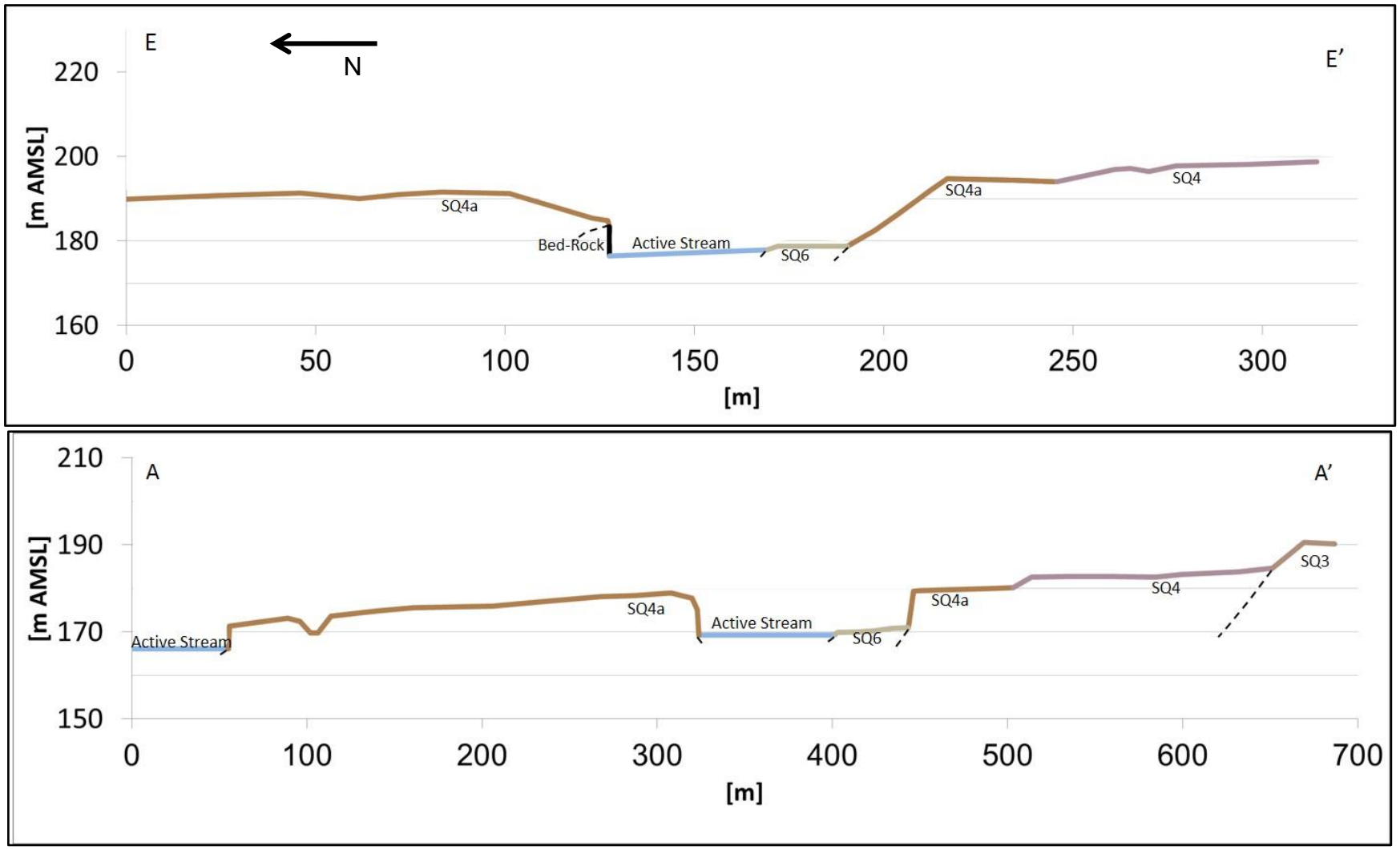
E
N
E'
220
200
180
160
[m AMSL]
SQ4a
Bed-Rock
Active Stream
SQ6
SQ4a
SQ4
0
50
100
150
200
250
300
[m]
A
A'
210
190
170
150
[m AMSL]
Active Stream
SQ4a
Active Stream
SQ6
SQ4a
SQ4
SQ3
0
100
200
300
400
500
600
700
[m]

3.4.3. OSL dating

In the Shehoret basin, ten sediment samples were collected for OSL dating (YEG-11 to 20 Table 5). Samples YEG- 13(SQ3), 16(SQ4b), 17(SQ4a), 18 (SQ4) and 19 (SQ1) were collected from directly under the salic-gypsic accumulation horizons at the base of the soil sequence overlying the fluvial material. Samples YEG-14 (SQ3), 15 (SQ4) and 20(SQ1) were collected from the lowest exposed sediment horizons of their respective terraces.

Using the average De value method for calculating the ages of samples YEG-11(SQ1 lowest sequence) and YEG-12 (SQ1 top sequence) yielded poor results. Therefore, unit SQ1 was resampled (YEG-19 and YEG-20) and the TT-OSL method was used to define the units' age.

Using the average De value method for calculating sample YEG- 16 age yielded poor results; therefore single grain measurements were performed. The De values used to calculate the age of sample YEG- 16 was obtained from the first component that represents the value of 10% and up of the grains (Table 6).

YEG-16				
Component	1	2	3	4
Dose [s]	173±5	320±12	804±40	1995±79
% of component	42	29	13	16

Table 6. Shehoret SG FMM: **Results of the FMM for the Shehoret SG sample. The component chosen for calculating the age is marked in blue.**

3.4.4 Discussion

3.4.4.1 Geomorphic outcomes

Relicts of the oldest fluvial deposits in the Shehoret basin, mapped as unit SQ1, are found mostly on hilltops, high above the present active channels. In one location, sediments of the lower layers of this unit fill a bed-rock channel, indicating that the topography upon which the drainage system evolved was not totally leveled, but rather cleft.

Between 526±94 and 202±60 ka incision formed south and southeast directed channels cut into the fluvial sedimentary cover, leaving relicts of unit SQ1 and the underlying bedrock as elongated ridges and isolated terraces upon bedrock hills. Units SQ2 and SQ3 were later deposited in these channels. Unit SQ2's lithological composition suggests that its sediment source was from the distant parts of the Shehoret basin (i.e. west of the Netafim fault). An increase in sediment supply from the eroding magmatic slopes, relative to the sediment supply from the carbonate sources, altered the lithologic composition of the aggradating sediments, and formed unit SQ3. This source alteration is currently unexplained.

The deposition of units SQ2 and SQ3 (202±68 ka) was followed by a significant degradation period, in which flow direction shifted from south-east to north-east and the basin's catchments area shifted northwards consequently. The deposition of unit SQ4 began at approximately 122±27ka and marks an extended period of continuous aggradation that ended shortly after 18±4ka.

Since the abandonment of unit SQ4's surface after 18±4ka the basin's main channel has been incising into the fluvial sediments and progressively shifting to the northeast as indicated by cut terraces SQ4a,b,c,d. . The small terrace located to the south of the main active channel (unit SQ6) is an additional observation supporting the gradual northwards shift of the basins main channel. This unit represents an additional surface that was abandoned as result of a northward shift of the incising channel.

The topographic cross-sections and the plan view geometry indicate a general surface tilt towards the North-East of units SQ4 to SQ6, thus indicating a north-east flow direction since the deposition of unit SQ4 and/or post deposition northwards tilt of the basin.

In response to the incision of the basin's main channel, channel capture of the channel that originally sourced SQ5 south of the main channel occurred. This channel capture occurred in two stages: (1) the channel shifted to a northeast direction while incising approximately two meters into unit SQ5. (2) Additional incision formed a cut terrace (mapped as unit SQ5a), and the channel was shifted further to the north, (Fig. 45).

The overall pattern obtained from the three channels (the basins main channel and the adjacent southern channels (the channel that formed SQ5a) is that since the

abandonment of unit SQ4, the basin underwent a gradual degradation process along with lateral northwards shifting of the channels.

3.4.4.2 Tectonic outcomes

The current configuration of the Shehoret basin has a relatively low elongation ratio of ~0.56, indicating that the height of the basin's base level relative to the basin's head waters height is still evolving resulting in immature basin geometry. Since the basin's geometry changes considerably as it crosses the Netafim fault, two separate elongation ratios were calculated for the two parts of the basin. The western part of the basin has an elongation ratio of ~0.8, while the eastern part's elongation ratio is ~0.48. The highly circler elongation ratio of the western part of the basin suggests it is rather geomorphically mature. In contrast, the very low elongation ratio of the eastern part suggests it is very immature. The partition of the basin to a mature area and an immature area separated by the Netafim fault indicates that the eastern part of the basin is considerably more influenced by tectonic perturbation than the western part. Reconstruction of the former configuration of the Shehoret basin (before the northward shift in flow direction) (Fig.33) based on the distribution of the fluvial sediments derived from bedrock outcrops within the basin, enables the estimation of the paleo-elongation ratio. The minimal calculated elongation ratio value is ~0.69, indicating that prior to the tectonic deformation that caused the change in flow direction the basin was in a relatively mature development stage.

The geomorphic observations described above help inform our understanding of tectonic deformation in the basin during the Quaternary:

(a) Faulting of unit SQ1- The lower bedding horizons of unit SQ1 are displaced by two normal faults striking north-south (Fig. 36). This observation suggests that besides deformation along the DST main faults, the basin's area was tectonically deformed during the middle Pleistocene (526±94 ka). On the other hand, no evidence of faulting was found to disrupt the younger units in the basin.

(b) Change in flow direction - The change in flow direction that occurred between the abandonment of units SQ2 and SQ3 surfaces and the deposition of unit SQ4 (between 202±68 and 123±28 ka) may be consistent with major tectonic deformation within the basin area.

(c) Time-progressive northward migration of channels during the incision period initiated after the deposition of unit SQ4 ceased (18±4 ka); the main channel monotonically shifted northwards and formed the degradation surfaces SQ4a and SQ4b. Furthermore, as northward shifting of channel flow direction occurred during two separate degradation periods divided by an aggradation period may indicate continuous tectonic deformation.

4. Tectonic discussion

Spatial tectonic deformation:

Aside of the faulted SQ1 unit, none of the other geomorphic observations discussed above is uniquely indicative of tectonic activity. However, tectonic surface tilting appears to be the single process that can explain all the observations. Combined with the OSL ages these observations suggest that the northern basins (Zefunot and Amram) experienced Pleistocene to late Holocene southward surface tilt. The Shehoret basin experienced Pleistocene to late Holocene surface tilt to the north. The southward tilt of the Amram and Zefunot mark the southward tilt of the Amram block and the northward tilt of the Shehoret basin marks the northward tilt of the adjacent Roded block (Fig. 7). Thus, the combined observations may be interpreted as resulting from compressional N-S tectonic deformation in the region.

During the late Miocene and over the formation of the Amir syncline (Beyth et al., 2012), the compressional stress vector was directed perpendicular to the syncline's hinge. However, since the structural blocks and the syncline were subjected to rotational deformation, it is possible that the synclines hinge direction is no longer perpendicular to the initial stress direction. Therefore, the compressional deformation inferred in this research was most likely not directed perpendicular to the synclines hinge but rather preserved an overall N-S direction. Since the geomorphic evidence indicating the deformation does not point to a precise direction but rather indicates a more general direction, it is not possible to spatially place the overall stress vectors leading to the recent deformation.

The deformation of the structural blocks subjected to compressional stress can occur through: (a) convergence of the blocks as whole rigid bodies, or (b) by faulting activity within the blocks. The formation of the Amir syncline at the boundary between the two blocks due to compressional forces since the Miocene (Garfunkel, 1970) indicates that these blocks converged as rigid blocks in the past. Thus similarly, it appears that Quaternary deformation within this segment of the DST was driven by the convergence of ridged bodies.

However, evidence for the existence of the Faulting mechanism is found in the research area. Several Precambrian, Neogene, and Pleistocene faults that dissect these

blocks in different directions (Garfunkel, 1969, 1970; Beyth et al., 2012) (Figs. 5 and 43) can serve as possible weakness plains for tectonic deformation. Furthermore, the observation of faulted terraces in the Shehoret basin (the lower layers of unit SQ1, Fig. 36), and late Pleistocene activity of faults in the Amram block (Sagy et al., 2013), indicate that faulting activity indeed occurred in these blocks during the Quaternary. Therefore, it seems reasonable to assume that the observed surface deformation was driven by both mechanisms. The compressional forces caused the blocks to collide and tilt as whole rigid bodies, and, in addition, part of the compressional force was expressed by faulting activity.

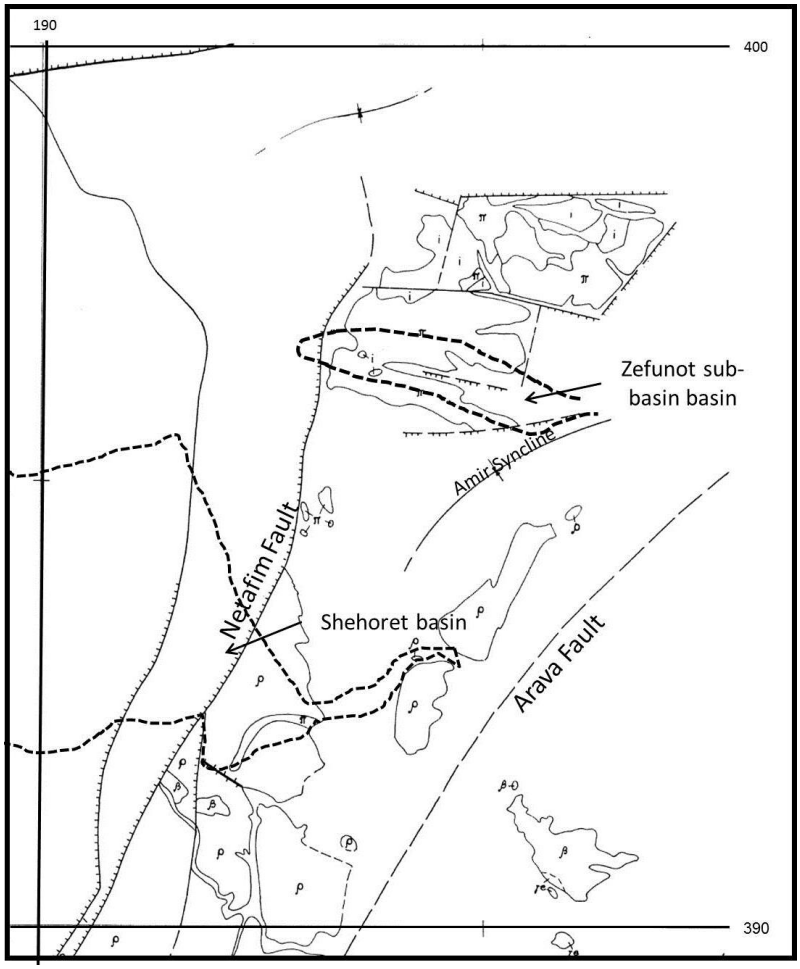

***Figure* 43*. Research area tectonic elements:* Map of research area showing the main tectonic features. Note that several faults dissect the Amram block and in particular two faults dissect the Zefunot basin (outlined with dashed line). (Modified from Garfunkel, 1970).**

Suggested mechanisms for the Formation of spatial compressional deformation:

Many of the DST deformational structures match the characteristics of the simple shear mechanisms. As the DST's displacement vector in the southern Arava region includes a considerable transverse component (Garfunkel, 1980), it can be considered a "divergent strike-slip fault". The divergent component dictates that the overall deformation of the region is expected to form extensional structures such as normal faults and grabens. This extensional regional deformation is expressed in the normal step-faults dividing the structural blocks descending towards the Arava Valley. Apart from the normal component of these faults, they accommodate considerable sinistral displacement, thus forming sub-regions between them, which contrary to the general regional trend, are subjected to compression and rotational deformation (Garfunkel, 1970).

The compression between the faults can be generated by two mechanisms: (a) Parallel strike-slip faults with the same displacement direction produce internal compressional deformation and rotational deformation of the area between the faults (Ron et al., 1984) (b) If the faults change their orientation along the dividing blocks, deformation is formed due to contradicting slip directions (Garfunkel, 1970). The compressional deformation inferred in this research is located between the Netafim and Eilat normal-sinistral faults. These faults contain features generating both mechanisms: their northern segments are parallel thus, producing compressional deformation and rotation across the research area, and in addition the change in strike along the faults likely forces clockwise rotation about a vertical axis (Garfunkel, 1970). Consequently, the research area was possibly subject to the two suggested deformation mechanisms, thus, experiencing compression deformation within the overall extensional region.

Dynamics of spatial deformation reactivation:

It has been previously suggested that with the cumulative offset of 105 km along the transform, the width of deformation along the DST should be localized to the center of the transform, and the offset accommodated by a single smooth 420 km long fault segment (Stirling et al., 1996; Wesnousky, 1988). While several previous studies indicated that such localization may have occurred within the southern Arava segment of the DST (Enzel et al., 1996; Amit et al., 2002; Zilberman et al., 2005), this study suggests that spatial distribution of deformation may be more complex.

Regeneration of spatial deformation in areas distant from the localized transform would be possible if the regional stress field was reoriented due to geometrical changes in the plate boundary configuration (Marco, 2007; Ten Brink et al., 1999; Zain et al., 2001). Along the DST, several indications of regeneration of spatial deformation, due to changes in plate boundary geometry, were found: (a) displacement of Pleistocene fluvial sediments by the Barak fault in the central Arava segment of the DST (previously defined by Marco (2007) as the segment of the transform extending from the Themed fault in the south to the dead sea basin in the north). This displacement indicates the central Arava crossed over from widening of the deformation zone during the Miocene, followed by a late Miocene to Plio-Pleistocene deformation localization phase that once again widened during the late Pleistocene (Marco, 2007). (b) A post middle-Pleistocene formation of a diagonal fault across the Hula basin (Schattner and Weinberger, 2008). Other examples can be found in Ten Brink et al., 1999 and in Schattner and Weinberger, 2008. In this context, the findings of this research which indicate a wider than previously considered Quaternary deformation belt along the Arava margins support such changes in the stress-field orientation. Furthermore, this work can be taken as additional evidence indicating the variation in spatial deformation as a result of rearrangement of the plate boundary motion.

5. Summary

The Quaternary geomorphic evolution of four adjacent fluvial basins in the southern Arava was investigated. OSL dating of the fluvial units that record these perturbations places the inferred tectonic activity responsible for the changes in drainage flow direction within a defined time frame. The geomorphic evolution of the northern basins (Zefunot sub-basin and the Amram basin) suggests that during the late Pleistocene - late Holocene the fluvial configurations were altered by tectonic deformation and southward tectonic surface tilting accrued. The geomorphic evolution of the southern basin (the Shehoret basin) suggests that during the middle Pleistocene - Holocene the fluvial configurations were altered by tectonic deformation and northward tectonic surface tilting accrued.

Since the Formation of the Amir syncline during the late Miocene, the Roded and Amram structural blocks underwent horizontal rotation. As the rotation continued and the angel between the synclines hinge and the bounding Arava fault decreased, the folding activity ceased and was locked. Conservation of the compressional force altered the active folding hinge location and angel, thus initiating the inward surface tilting and the present formation of a subsurface syncline between the Roded and Amram adjacent blocks.

These findings expand the previously considered spatial extent of tectonic deformation along the southern DST's margins. The wide deformation belt contradicts the expected deformation width matching the maturity and cumulative offset of the DST. The widening of the tectonic deformation belt was most likely generated as a result of changes in the geometry of relative movement between the Arabian plate and the Sinai sub-plate. This assertion is consistent with previous similar findings along the DST that reinforce this possibility. The expansion of spatial deformation resulted in the formation of compressional forces initiated by reactivation of the marginal faults of the southern DST and the relative collision of the Roded and Amram structural blocks.

These findings shed new light on the deformation width along the DST and suggest the existence of additional similar zones along the DST that might have experienced similar deformation history. Additionally, the findings of this study support the theoretical assumption that changes in the geometric features between tectonic plates will initiate re-expansion of the deformation belt.

6. Bibliography

Aitken, M. J. (1998). An introduction to optical dating: the dating of Quaternary sediments by the use of photon-stimulated luminescence. Oxford university press.

Ambraseys, N. N., & Jackson, J. A. (1998). Faulting associated with historical and recent earthquakes in the Eastern Mediterranean region. Geophysical Journal International, 133(2), 390-406.

Amiran, D. H., Arieh, E., & Turcotte, T. (1994). Earthquakes in Israel and adjacent areas: macroseismic observations since 100 BCE. Israel Exploration Journal, 260-305.

Amit, R., Gerson, R., & Yaalon, D. H. (1993). Stages and rate of the gravel shattering process by salts in desert Reg soils. Geoderma, 57, 295–324. doi:10.1016/0016-7061(93)90011-9

Amit, R., Harrison, J. B. J., Enzel, Y., & Porat, N. (1996). Soils as a tool for estimating ages of Quaternary fault scarps in a hyperarid environment—the southern Arava valley, the Dead Sea Rift, Israel. *Catena*, *28*(1), 21-45.

Amit, R., & Yaalon, D. H. (1996). The micromorphology of gypsum and halite in Reg soils -- The Negev Desert, Israel. Earth Surface Processes and Landforms, 21, 127–1143. doi: 10.1002/ (SICI) 1096-9837(199612)21:12<1127::AID-ESP656>3.0.CO;2-G

Amit, R., Zilberman, E., Porat, N., & Enzel, Y. (1999). Relief Inversion in the Evrona Playa as Evidence of Large-Magnitude Historical Earthquakes, Southern Arava Valley, Dead Sea Rift. Quaternary Research, 52(1999), 76–91. doi:10.1006/qres.1999.2050

Amit, R., Zilberman, E., Enzel, Y., & Porat, N. (2002). Paleoseismic evidence for time dependency of seismic response on a fault system in the southern Arava Valley, Dead Sea rift, Israel. *Geological Society of America Bulletin*,*114*(2), 192-206.

Amit, R., Enzel, Y., & Sharon, D. (2006). Permanent Quaternary hyperaridity in the Negev, Israel, resulting from regional tectonics blocking Mediterranean frontal systems. Geology, 34, 509–512. doi:10.1130/G22354.1

Anderson, E. M. (1905). The dynamics of faulting. Transactions of the Edinburgh Geological Society, 8(3), 387-402.

Avni, Y. 1998, Paleogeography and tectonics of the central Negev and the Dead Sea Rift western margins during the Late Neogene and the Quaternary: Isr. Geol. Surv.. Rep. GSI/24/98, 231 pp. (in Hebrew, English abstract)

Aydin, A., & Page, B. M. (1984). Diverse Pliocene-Quaternary tectonics in a transform environment, San Francisco Bay region, California Diverse Pliocene-Quaternary tectonics in a transform environment, San Francisco Bay region, California. Geological Society of America Bulletin, 95, 1303–1317. doi:10.1130/0016-7606(1984)95<1303

Baer, G., Funning, G. J., Shamir, G., & Wright, T. J. (2008). The 1995 November 22, Mw 7.2 gulf of elat earthquake cycle revisited. Geophysical Journal International, 175, 1040–1054. doi:10.1111/j.1365-246X.2008.03901.x

Bartov, J., 1967, The geology of Beer Ora area, unpublished M.Sc. thesis, Hebrew University, Jerusalem (in Hebrew), 39 pp.

Bartov Y., (1974) A Structural and Paleogeographic Study of the Central Sinai Faults and Domes Phd. Thesis Hebrew University, Jerusalem, p. 143 (in Hebrew, English abstr.).

Barzilai, E., Enzel, Y., Amit, R., 2000. Constructing synthetic time-series of rainfall events for environmental modeling in a hyperarid environment, Southern Arava, Israel. International Association of Hydrological Sciences (IAHS) Publication 261, 29–42.

Ben-Avraham, Z., Garfunkel, Z., & Lazar, M. (2008). Geology and Evolution of the Southern Dead Sea Fault with Emphasis on Subsurface Structure. Annual Review of Earth and Planetary Sciences, 36, 357–387. doi:10.1146/annurev.earth.36.031207.124201

Bentor, Y. K., (1961), Petrographical outline of the Precambrian in Israel: Bul. Research Counc. Isr. 10G:19-63.

Bentor, Y.K., Vroman, A. 1957. The geological map of Israel, 1:100,000 Sheet 19: Arava Valley, with explanatory notes. Geol. Surv. Isr., 66 pp.

Beyth, M., Eyal, Y., Garfunkel, Z., 2012, Geological map of the Eilat Sheet: Geological Survey of Israel.

Bull, W. B. (1991). Geomorphic responses to climatic change.

Bull, W. B. (2009). Tectonically Active Landscapes. Tectonically Active Landscapes (pp. 1–326). doi:10.1002/9781444312003

Burbank, D. W., & Anderson, R. S. (2011). Tectonic Geomorphology: Second Edition. Tectonic Geomorphology: Second Edition. doi:10.1002/9781444345063

Castelltort, S., Goren, L., Willett, S. D., Champagnac, J.-D., Herman, F., & Braun, J. (2012). River drainage patterns in the New Zealand Alps primarily controlled by plate tectonic strain. Nature Geoscience, 5(10), 744–748. doi:10.1038/ngeo1582

Chester, F. M., Evans, J. P., & Biegel, R. L. (1993). Internal structure and weakening mechanisms of the San Andreas fault. Journal of Geophysical Research: Solid Earth (1978–2012), 98(B1), 771-786.

Christie-Blick, N., & Biddle, K. (1985). Deformation and basin formation along strike-slip faults. Strike-Slip Deformation, Basin Formation and Sedimentation, 1–34. doi:10.2110/pec.85.37.0001

Duller, G. A. (2008). Single-grain optical dating of Quaternary sediments: why aliquot size matters in luminescence dating. Boreas, 37(4), 589-612.

Enzel, Y., Amit, R., Porat, N., Zilberman, E., & Harrison, B. J. (1996). Estimating the ages of fault scarps in the Arava, Israel. Tectonophysics, 253, 305–317. doi:10.1016/0040-1951(95)00072-0.

Enzel, Y., Amit, R., Dayan, U., Crouvi, O., Kahana, R., Ziv, B., & Sharon, D. (2008). The climatic and physiographic controls of the eastern Mediterranean over the late Pleistocene climates in the southern Levant and its neighboring deserts. Global and Planetary Change, 60, 165–192. doi:10.1016/j.gloplacha.2007.02.003

Enzel, Y., Amit, R., Grodek, T., Ayalon, A., Lekach, J., Porat, N. & Erel, Y. (2012). Late Quaternary weathering, erosion, and deposition in Nahal Yael, Israel: An "impact of climatic change on an arid watershed"?. Geological Society of America Bulletin, 124(5-6), 705-722.

Eyal, M., Eyal, Y., Bartov, Y., & Steinitz, G. (1981). The tectonic development of the western margin of the Gulf of Elat (Aqaba) rift. Tectonophysics, 80, 39–66. doi:10.1016/0040-1951(81)90141-4

Eyal, Y. (1996). Stress field fluctuations along the Dead Sea rift since the middle Miocene. Tectonics. doi:10.1029/95TC02619

Freund, R. (1971). The Hope Fault, a strike slip fault in New Zealand (Vol. 86). Dept. of Scientific and Industrial Research.

Freund, R. (1974). Kinematics of transform and transcurrent faults. Tectonophysics, 21, 93–134. doi:10.1016/0040-1951(74)90064-X

Freund, R., Garfunkel, Z., Zak, I., Goldberg, M., Weissbrod, T., Derin, B., (1970). The Shear along the Dead Sea Rift [and Discussion]. Philosophical Transactions of the Royal Society A: Mathematical, Physical and Engineering Sciences, 267(October), 107–130. doi:10.1098/rsta.1970.0027

Frieslander, U. (2000). The structure of the Dead Sea Transform emphasizing the Arava, using new geophysical data. The Hebrew University of Jerusalem,101(7).

Galbraith, R. F., Roberts, R. G., Laslett, G. M., Yoshida, H., & Olley, J. M. (1999). Optical dating of single and multiple grains of quartz from jinmium rock shelter, northern Australia: Part I, experimental design and statistical models*.Archaeometry, 41(2), 339-364.

Garfunkel, Z., (1970). The Tectonics of the Western Margins of the Southern Arava. Phd. Thesis, Hebrew University, 204 pp. (in Hebrew, English abstract).

Garfunkel, Z., (1978). The Negev Regional synthesis of sedimentary basins. Int. Congr. sedimentol., 10th (Jerusalem) Guideb. 1, pp. 35-101.

Garfunkel, Z. (1981). Internal structure of the Dead Sea leaky transform (rift) in relation to plate kinematics. Tectonophysics, 80, 81–108. doi:10.1016/0040-1951(81)90143-8

Garfunkel, Z. (1988). The pre-Quaternary geology of Israel. Monographiae biologicae, 62, 7-34.

Garfunkel, Z., Zak, I., & Freund, R. (1981). Active faulting in the Dead Sea rift. Tectonophysics, 80, 1–26. doi:10.1016/0040-1951(81)90139-6

Garfunkel, Z., & Horowitz, A. (1966). The upper Tertiary and Quaternary morphology of the Negev, Israel. Isr. J. Earth Sci, 15(3), 101-117.

Gerson, R., & Amit, R. (1987). Rates and modes of dust accretion and deposition in an arid region--the Negev, Israel. Geological Society, London, Special Publications, 35, 157–169. doi:10.1144/GSL.SP.1987.035.01.11

Gerson, R., Grossman, S., Amit, R., & Greenbaum, N. (1993). Indicators of faulting events and periods of quiescence in desert fluvial fans. Earth Surface processes and landforms, 18(3), 181-202.

Ginat, H., Enzel, Y., & Avni, Y. (1998). Translocated Plio-Pleistocene drainage systems along the Arava fault of the Dead Sea transform. *Tectonophysics*,*284*(1), 151-160.

Ginat, H., Beyth, M., & Crouvi, O. (2009). Geomorphic evidence for young tectonic activity around Har Timna. Israel Journal of Earth Sciences, 57, 213–229. doi:10.1560/IJES.57.3-4.213

Guralnik, B., Matmon, A., Avni, Y., & Fink, D. (2010). 10 Be exposure ages of ancient desert pavements reveal Quaternary evolution of the Dead Sea drainage basin and rift margin tilting. Earth and Planetary Science Letters,290(1), 132-141.

Hamiel, Y., Amit, R., Begin, Z. B., Marco, S., Katz, O., Salamon, A., Zilberman, E. & Porat, N. (2009). The seismicity along the Dead Sea Fault during the last 60,000 years. Bulletin of the Seismological Society of America, 99(3), 2020-2026.

Harding, T. P., Vierbuchen, R. C. & Christie-Bhck, N. (1985). Structural styles, plate-tectonic settings, and hydrocarbon traps of divergent (transtensional) wrench faults. In: Strike-slip Basin Deformation, Basin Formation and Sedimentation (edited by Biddie, K. T. and Christie-Blick, N.). Spec. Pubs. Sot. econ. Paleont. Miner. 37,51-77.

Hill, M. L., & Dibblee, T. W. (1953). San Andreas, Garlock, and Big Pine faults, California a study of the character, history, and tectonic significance of their displacements. Geological Society of America Bulletin, 64(4), 443-458.

Hoffman, P. F., & St-Onge, M. R. (1981). Contemporaneous thrusting and conjugate transcurrent faulting during the second collision in Wopmay orogen: implications for the subsurface structure of post-orogenic outliers. Current Research, Part A, Geological Survey of Canada, Paper, 251-257.

Horowitz, A. (1979) The Quaternao, of Israel. Academic Press, New York, 394 pp.

Jaeger, J. C., Cook, N. G., & Zimmerman, R. (2009). Fundamentals of rock mechanics. John Wiley & Sons.

Lian, O. B., & Roberts, R. G. (2006). Dating the Quaternary: progress in luminescence dating of sediments. Quaternary Science Reviews, 25(19), 2449-2468.

Malik, J. N., & Mohanty, C. (2007). Active tectonic influence on the evolution of drainage and landscape: Geomorphic signatures from frontal and hinterland areas along the Northwestern Himalaya, India. Journal of Asian Earth Sciences, 29, 604–618. doi:10.1016/j.jseaes.2006.03.010

Marco, S. (2007). Temporal variation in the geometry of a strike-slip fault zone: Examples from the Dead Sea Transform. Tectonophysics, 445, 186–199. doi:10.1016/j.tecto.2007.08.014

Murray, A. S., & Wintle, A. G. (2000). Luminescence dating of quartz using an improved single-aliquot regenerative-dose protocol. Radiation measurements,32(1), 57-73.

Olley, J. M., Pietsch, T., & Roberts, R. G. (2004). Optical dating of Holocene sediments from a variety of geomorphic settings using single grains of quartz. Geomorphology, 60, 337–358. doi:10.1016/j.geomorph.2003.09.020

Picard, L. Y. (1943). Structure and evolution of Palestine: with comparative notes on neighbouring countries. Geological Department Hebrew Univ.

Porat, N., Amit, R., Zilberman, E., & Enzel, Y. (1997). Luminescence dating of fault-related fluvial fan sediments in the Southern Arava Valley, Israel. Quaternary Science Reviews, 16(96), 397–402. doi:10.1016/S0277-3791(96)00101-1

Porat, N., Duller, G. a T., Amit, R., Zilberman, E., & Enzel, Y. (2009). Recent faulting in the southern Arava, Dead Sea Transform: Evidence from single grain luminescence dating. Quaternary International, 199, 34–44. doi:10.1016/j.quaint.2007.08.039

Porat, N., Amit, R., Enzel, Y., Zilberman, E., Avni, Y., Ginat, H., & Gluck, D. (2010). Abandonment ages of fluvial landforms in the hyperarid Negev determined by luminescence dating. Journal of Arid Environments, 74(7), 861–869. doi:10.1016/j.jaridenv.2009.10.018

Quennell, A. M. (1958). The structural and geomorphic evolution of the Dead Sea Rift. Quarterly Journal of the Geological Society, 114(1-4), 1-24.

Rinat, Y., Matmon, A., Arnold, M., Aumaître, G., Bourlès, D., Keddadouche, K., ... & Finkel, R. C. (2014). Holocene rockfalls in the southern Negev Desert, Israel and their relation to Dead Sea fault earthquakes. Quaternary Research,81(2), 260-273.

Riquelme, R., Martinod, J., Hérail, G., Darrozes, J., & Charrier, R. (2003). A geomorphological approach to determining the Neogene to Recent tectonic deformation in the Coastal Cordillera of northern Chile (Atacama). Tectonophysics, 361, 255–275. doi:10.1016/S00401951(02)006492

Roberts, R. G., Galbraith, R. F., Yoshida, H., Laslett, G. M., & Olley, J. M. (2000). Distinguishing dose populations in sediment mixtures: a test of single-grain optical dating procedures using mixtures of laboratory-dosed quartz.Radiation Measurements, 32(5), 459-465.

Ron, H., Freund, R., Garfunkel, Z., & Nur, A. (1984). Block rotation by strike-slip faulting: Structural and paleomagnetic evidence. Journal of Geophysical Research: Solid Earth (1978–2012), 89(B7), 6256-6270.

Ron, H., & Eyal, Y. (1985). Intraplate deformation by block rotation and mesostructures along the Dead Sea transform, northern Israel. Tectonics, 4(1), 85-105.

Sagy, a., Snch, a., Rosensaft, m., Bartov, y. (2013), Map of active faults and potential active faults for the Israel standard 413 "design provision for earthquakes resistance of structures" amendment No.5,2013: Geological Survey of Israel.

Schattner, U., & Weinberger, R. (2008). A mid-Pleistocene deformation transition in the Hula basin, northern Israel: Implications for the tectonic evolution of the Dead Sea Fault. Geochemistry, Geophysics, Geosystems, 9(December 2007). doi:10.1029/2007GC001937

Schumm, S. A. (1977). The fluvial system (Vol. 338). New York: Wiley.

Skempton, A. W. (1966, January). Some observations on tectonic shear zones. In 1st ISRM Congress. International Society for Rock Mechanics.

Stirling, M. W., Wesnousky, S. G., & Shimazaki, K. (1996). Fault trace complexity, cumulative slip, and the shape of the magnitude-frequency distribution for strike-slip faults: a global survey. Geophysical Journal International, 124(3), 833-868.

Stokes, S. (1999). Luminescence dating applications in geomorphological research. Geomorphology, 29(1), 153-171.

Strahler, A. N. (1964). Quantitative geomorphology of drainage basin and channel networks. Handbook of applied hydrology.

Sylvester, A. G. (1988). Geological Society of America Bulletin Strike-slip faults. Geological Society of America Bulletin Strike-Slip Faults, (11), 1666–1703. doi:10.1130/0016-7606(1988)100<1666

Tchalenko, J. S. (1970). Similarities between shear zones of different magnitudes. Geological Society of America Bulletin, 81(6), 1625-1640.

Ten Brink, U. S., Rybakov, M., Al-Zoubi, A. S., Hassouneh, M., Frieslander, U., Batayneh, A. T., … Hall, J. K. (1999). Anatomy of the Dead Sea transform: Does it reflect continuous changes in plate motion? Geology, 27, 887–890. doi:10.1130/0091-7613(1999)027<0887:AOTDST>2.3.CO;2

Wang, X. L., Wintle, A. G., & Lu, Y. C. (2006). Thermally transferred luminescence in fine-grained quartz from Chinese loess: basic observations.*Radiation Measurements*, *41*(6), 649-658.

Weissbrod, T., (1961), The geology and petrography of the Roded Massif: unpubl. M.Sc. thesis; Hebrew University, Jerusalem (in Hebrew), 64 pp.

Wellman, H. W., & Willett, R. W. (1942). The geology of the west coast from Abut Head to Milford Sound. Royal Society of New Zealand.

Wesnousky, S. G. (1988). Seismological and structural evolution of strike-slip faults. Nature. doi:10.1038/335340a0

Westaway, R. (1990). Block rotation in western Turkey: 1. Observational evidence. Journal of Geophysical Research: Solid Earth (1978–2012), 95(B12), 19857-19884.

wilcox, R. E., Harding, T. P., & Seely, D. R. (1973). BASIC WRENCH TECTONICS. American Association of Petroleum Geologists Bulletin. doi:10.1306/819A424A-16C5-11D7-8645000102C1865D

Zain Eldeen, U., Delvaux, D., & Jacobs, P. (2001). Tectonic evolution in the Wadi Araba Segment of the Dead Sea Rift, South-West Jordan. Stephan Mueller Special Publication Series, 2, 63–81. doi:10.5194/smsps-2-63-2002

Zak, I., & Freund, R. (1981). Asymmetry and basin migration in the dead sea rift. Tectonophysics, 80, 27–38. doi:10.1016/0040-1951(81)90140-2

Zilberman, E. (1991). Landscape evolution in the central, northern and northwestern Negev during the Neogene and the Quaternary. Geological Survey of Israel, Jerusalem, 1-164.

Zilberman, E., Baer, G., Avni, Y., & Feigin, D. (1996). Pliocene fluvial systems and tectonics in the central Negev, southern Israel. Isr. J. Earth Sci, 45, 113-126.

Zilberman, E., Amit, R., Porat, N., Enzel, Y., & Avner, U. (2005). Surface ruptures induced by the devastating 1068 AD earthquake in the southern Arava valley, Dead Sea Rift, Israel. Tectonophysics, 408, 79–99. doi:10.1016/j.tecto.2005.05.030

Appendix A. Figures locations

Appendix B. Detailed description of mapping units

Unit ZQ1:

Unit ZQ1 is the most elevated terrace in this drainage basin and covers about 3% of the total surface area. The exposed base of the unit is deposited on Precambrian magmatic rocks and Cambrian sandstones. Well-developed desert pavement coats this unit. A soil sequence with a reddish Av horizon and a large concentration of gypsum and salt at the depth of approximately 20cm developed at the top of this unit. In the upper 35cm of the soil profile the gravel is highly shattered. Boulders larger than 40 cm are sparsely scattered all through the deposited sequence and interfere with the unit's coating. This unit exhibits two types of alternating beddings:

Type A: coarse-grained fluvial gravel. This type is composed of 50% carbonate pebbles and 50% magmatic clasts. The components are mud supported and moderately consolidated by a silty matrix that contains gypsum. The carbonate pebbles are moderately spherical and the magmatic clasts are angular. Grain sizes vary from 1 to 5cm, are poorly rounded and poorly sorted. General color appearance of these horizons is light.

Type B: coarse-grained bedded fluvial gravel. These horizons are composed of 65% carbonates pebbles and 35% magmatic clasts. The components are grain supported and poorly consolidated. A silty matrix that contains gypsum fills the space between the grains. The carbonate pebbles are moderately spherical and the magmatic clasts are angular. Grain sizes vary from 5 to 10cm, are poorly rounded and poorly sorted. General color appearance of these horizons is light.

Type A horizons are generally thicker (100-170 cm) as opposed to Type B (~30cm).

Unit ZQ2:

Unit ZQ2 is a coarse to medium-grained and moderate to fine-bedded fluvial sequence. The unit is composed of 30% moderately spherical carbonate pebbles and 70% angular magmatic clasts. The components are mud supported by a moderately consolidated silty matrix that contains gypsum. Grain sizes vary from 1 to 5 cm, are poorly rounded and poorly to moderately sorted. This unit's general color appearance is bark and it covers about 10% of the total surface area. At approximately 50cm beneath the surface there is a horizon that contains boulders larger than 40cm. The unit is coated by a moderately developed desert pavement. A soil sequence with a large concentration of gypsum and salt at the depth of approximately 5cm developed upon this unit. In the upper 25cm of the soil profile the gravel is highly shattered.

Unit ZQ3:

Unit ZQ3 is a coarse-grained and fine-bedded fluvial sequence. The unit is composed of 10% moderately spherical sandstone pebbles, 30% moderately spherical carbonate pebbles and 60% angular magmatic clasts. The components are mud supported by a moderately consolidated silty matrix. Grain sizes vary from 1 to 10 cm, are poorly rounded and poorly to moderately sorted. This unit's general color appearance is bark/gray and it covers about 5% of the total surface area. The base of the unit is deposited on Cambrian sand stones. At the top of this unit a soil horizon containing gypsum and salt developed. Well-developed desert pavement with an underlying reddish Av horizon coats this unit.

Unit ZQ4:

Unit ZQ4 is a coarse-grained and fine-bedded fluvial sequence. The unit is composed of 30% moderately spherical carbonate pebbles and 70% angular magmatic clasts. The components are mud supported by a moderately consolidated silty matrix that contains gypsum. There are three grain size groups (1-3cm; 5-7cm; 3-30cm) that occupy different bedding horizons and are poorly rounded and moderately sorted. This unit's general color appearance is bark-reddish and it covers about 20% of the total surface area. The unit is coated by a poorly developed desert pavement and still preserves a bar and swell pattern. The unit's surface is very rough and is covered with boulders. An immature soil sequence with an Av horizon and gypsum and salt scarcely scattered throughout the top 20cm developed upon this unit.

Unit AQ2:

Unit AQ2 is a coarse-grained and coarse-bedded fluvial sequence. The unit is composed of 90% moderately to poorly spherical carbonate pebbles and 10% angular magmatic clasts. The components are mud supported by a well to moderately consolidated silty matrix that contains gypsum. Grain sizes vary from 5 to 20 cm, are poorly rounded and well sorted. Throughout the sequence of the terrace there are scattered boulders of varies sizes up to 150cm. This unit's general color appearance is light and it covers less than 2% of the total surface area. The base of the unit is deposited on Pre-Cambrian magmatic stones. Moderately-developed desert pavement with an underlying reddish Av horizon coats this unit.

Unit AQ3:

Unit AQ3 is a coarse-grained and fine-bedded fluvial sequence. The unit is composed of 40% moderately spherical carbonate pebbles and 60% angular magmatic clasts. There are horizons that contain carbonate and magmatic components and those that contain only carbonates, but there are no horizons that contain only magmatic clasts. The components are mostly grain sported and partly mud supported by a moderately consolidated silty matrix. A 40cm thick horizon containing gypsum and salt developed at a depth of 120cm from the top of the unit. Grain sizes vary from 1 to 5 cm, are poorly rounded and well sorted. Throughout the sequence of the terrace there are scattered boulders that range in size between 20 and 40cm. This unit's general color appearance is dark/gray and it covers about 10% of the total surface area. The base of the unit is deposited on Pre-Cambrian magmatic stones and partly deposited upon AQ2. Moderately-developed desert pavement with an underlying reddish Av horizon coats this unit.

Unit AQ4:

Unit AQ4 is a coarse-grained and coarse-bedded fluvial sequence. The unit is composed of 80% carbonate, 20% sand stone and <1% chert moderately spherical pebbles. The components are mud supported by a moderately consolidated silty matrix. Grain sizes vary from 1 to 3cm in the thinnest horizons and from 5 to 10 cm in the thicker horizons, are moderately rounded and poorly to moderately sorted. Throughout the sequence of the terrace there are scattered boulders that range in size between 30 and 100cm. This unit's general color appearance is light and it covers about 60% of the total surface area. The base of the unit is partly deposited on Cambrian sand stones and partly deposited

on unit AQ3. The unit is coated by a poorly developed desert pavement with an underlying reddish Av horizon and a soil horizon approximately 5cm thick containing gypsum and salt beneath it.

Unit AQ5:

Unit AQ5 is a coarse-grained and coarse-bedded fluvial sequence. The unit is composed of 70% carbonate and 30% sand stone pebbles which are moderately spherical. The components are mud supported by a moderately consolidated silty matrix. Grain sizes vary from 2 to 10cm, are moderately rounded and poorly to moderately sorted. This unit's general color appearance is light and it covers about 15% of the total surface area. The unit is coated by a poorly developed desert pavement with an underlying reddish Av horizon and a soil horizon approximately 5cm thick containing gypsum and salt beneath it. The surface of the unit is very rough and is not leveled.

Unit SQ1:

Unit SQ1 is a coarse-grained and coarse-bedded fluvial sequence. The unit is composed of 60% moderately spherical carbonate pebbles, 10% angular chert clasts and 30% angular magmatic clasts. The components are grain supported and well to moderately consolidated, with the addition of a silty matrix containing gypsum and salt. Grain sizes vary from 2 cm to 1 m, are poorly rounded and poorly sorted. This unit's general color appearance is light and it covers about 10% of the total surface area. The unit is coated by a well-developed desert pavement, composed mostly of chert, with an underlying reddish Av horizon.

Unit SQ2:

Unit SQ2 is a coarse-grained and coarse-bedded fluvial sequence. The unit is composed of 5% moderately spherical carbonate pebbles, 95% angular magmatic clasts. As the distance from the basin's origin increases there is an increase in the carbonate and chert component alongside a decrease in their grain size. The components are grain supported and moderately consolidated, with the addition of a silty matrix containing salt. Grain sizes vary from 1 cm to 1 m, are poorly rounded and poorly sorted. This unit's general color appearance is dark and it covers about 10% of the total surface area. The unit is coated by a well-developed desert pavement with an underlying reddish Av horizon.

Unit SQ3:

Unit SQ3 is a coarse-grained and coarse-bedded fluvial sequence. The unit is composed of 95% moderately spherical carbonate pebbles and 5% angular magmatic clasts. The components are grain supported and poorly consolidated, with the addition of a silty matrix containing gypsum. Grain sizes vary from 1 to 20 cm, are moderately rounded and moderately sorted. This unit's general color appearance is light and it covers about <1% of the total surface area. The unit is coated by a moderately-developed desert pavement with an underlying reddish Av horizon.

Unit SQ4:

Unit SQ4 is a coarse-grained and coarse-bedded fluvial sequence. The unit is composed of moderately spherical carbonate pebbles. The components are grain supported and poorly consolidated, with the addition of a silty matrix containing gypsum. Grain sizes vary from 1 cm to 1 m, are poorly rounded and poorly sorted. Al threw the unit there are elongated nodules of grain sizes that are different from the surrounding grain size. This unit's general color appearance is light and it covers about 30% of the total surface area. The unit is coated by a moderately-developed desert pavement located between the overlying boulders with an underlying reddish Av horizon.

Unit SQ4 is composed of five subunits that share the same flow direction but differ in their heights and roughness of surface:

SQ4: The highest subunit, its surface is coated with scattered boulders.

SQ4a: Lower than and not as rough as subunit SH_Q_4.

SQ4b: Lower than and not as rough as subunit SH_Q_4_1.

SQ4c: Its surface is coated with a thin dark colored horizon that is composed of magmatic and sand stone rocks of smaller grain size that do not appear in the other subunits.

SQ4d: The lowest sub unit.

Unit SQ5:

Unit SQ5 is a coarse-grained and fine-bedded fluvial sequence. The unit is composed of angular magmatic clasts. The components are grain supported and poorly consolidated.

Grain sizes vary from 1 cm to 20 cm, are poorly rounded and moderately sorted. All through the unit there are elongated nodules of grain sizes that are different from the surrounding grain size. This unit's general color appearance is dark/red and it covers about 20% of the total surface area. The unit is coated by a moderately-developed desert pavement with an underlying reddish Av horizon.

Appendix C. Detailed OSL results:

Sample	Unit	Depth (cm)	K (ppm)	U (ppm)	Th (ppm)	Ext. α (µGy/a)	Ext. β (µGy/a)	Ext. γ (µGy/a)	Cosmic (µGy/a)	Total dose (µGy/a)	No. aliquots	OD (%)	De (Gy)	Age (ka)
Zefunot														
YEG-1	ZQ1	180	2.74	2.3	6.9	2	2101	1316		3420±128	9/18		137±36	40±10
YEG-2	ZQ4 t	65	2.822	3.8	12.8	18	2725	1686	199	4628±96	14/17	58	33±9	7.1±1.9
YEG-3	ZQ4 b	210	1.577	2.2	6.6	10	1522	926	162	2620±53	14/16	50	62±24	24±9
YEG-4	ZQ1 t	70	2.407	2.6	8.5	12	2188	1255	196	3651±65	12/12	36	171±65	47±18
SG											60/113/1100	34	176±7	48±2
YEG-5	ZQ1 b	350	1.66	3.1	7.1	13	1704	1067	137	2921±60	10/13	46	170±66	58±23
YEG-6	ZQ4 t	45	2.407	2.9	9.1	14	2242	1316	214	3787±70	20/29	71	20±8	5.2±2
YEG-7	ZQ1 t	120	2.656	3.1	11.1	15	2485	1491	181	4172±87	9/9	29	206±63	49±15
SG											68/166/1100	42	205±12	50±3
YEG-8	ZQ2 t	80	2.158	2.4	8.2	12	1984	1160	190	3345±69	13/13	31	197±68	59±20
YEG-9	ZQ3 t	110	2.739	2.5	10.1	13	2439	1397	183	4033±84	11/11	46	199±93	49±23
YEG-10	ZP	120	4.4	3.5	13.1	19	3799	2042	181	6041±125	24/29	86	3.9±2.6	0.6±0.4
SG											74/75/500			0.4±0.1

Table 7. Detailed OSL results of the Zefunot basin: **OSL dating results. SG = Single grain measurement; t = sample collected from top of mapping unit; b = sample collected from base of mapping unit.**

Sample	Unit	Depth (cm)	K (ppm)	U (ppm)	Th (ppm)	Ext. α (µGy/a)	Ext. β (µGy/a)	Ext. γ (µGy/a)	Cosmic (µGy/a)	Total dose (µGy/a)	No. aliquots	OD (%)	De (Gy)	Age (ka)
Shehoret														
YEG-11	SQ1 t	100	0.17	2.3	0.6	6	425	322	185	939±23	19/19	83	100±59	107±63 *
YEG-12	SQ1 b	800	0.25	4.4	0.7	12	751	578	85	1426±42	38/38	100	108±74	73±51 *
YEG-13	SQ2 t	130	0.42	0.9	0.8	3	422	236	178	840±17	17/17	34	170±57	202±68
YEG-14	SQ2 b	350	0.58	1.1	1.2	4	570	315	137	1026±87	15/18	55	208±59	202±60
YEG-15	SQ4 b	2000	0.25	1.2	0.9	4	346	234	33	617±19	13/13	23	76±17	123±28
YEG-16	SQ4b t	50	0.5	1.1	1	5	452	338	210	1006±21	19/20	65	31±16	31±16
SG											29/68/600	100	8.3±0.2	8.3±0.3
YEG-17	SQ4a t	120	0.58	1.2	0.9	4	576	312	174	1066±21	16/22	52	32±10	30±9
YEG-18	SQ4 t	65	0.58	1.1	1.1	4	568	311	199	1082±19	15/20	53	20±5	18±4
YEG-19-TT	SQ1 t	40	0.61	2.8	1.5	9	807	518	219	1553±52	9/9	16	817±143	526±94
YEG-20-TT	SQ1 b	300	0.66	2.1	2.3	7	771	490	145	1414±50	9/9	22	777±185	549±133

Table 8. Detailed OSL results of the Shehoret basin: **OSL dating results. SG = Single grain measurement; TT= thermally transferred OSL; t = sample collected from top of mapping unit; b = sample collected from base of mapping unit; *= samples that were not included in the research results do to their poor results (this unit was resampled and processed with the TT-OSL method: YEG-19 and YEG-20).**

תקציר

אזור אילת נחשב לאזור בעל סיכון סיסמולוגי רב בשל פעילות טקטונית צעירה לאורך מערכת העתקי אילת. בעוד הכרונולוגיה של פעילות זו נחקר ביסודיות בסדרת מחקרים פלאו-סיסמיים והיסטוריים, הבנת ההשתרעות המרחבית של דפורמציה טקטונית צעירה בשולי אזור ההעתקה העיקרית פחות ברורה. בהקשר זה, מטרת מחקר זה היא שיפור הבנת הפריסה המרחבית של הדפורמציה הטקטונית בתקופת הרביעון בדרום הערבה. לשם כך נחקרו השינויים הגאומורפולוגיים ומאפייני מערכות הניקוז תחת השפעתה של פעילות זו. עבודת השדה שכללה מיפוי יחידות סחף רבעוניות ומדידת חתכים טופוגרפיים בהפרדה גבוהה באגני הניקוז צפונות, עמרם, ושחורת מצביעה על שינוים בכיווני הזרימה. יתכן ששינויים אלה נגרמו מהטיית פני השטח כתוצאה מדפורמציה טקטונית. מספר עדויות גאומורפולוגיות מצביעות על הטיה לכיוון דרום של מניפת הסחף של אגן צפונות ואגן עמרם והטיה לכיוון צפון של מניפות הסחף באגן שחורת. שינוים אלה מעלים את האפשרות לנוכחותו של מאמץ טקטוני לחיצתי בכיוון צפ'-דר' בשולי טרנספורם ים המלח. תוצאות תיארוך יחידות המיפוי בשיטת הלומינסנציה (OSL) הראו שאזור המחקר הושפע מדפורמציה טקטונית במהלך אמצע הפליסטוקן ועד ההולוקן המאוחר. תוצאות מחקר זה מצביעות על כך שהדפורמציה הטקטונית לאורך שולי חלקו הדרומי של טרנספורם ים המלח משתרע על רוחב גדול יותר מהידוע עד כה. רוחב השתרעות הדפורמציה שנצפה במחקר זה סותר את רוחב ההשתרעות המצופה בהינתן בגרותו ומידת ההסתה הכוללת לאורך כלל טרנספורם ים המלח. יתכן ששינוים פליסטוקנים-הולוקנים בגיאומטרית התנועה בין הלוח הערבי ותת הלוח של סיני הם הגורמים ליצירת חגורת הדפורמציה הרחבה.

דפורמציה טקטונית מרחבית לאורך טרנספורם ים המלח, בשולי הערבה הדרומית, כפי שמבוטאת בסמנים גיאומורפולוגיים

עבודת גמר לתואר מוסמך במדעי הטבע
מוגשת על ידי:
ידידיה גלמן

בהדרכת:
ד"ר עמית מושקין
פרופ' ארי מטמון

30.3.2015
י' ניסן תשע"ה

החוג לגיאולוגיה
המכון למדעי כדור הארץ
הפקולטה למדעי הטבע
האוניברסיטה העברית בירושלים